

# MODELLING AND ANALYSIS OF A S-SP TOPOLOGY BASED WPT SYSTEM

*A Project Report*

*submitted by*

**B. ABHILASH**

*in partial fulfilment of the requirements  
for the award of the degree of*

**DUAL DEGREE**



**DEPARTMENT OF ELECTRICAL ENGINEERING  
INDIAN INSTITUTE OF TECHNOLOGY MADRAS.**

**MAY 2022**

# THESIS CERTIFICATE

This is to certify that the thesis titled **MODELLING AND ANALYSIS OF A S-SP TOPOLOGY BASED WPT SYSTEM**, submitted by **B. ABHILASH**, to the Indian Institute of Technology, Madras, for the award of the degree of **DUAL DEGREE IN ELECTRICAL ENGINEERING**, is a bona fide record of the research work done by him under my supervision. The contents of this thesis, in full or in parts, have not been submitted to any other Institute or University for the award of any degree or diploma.

Place: Chennai  
Date: 15th May, 2022

**Dr. Arun Karuppaswamy B**  
Research Guide  
Assistant Professor  
Dept. of Electrical Engineering  
IIT Madras, 600 036

# ACKNOWLEDGEMENTS

Foremost, I would like to thank my advisor Dr.Arun Karupaswamy B for his guidance over the entire project duration in terms of giving suggestions, helping with doubts, discussions, and his time and attention. I'm also grateful for the Power Electronics course(Btech level) he took which kindled my interest to start and explore power electronics deeper which eventually led me to this project.

I'm grateful to my lab mates and the weekly lab discussions which made my understanding more concrete. I thank Mr. Ravi Teja and Mr. Satheesh for their help with doubts, discussions and motivation.

I thank all the authors whose papers I had referred, for their efforts which gave me different perspectives of understanding the subject.

Finally, I thank all the IITM professors whose power electronics and motor control related courses I took, as they helped me comprehend different aspects related to the project.

# ABSTRACT

KEYWORDS: WPT ; S-SP topology; CC-CV charging; Unified Steady State model; Phasor DQ modelling.

Electric vehicles (EVs) have benefits such as lesser pollution and higher efficiency compared to internal combustion (IC) engine vehicles. As the usage of EVs grow, the need for public charging infrastructure becomes important. Static wireless power transfer (WPT) has several advantages compared to plug-in charging in terms of better safety, lesser maintenance requirement, etc. In public places like say, shopping malls, office parking and the like, WPT also ensures ease of use. EVs generally use Li-ion batteries due to their high power densities. Constant current (CC)- constant voltage (CV) charging is the preferred charging method for Li-ion. Further, ZPA is desirable to ensure a lower power rating requirement for the switching converter. This project aims to design a WPT system with minimum number of components to achieve CC-CV charging along with zero phase angle (ZPA). A S-SP topology is chosen as it is the simplest possible one with less component count. The use of the additional dc-dc converter is eliminated by the load-independent characteristics of S-SP topology. The topology is modelled using unified steady state model and a phasor DQ model with suitable order-reduction techniques. A voltage regulation based control strategy is used.

# TABLE OF CONTENTS

<b>ACKNOWLEDGEMENTS</b>	<b>i</b>
<b>ABSTRACT</b>	<b>ii</b>
<b>LIST OF TABLES</b>	<b>vii</b>
<b>LIST OF FIGURES</b>	<b>x</b>
<b>ABBREVIATIONS</b>	<b>xi</b>
<b>NOTATION</b>	<b>xii</b>
<b>1 INTRODUCTION</b>	<b>1</b>
1.1 Wireless Charging and its uses . . . . .	1
1.2 Research objectives . . . . .	1
1.3 Organization of the thesis . . . . .	2
<b>2 SYSTEM OVERVIEW</b>	<b>3</b>
2.1 Battery of an EV . . . . .	3
2.2 Working Principle and Components Overview . . . . .	4
<b>3 COMPENSATION NETWORKS</b>	<b>5</b>
3.1 Short Survey of Methods to Realize CC/CV . . . . .	5
3.2 Modelling Compensation Network System . . . . .	6
3.2.1 Input Port Model . . . . .	6
3.2.2 Output Port Model . . . . .	7
3.2.3 Coil Model . . . . .	8
3.3 Desirable Features of a Compensation Network . . . . .	9
3.3.1 Constant load-independent output (CC/CV) . . . . .	10
3.3.2 Zero Phase Angle (ZPA) . . . . .	20
3.3.3 Zero Voltage Switching (ZVS) . . . . .	21

3.3.4	Bifurcation . . . . .	22
3.3.5	Frequency-splitting . . . . .	22
3.3.6	Filtering action . . . . .	23
3.3.7	High circulating currents/voltage stresses . . . . .	23
3.3.8	Efficiency . . . . .	24
3.3.9	Parameter Variation(PV) and misalignment tolerance . .	25
3.3.10	Maximum Power Transfer(MPT) . . . . .	25
3.3.11	Others: Size, Bidirectional power flow . . . . .	26
3.4	Summary of basic topologies . . . . .	26
<b>4</b>	<b>STEADY STATE ANALYSIS AND DESIGN OF S-SP TOPOL- OGY</b>	<b>27</b>
4.1	Choosing the topology . . . . .	27
4.2	Steady State Requirements (design objective) . . . . .	28
4.3	Steady State Model equations of S-SP topology . . . . .	29
4.4	Simplified Equations: . . . . .	31
4.4.1	CV mode . . . . .	31
4.4.2	CC mode . . . . .	31
4.4.3	Components Calculation: . . . . .	32
4.5	Design Procedure of Compensation Topology . . . . .	32
4.6	Final Results . . . . .	34
4.7	Conclusion . . . . .	35
<b>5</b>	<b>DYNAMIC MODELLING OF S-SP TOPOLOGY AND WPT SYSTEM</b>	<b>36</b>
5.1	Choice of States . . . . .	36
5.2	Modelling of Compensation Topology . . . . .	38
5.2.1	Time domain to Phasor domain . . . . .	38
5.2.2	Phasor domain to DQ domain . . . . .	40
5.3	State Equations of S-SP topology . . . . .	42
5.4	Order-reduction techniques and approximations . . . . .	44
5.4.1	C-L or SVADP approximation . . . . .	44
5.4.2	Neglecting Mutual-Inductance dynamics partly . . . . .	45
5.4.3	Static element approximation . . . . .	46

5.4.4	Constant phase approximation . . . . .	46
5.4.5	Other mathematical approximations . . . . .	48
5.4.6	Comparison of Approximations . . . . .	48
5.5	The Final reduced-order model of S-SP topology . . . . .	49
5.6	Combined WPT model . . . . .	49
5.7	The Monotonicity theorem . . . . .	51
5.8	Conclusion . . . . .	52
<b>6</b>	<b>CONTROL SYSTEM</b>	<b>53</b>
6.1	Choosing a control strategy . . . . .	53
6.2	Controller Block Diagram . . . . .	54
6.3	Controller Design . . . . .	54
6.3.1	CC mode Controller Design . . . . .	54
6.3.2	CV mode Controller Design . . . . .	55
6.4	Bode Plots of Controller and Closed-loop response . . . . .	56
6.4.1	CC mode . . . . .	56
6.4.2	CV mode . . . . .	57
6.5	Conclusion . . . . .	58
<b>7</b>	<b>SIMULATION RESULTS</b>	<b>59</b>
7.1	Steady State Simulations . . . . .	59
7.2	DQ Model Verification . . . . .	62
7.3	Transient Waveform Simulations . . . . .	62
7.4	Conclusion . . . . .	65
<b>8</b>	<b>CONCLUSION AND FUTURE SCOPE</b>	<b>66</b>
8.1	Conclusion . . . . .	66
8.2	Future Scope . . . . .	66
<b>9</b>	<b>APPENDIX I - Actual equations and integrated ZPA model</b>	<b>67</b>
9.1	CC/CV LIO Analysis of S-SP topology using Resonant Tank Model	67
9.1.1	CV mode LIO analysis . . . . .	67
9.1.2	CC mode LIO analysis . . . . .	67
9.2	Integrated ZPA analysis using resonant tank approach . . . . .	68

9.2.1	CV mode ZPA analysis: . . . . .	69
9.2.2	CC mode ZPA analysis: . . . . .	72
9.2.3	Comments . . . . .	73
9.3	Summary of equations . . . . .	74
<b>REFERENCES</b>		<b>77</b>



# LIST OF TABLES

2.1	Some commonly used charging methods . . . . .	4
3.1	Simplified Gain and Input Impedance of L-Networks under resonance . . . . .	17
3.2	Equations in Unified Model . . . . .	18
3.3	Summary of Compensation Topology Models . . . . .	21
4.1	Unified model Steady-State Equations of S-SP topology . . . . .	30
4.2	Steady-State actual Steady-State Equations of S-SP Topology . . . . .	30
4.3	WPT system Steady-State Design . . . . .	34
5.1	States in DC-DC converter . . . . .	37
5.2	States in Compensation Topology for inductor current . . . . .	38

# LIST OF FIGURES

2.1	Li-ion battery CC/CV Charging Profile . . . . .	3
2.2	A Typical EV-WPT system . . . . .	4
3.1	Realizing CC and CV modes with a secondary dc-dc converter .	5
3.2	A hybrid SS, PS compensation network . . . . .	6
3.3	Modelling of the input and output Ports . . . . .	7
3.4	Modelling of the coil . . . . .	8
3.5	Thevenin and Norton equivalent representation of a 2-port network	10
3.6	List of basic resonance-tanks and their resonance conditions . .	11
3.7	Detailed list of basic resonance-tanks and their resonance conditions [28] . . . . .	12
3.8	Representing different topologies using resonant tanks . . . . .	12
3.9	Visual representation of CC/CV and ZPA solutions with circles	13
3.10	Modelling 2-port networks with impedance parameters as a Net- work or Controlled Source . . . . .	14
3.11	Representing different topologies using resonant tanks . . . . .	14
3.12	Modelling and Analysis of DLCC topology - CC mode . . . . .	15
3.13	Normal and Reversed L-Networks . . . . .	16
3.14	Modelling by breaking impedances and grouping into L-Networks to get CC and CV modes . . . . .	17
3.15	A visual representation of ZPA condition in CV mode (similar for CC mode also) . . . . .	18
3.16	Using Unified Model in SS topology to get resonance conditions in terms of original impedances . . . . .	19
3.17	Impedance Inverter Circuits . . . . .	19
3.18	ZPA block modelling of DLCC topology [16] . . . . .	20
3.19	Plot by [19] depicting frequency splitting with coupling coefficient( $k$ )	22
3.20	Stress on Primary side components of SS and PS topologies in de- sign by [18] . . . . .	24
3.21	Comparison of basic topologies in terms of CC/CV and ZPA by [24]	26

4.1	S-SP Topology . . . . .	27
4.2	S-SP topology Unified Model . . . . .	29
4.3	Plot of Thevenin impedance $Z_{th}$ and Input phase angle $\theta_{in}$ over 75-98 kHz input frequency . . . . .	34
5.1	Illustration of Actual Vs Modelled quantities waveforms . . . . .	37
5.2	Phasor transforms of circuit elements . . . . .	40
5.3	S-SP topology Time-Phasor domain transformation . . . . .	40
5.4	Transforming a capacitor . . . . .	41
5.5	S-SP topology DQ model . . . . .	42
5.6	S-SP topology DQ model (laplace transformed) . . . . .	42
5.7	SVADP approximation . . . . .	45
5.8	S-SP topology SVADP approximation . . . . .	45
5.9	S-SP topology Mutual Inductance approximation . . . . .	46
5.10	S-SP topology Static $C_{sp}$ approximation . . . . .	46
5.11	Steady-State Unified Model of S-SP topology . . . . .	47
5.12	S-SP topology Constant Phase approximation . . . . .	47
5.13	Comparison of Approximations Plots . . . . .	48
5.14	The Reduced-Order Model of S-SP Topology . . . . .	49
5.15	Comparison of Actual and Reduced-Order Model . . . . .	49
5.16	Dynamic Model of the entire WPT System . . . . .	50
5.17	Illustration of Monotonicity Theorem (CC mode) . . . . .	51
5.18	Illustration of Monotonicity Theorem (CV mode) . . . . .	52
6.1	Control block diagram of the WPT system . . . . .	54
6.2	Closed Loop Response(15 $\Omega$ - CC mode) . . . . .	56
6.3	Closed Loop Response(22 $\Omega$ - CC mode) . . . . .	57
6.4	Closed Loop Response(22 $\Omega$ - CV mode) . . . . .	57
6.5	Closed Loop Response(140 $\Omega$ - CV mode) . . . . .	58
7.1	Output voltage and current gains and input phase angle for different loads . . . . .	59
7.2	Compensation topology input waveforms with $R_{ac} = 15\Omega$ for (a)load modelled as pure resistance (b) load is rectifier . . . . .	60

7.3	Compensation topology input waveforms with $R_{ac} = 140\Omega$ for (a)load modelled as pure resistance (b) load is rectifier . . . . .	61
7.4	Compensation topology input and output waveforms with $R_{ac} = 15\Omega$ depicting input-output phase relation in cc mode . . . . .	61
7.5	Compensation topology input and output waveforms with $R_{ac} = 22\Omega$ depicting input-output phase relation in cv mode . . . . .	62
7.6	Compensation topology output waveforms with $R_{ac} = 15\Omega$ depicting phase deviation at output . . . . .	63
7.7	Circuit diagram of dq model (10th order) . . . . .	63
7.8	Simulation of dq model (10th order) and actual waveform . . . .	64
7.9	$I_{bat}$ closed-loop waveform in cc mode for $R_{ac} = 15\Omega$ . . . . .	64
7.10	$I_{bat}$ closed-loop waveform in cc mode for $R_{ac} = 22\Omega$ . . . . .	64
7.11	$V_{bat}$ closed-loop waveform in cv mode for $R_{ac} = 22\Omega$ . . . . .	65
7.12	$V_{bat}$ closed-loop waveform in cv mode for $R_{ac} = 140\Omega$ . . . . .	65
9.1	CC mode LIO condition derivation . . . . .	68
9.2	Unified Model of S-SP topology . . . . .	69

# ABBREVIATIONS

<b>AC</b>	Alternating Current
<b>CC</b>	Constant Current
<b>C-L</b>	Capacitor to Inductor Transform
<b>CV</b>	Constant Voltage
<b>DC</b>	Direct Current
<b>DQ</b>	Direct Quadrature
<b>EDF</b>	Extended Describing Function
<b>EV</b>	Electric Vehicle
<b>IPT</b>	Inductive Power Transfer
<b>MPT</b>	Maximum Power Transfer
<b>PP</b>	Parallel Parallel
<b>PS</b>	Parallel Series
<b>PV</b>	Parameter Variation
<b>SP</b>	Series Parallel
<b>SS</b>	Series Series
<b>S-SP</b>	Series-Series Parallel Topology
<b>SVADP</b>	Slowly Varying Amplitude Dynamic Phasor
<b>TF</b>	Transfer Function
<b>WPT</b>	Wireless Power Transfer
<b>ZPA</b>	Zero Phase Angle
<b>ZVS</b>	Zero Voltage Switching

## NOTATION

$\Phi_{in}$	Input Phase Angle
$C_f$	Filter capacitance
$C_p$	Primary side capacitance
$C_{sp}$	Secondary side parallel capacitance
$C_{ss}$	Secondary side series capacitance
$f_s$	Switching Frequency
$f_{cc}$	Frequency at CC mode
$f_{cv}$	Frequency at CV mode
$I_{bat}$	Battery Current
$I_{in}$	Input Current of Compensation Topology
$I_o$	Output Current of Compensation Topology
$K$	coupling coefficient
$L_f$	Filter Inductance
$L_p$	Primary side self inductance
$L_s$	Secondary side self inductance
$L_{lp}$	Primary side leakage inductance
$L_{ls}$	Secondary side leakage inductance
$M$	Mutual inductance
$R_{ac}$	Equivalent AC resistance of Battery
$R_{bat}$	Battery Resistance

$V_o$	Output Voltage of Compensation Topology
$V_{bat}$	Battery Voltage
$V_{in}$	Input Voltage of Compensation Topology
$Z_{eq}$	Equivalent thevenin/Norton impedance
$Z_{in}$	Input Impedance
$Z_{th}$	Thevenin Impedance

# CHAPTER 1

## INTRODUCTION

### 1.1 Wireless Charging and its uses

Electric vehicles (EVs) have gained momentum because of their advantages over conventional IC engine vehicles. EVs are environmental friendly, have lesser maintenance costs and more efficient than IC engine vehicles.

EVs can be charged using a cable(plug-in) or through wireless. Wireless charging can be static or dynamic. In static wireless charging the vehicle is charged while it is at rest, say when it is parked or in traffic. In semi-dynamic charging the vehicle is moving at a slow speed, for example in a congested road or near a speed-breaker. In dynamic charging the vehicle is moving on the road. This project focusses on static charging.

Static wireless charging eliminates several disadvantages of plug-in charging like shock hazards and maintenance costs. Another advantage of static charging is that charging can be automated while the vehicle is parked.

### 1.2 Research objectives

1. Gain a basic understanding of wireless power transfer (WPT) system.
2. Understand compensation topology: Its working principle and applications.
3. Understand steady state modelling of compensation topology and select a suitable topology and design it to achieve constant current (CC)/constant voltage (CV) and zero phase angle (ZPA).
4. Understand the dynamic modelling of compensation topology and derive a reduced-order linear large-scale model.
5. Understand the different control strategies and design a suitable control system for control in CC and CV modes.



## 1.3 Organization of the thesis

Chapter 2 gives an overview of the different components of a WPT system and its working.

Chapter 3 discusses the purpose of a compensation network, different desirable features of compensation networks and steady state models of different components of WPT system and compensation networks.

Chapter 4 discusses the modelling and design of a S-SP compensation topology to satisfy CC/CV and ZPA conditions.

Chapter 5 discusses dynamic modelling of compensation topology, order reduction-techniques to reduce the order of the model, an approximation to get a linear large-signal model, and finally creating a circuit model for the entire WPT system. The dynamic model of the S-SP topology is obtained.

Chapter 6 describes different control techniques and a controller for the developed WPT system is designed for CC/CV modes.

Chapter 7 presents the simulation results which verify the steady state analysis, dq model, and dynamic analysis.

Appendix I explains the integrated ZPA model and derives the resonant conditions for S-SP topology in terms of actual impedances.

# CHAPTER 2

## SYSTEM OVERVIEW

In this chapter we will look at the components present in an EV WPT system and briefly understand the working principle of the system. The purpose of this work is to charge the battery, hence first we will look at what the battery demands.

### 2.1 Battery of an EV

EVs commonly use Li-ion batteries. There are several charging methods, some are described in table 2.1 [7]. The usual charging method is CC/CV charging, which consists of 3 stages[5]:

1. **Pre-charge(CC)**: When the battery is deeply discharged (very low battery voltage,  $V_{bat}$ ), it is charged with a very low constant current  $I_{pre}$ . This is because a high current can damage the battery.
2. **Fast-charge(CC)**: Now battery is charged with a higher constant current until  $V_{bat}$  reaches close to maximum voltage (say around 80% ).
3. **Absorption(CV)**: When  $V_{bat}$  is almost fully-charged, we shift into constant voltage charging, because continuing in CC mode can cause overcharging and damage the battery.

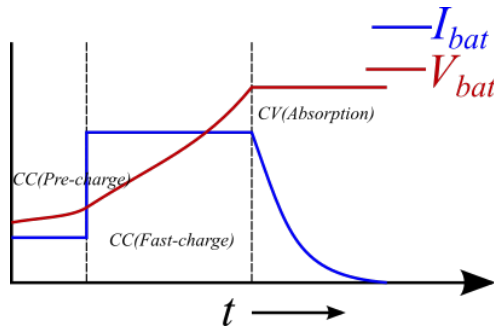


Figure 2.1: Li-ion battery CC/CV Charging Profile

Table 2.1: Some commonly used charging methods

Charging method	Description
CC charging	Constant current is applied
CV charging	Constant voltage is applied
CC/CV charging	First fast-charging is done in CC mode, then a slow charging is done in CV mode to avoid overcharging
Burp charging	A negative current is applied for a short time to avoid over-heating of battery
Random charging	Regenerative charging while braking

## 2.2 Working Principle and Components Overview

We have utility mains which provide low frequency ac. To have a smaller size for the isolation transformer, high frequency ac is usually preferred. Figure 2.2 shows a typical EV-WPT system. A power factor correction (PFC) circuit is used at the input to get a dc. Then, a H-bridge inverter converts the dc into high frequency ac square wave. This inverter is controlled to operate at two frequencies  $f_{cc}$  and  $f_{cv}$  to achieve CC and CV modes of operation.

A compensation network consisting of capacitors and inductors is used to reduce the reactive power drawn from the input line frequency ac. This helps in keeping the losses minimal at the PFC and the H-bridge. It also ensures that while operating at  $f_{cc}$ , the battery effectively receives a constant current independent of its state of charge. Similarly at  $f_{cv}$ , battery receives a constant voltage.

Magnetic coils are responsible for transferring the power inductively from the primary coil which is fitted under the charging pad to the secondary coil which is present at the bottom of the electric vehicle.

To control the output voltage or current magnitudes, the dc/ac inverter can be controlled accordingly (say duty-cycle control).

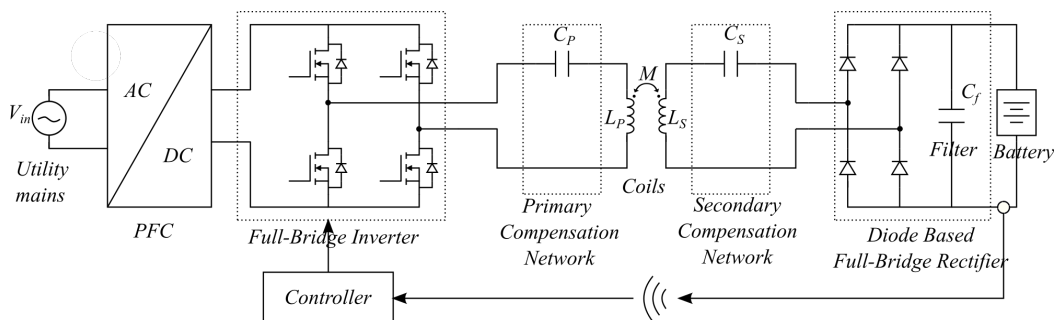


Figure 2.2: A Typical EV-WPT system

# CHAPTER 3

## COMPENSATION NETWORKS

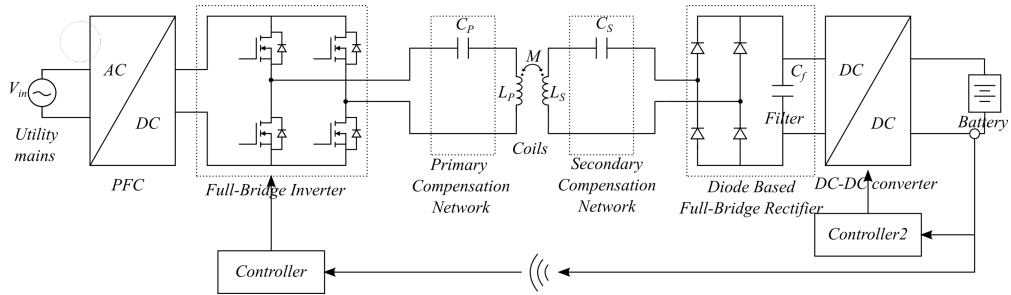
In this chapter, first we will look at some methods adopted to realize CC/CV output. Then we will model some components like coils, input/output ports, which are required for analysing compensation networks. Then we will look into the desirable features of a compensation network one by one. Different models for understanding compensation networks will also be explained.

### 3.1 Short Survey of Methods to Realize CC/CV

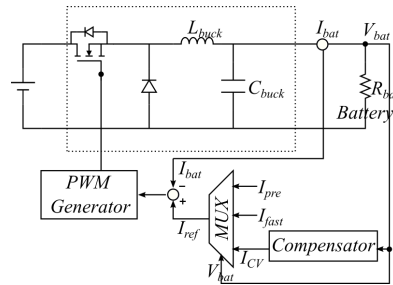
Three major methods proposed by researchers to achieve CC/CV output are:

#### 1. Using a secondary dc-dc converter [2]

An additional dc-dc converter is used on the secondary side of the coil, before the battery to achieve CC/CV mode as shown in Figure 3.1. Two frequencies  $f_{cc}$  and  $f_{cv}$  are not required and the inverter will be operated at a single frequency. The compensation network design will be simple, but the extra components in buck converter make it bulkier and less reliable.



(a) EV-WPT system with a secondary dc-dc converter



(b) A representative control block diagram for realizing CC/CV modes using a buck converter

Figure 3.1: Realizing CC and CV modes with a secondary dc-dc converter

## 2. Hybrid Compensation Network [17]

Two compensation networks are used here as shown in Fig. 3.2. When  $S$  is ON, the equivalent circuit is shown and it gives CC output. When  $\bar{S}$  is ON, the equivalent circuit is different and it gives a CV output. In this method also extra components and switches are present making it bulkier and lesser efficient. Further, care is required to handle the transients arising due to switching between the two networks.

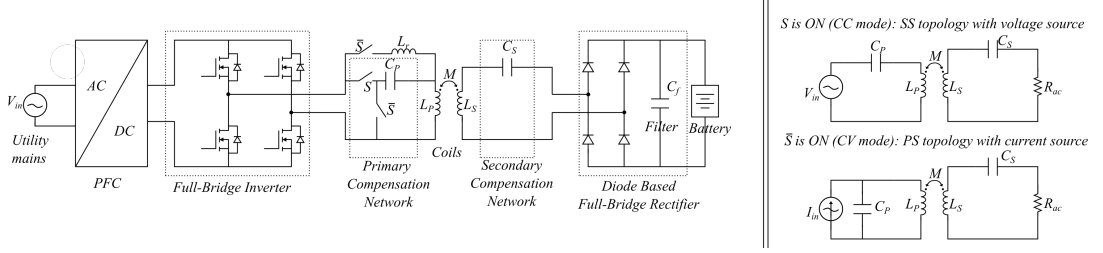


Figure 3.2: A hybrid SS, PS compensation network

## 3. Operating inverter at two frequencies [24]

The inverter is switched at a frequency  $f_{cc}$  for CC output and at  $f_{cv}$  for CV output. This strategy will be adopted in this work since it uses lesser number of passive components and switches, which makes it more compact and efficient.

## 3.2 Modelling Compensation Network System

The coil, primary and secondary compensation networks will be analysed together. This requires the input port(dc/ac inverter), output port (rectifier, filter, load), and the coil to be modelled [4].

### 3.2.1 Input Port Model

The input port voltage will be a square wave at the switching frequency  $f_s$  of the inverter. Since switching frequency is set at the resonant frequency of  $Z_{in}$  of the compensation topology ( $f_{cc}/f_{cv}$ ), the harmonics will largely be attenuated by  $Z_{in}$  and the current will predominantly be sinusoidal at the fundamental component  $f_s$ . So we can effectively replace input voltage with its fundamental component. The current on inverter input will be as in Figure 3.3, whose dc value is  $\frac{2}{\pi} I_{in} \cos(\phi_{in})$ . Thus the input port can be modelled as shown in Figure 3.3

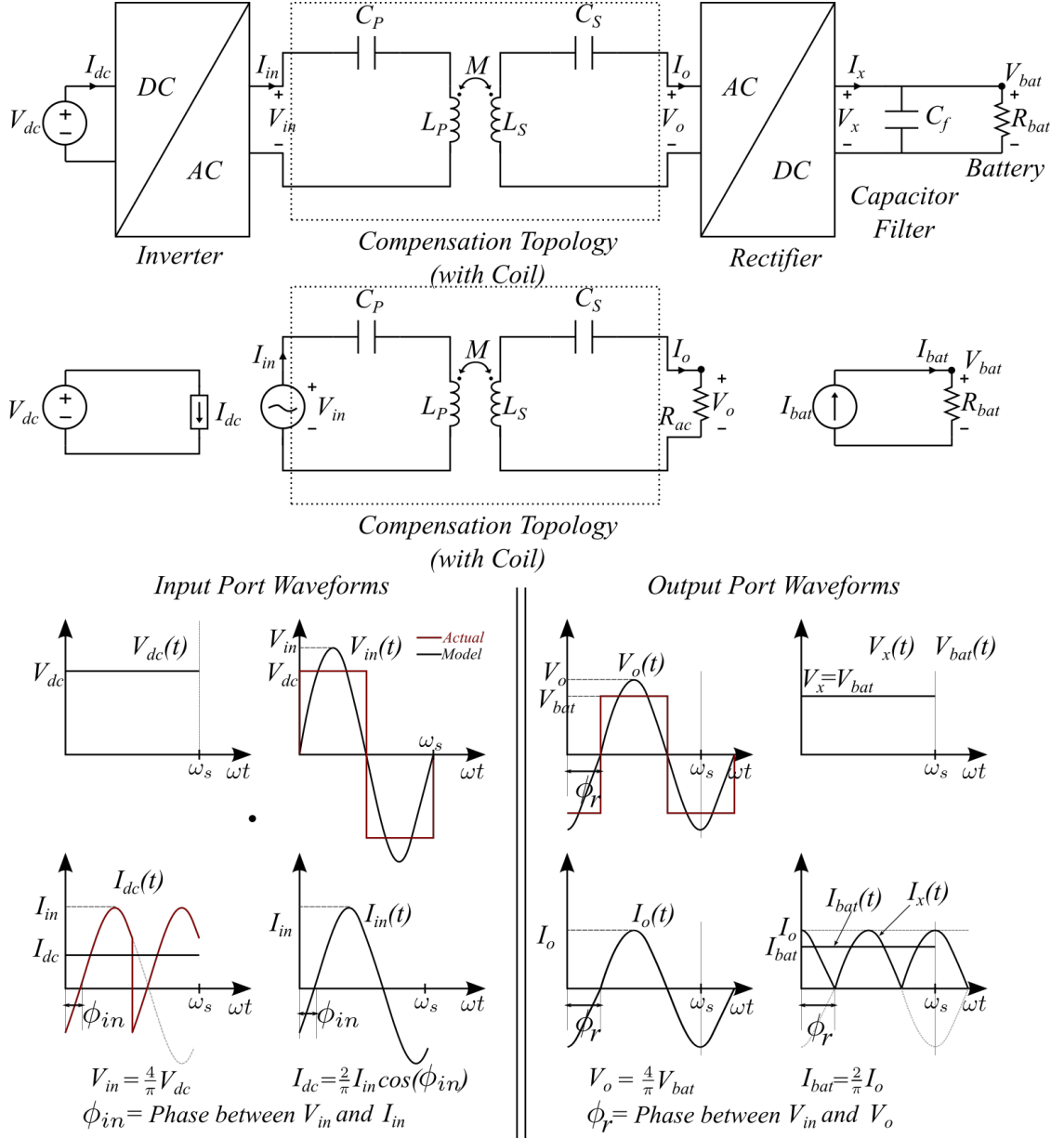


Figure 3.3: Modelling of the input and output Ports

### 3.2.2 Output Port Model

The output current will be  $I_o \sin(\omega t - \phi_r)$  ( $I_o$  is decided by  $V_{in}$  and the compensation network impedances). The rectifier output current  $I_x$  will have a dc component  $I_{bat} = \frac{2}{\pi} I_o$  which will pass through  $R_{bat}$  and the ac components will go through the filter capacitor. Hence magnitude of load voltage is  $V_{bat} = I_{bat} R = \frac{2}{\pi} I_o R$ .

At the output of the rectifier a capacitor filter is used here. So, the output voltage  $V_x$  of the rectifier is constrained to be a constant [Note: if an L or LC filter is used, the output current  $I_x$  of the rectifier will be constrained to be a

constant]. Hence the voltage  $V_o$  at the compensation network output will be a square wave. The output impedance  $Z_{th}$  will pass only the fundamental component and attenuate the harmonics since  $f_s$  is its resonance frequency. Hence, effectively the output voltage of the compensation network can be modelled to be  $V_o \sin(\omega t)$ .

Thus, the output port (rectifier+filter+load) can effectively be modelled as an equivalent ac resistance  $R_{ac} = \frac{8}{\pi^2} R_{bat}$ .

### 3.2.3 Coil Model

Let us consider the example of SS topology to understand the coil model. A coil is nothing but a transformer, but without a core [4].

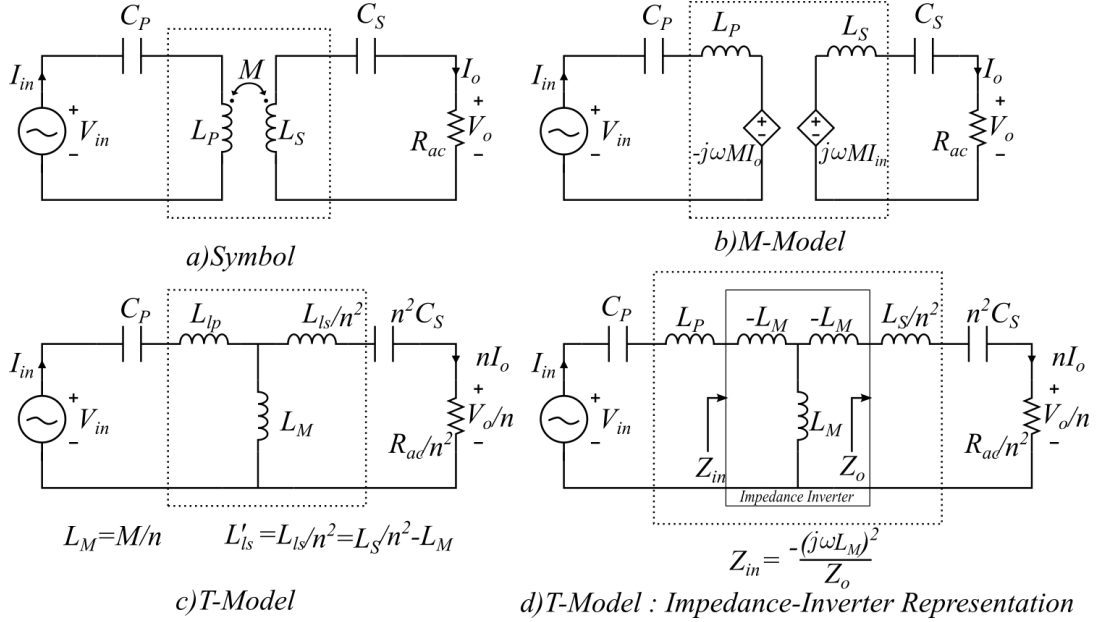


Figure 3.4: Modelling of the coil

A coil is represented as in Figure 3.4(a), where ‘M’ is the mutual inductance (a measure of how much flux is linked between the coils),  $L_p$  and  $L_s$  are the self inductances of the primary and secondary coils respectively. Coupling coefficient (k) and turns ratio (n) can be calculated as  $k = \frac{M}{\sqrt{L_p L_s}}$  and  $n = \sqrt{\frac{L_s}{L_p}}$ . For an ideal transformer,  $L_p$  and  $L_s$  are infinite since the reluctance is zero and  $k = 1$ .

The M-model in Figure 3.4(b) is based on current controlled voltage source (CCVS) and helps in deriving the equations directly.

The T-model in Figure 3.4(c) helps to represent coil as a two-port impedance

network.  $L_{lp}$  and  $L_{ls}$  are the leakage inductances and  $L_M$  is the magnetizing inductance. Usually secondary side is referred to the primary side as shown in the figure.

The T-model impedance inverter representation as in Figure 3.4(d) [8] is useful for calculation purposes. The secondary side impedance looks inverted as seen from the primary side.

### 3.3 Desirable Features of a Compensation Network

Different useful features a compensation network may be required to satisfy are listed below [20]:

1. Constant load-independent output (CC/CV)
2. Zero Phase Angle (ZPA)
3. Zero Voltage Switching (ZVS)
4. Bifurcation
5. Frequency-splitting
6. Filtering action
7. High circulating currents/voltage stresses
8. Efficiency
9. Parameter Variation(PV) and misalignment tolerance
10. Maximum Power Transfer(MPT)
11. Others: Size, Bidirectional power flow

In this work, the compensation topology design will be based on the first three features. Now each feature will be explained one-by-one in detail.



### 3.3.1 Constant load-independent output (CC/CV)

#### Introduction

The battery needs CC-CV charging. Now it will be explained how a single compensation network can provide CC and CV outputs by operating at different frequencies.

#### CC/CV General Condition [22]

Consider any 2-port network with L,C, with a voltage or current source at port-1.

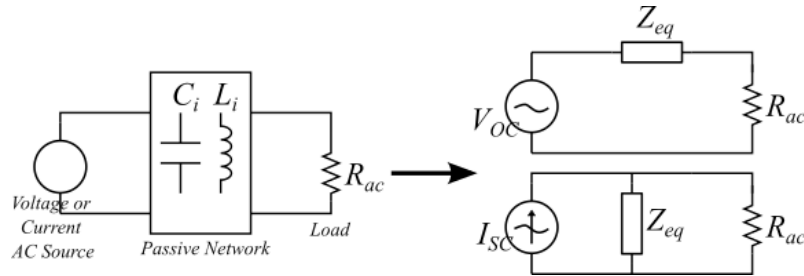


Figure 3.5: Thevenin and Norton equivalent representation of a 2-port network

It can be reduced into its thevenin or norton equivalent as in Figure 3.5. It consists of open-circuit voltage  $V_{oc}$ , short circuit current  $I_{sc}$ , and equivalent impedance  $Z_{eq}$  ( $= \frac{V_{oc}}{I_{sc}}$ ), which are functions of component values and source frequency  $\omega$ (rad/sec).

As the load  $R_{ac}$  changes, the voltage across it also changes usually ( $V_o = \frac{R_{ac}}{(R_{ac} + Z_{eq})} V_{oc}$ ).

**CC mode:** Find solutions simultaneously satisfying (1)  $Z_{eq}(\omega) = \infty$  (2)  $I_{sc}(\omega) \neq 0$  or  $\infty$ . At these frequencies ( $f_{cc}$ ) the circuit behaves as a load-independent current source.

**CV mode:** Find solutions simultaneously satisfying (1)  $Z_{eq}(\omega) = 0$  (2)  $V_{oc}(\omega) \neq 0$  or  $\infty$ . At these frequencies ( $f_{cv}$ ) the circuit behaves as a load-independent voltage source.

Note that solutions may not exist in some networks (eg: no  $f_{cc}$  solution in PS topology) and more than one solution may exist in some networks(eg: 2  $f_{cv}$  solutions in SS topology).

This method holds true for all topologies, but the mathematics involved (solving a polynomial equation) becomes complicated in higher order topologies. So a model is required which is simple to analyse in-order to determine  $f_{cc}$ ,  $f_{cv}$ , component values.[28,13,16] propose some ways of modelling/understanding. These models fundamentally try to split certain components and group a set of components as a unit. Hence bigger topologies can be broken down into small building blocks which can be cascaded one by one. Thus the mathematics involved is also broken down and simplified. Four such models will be described now.

### Resonant-tank Model [28]

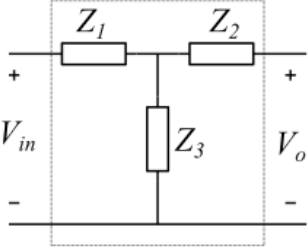
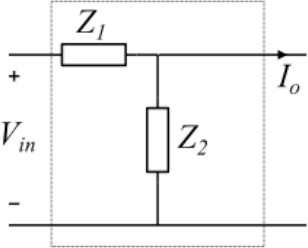
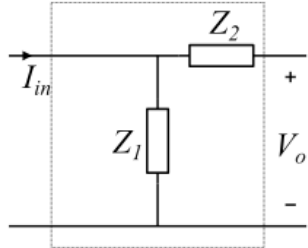
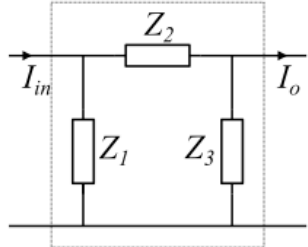
Input - Output	Network	Resonance Condition
$V - V$		$\frac{1}{Z_1} + \frac{1}{Z_2} + \frac{1}{Z_3} = 0$ <i>(i.e.)</i> $Y_1 + Y_2 + Y_3 = 0$ <u>Special cases :</u> a) $Z_1 + Z_2 = 0$ & $Z_3 = \infty$ b) $Z_1 = Z_2 = 0$
$V - C$		$Z_1 + Z_2 = 0$
$C - V$		$Z_1 + Z_2 = 0$
$C - C$		$Z_1 + Z_2 + Z_3 = 0$ <u>Special cases :</u> a) $Z_1 + Z_3 = 0$ & $Z_2 = 0$ b) $Z_1 = Z_3 = 0$

Figure 3.6: List of basic resonance-tanks and their resonance conditions

TABLE I. SUMMARY OF CONSTANT-VOLTAGE OUTPUT FROM A VOLTAGE SOURCE			TABLE II. SUMMARY OF CONSTANT-VOLTAGE OUTPUT FROM A CURRENT SOURCE			TABLE III. SUMMARY OF CONSTANT-CURRENT OUTPUT FROM A VOLTAGE SOURCE			TABLE IV. SUMMARY OF CONSTANT-CURRENT OUTPUT FROM A CURRENT SOURCE		
Number	Passive resonant network	Resonant frequency	Number	Passive resonant network	Resonant frequency	Number	Passive resonant network	Resonant frequency	Number	Passive resonant network	Resonant frequency
V-V-1		$\omega = \sqrt{\frac{1}{L_1 C} + \frac{1}{L_2 C}}$	C-V-1		$\omega = \sqrt{\frac{1}{LC}}$	V-C-1		$\omega = \sqrt{\frac{1}{LC}}$	C-C-1		$\omega = \sqrt{\frac{1}{L_1 C_1} + \frac{1}{L_2 C_2}}$
V-V-2		$\omega = \frac{1}{\sqrt{L C_1 + L C_2}}$	C-V-2		$\omega = \sqrt{\frac{1}{LC}}$	V-C-2		$\omega = \sqrt{\frac{1}{LC}}$	C-C-2		$\omega = \frac{1}{\sqrt{L C_1 + L C_2}}$
V-V-3		$\omega = \frac{1}{\sqrt{L C_1 + L C_2}}$				V-C-3		$\omega = \frac{1}{\sqrt{L C_1 + L C_2}}$	C-C-3		$\omega = \frac{1}{\sqrt{L C_1 + L C_2}}$
V-V-4		$\omega = \frac{1}{\sqrt{L C_1 + L C_2}}$				V-C-4		$\omega = \frac{1}{\sqrt{L C_1 + L C_2}}$	C-C-4		$\omega = \frac{1}{\sqrt{L C_1 + L C_2}}$
V-V-5		$\omega = \sqrt{\frac{1}{L_1 C} + \frac{1}{L_2 C}}$				V-C-5		$\omega = \sqrt{\frac{1}{L_1 C} + \frac{1}{L_2 C}}$	C-C-5		$\omega = \sqrt{\frac{1}{L_1 C} + \frac{1}{L_2 C}}$
V-V-6		$\omega = \sqrt{\frac{1}{L_1 C} + \frac{1}{L_2 C}}$				V-C-6		$\omega = \sqrt{\frac{1}{L_1 C} + \frac{1}{L_2 C}}$	C-C-6		$\omega = \sqrt{\frac{1}{L_1 C} + \frac{1}{L_2 C}}$
V-V-7		$\omega = \frac{1}{\sqrt{LC}}$				V-C-7		$\omega = \frac{1}{\sqrt{LC}}$	C-C-7		$\omega = \frac{1}{\sqrt{LC}}$
V-V-8		—				V-C-8		—	C-C-8		—

Figure 3.7: Detailed list of basic resonance-tanks and their resonance conditions [28]

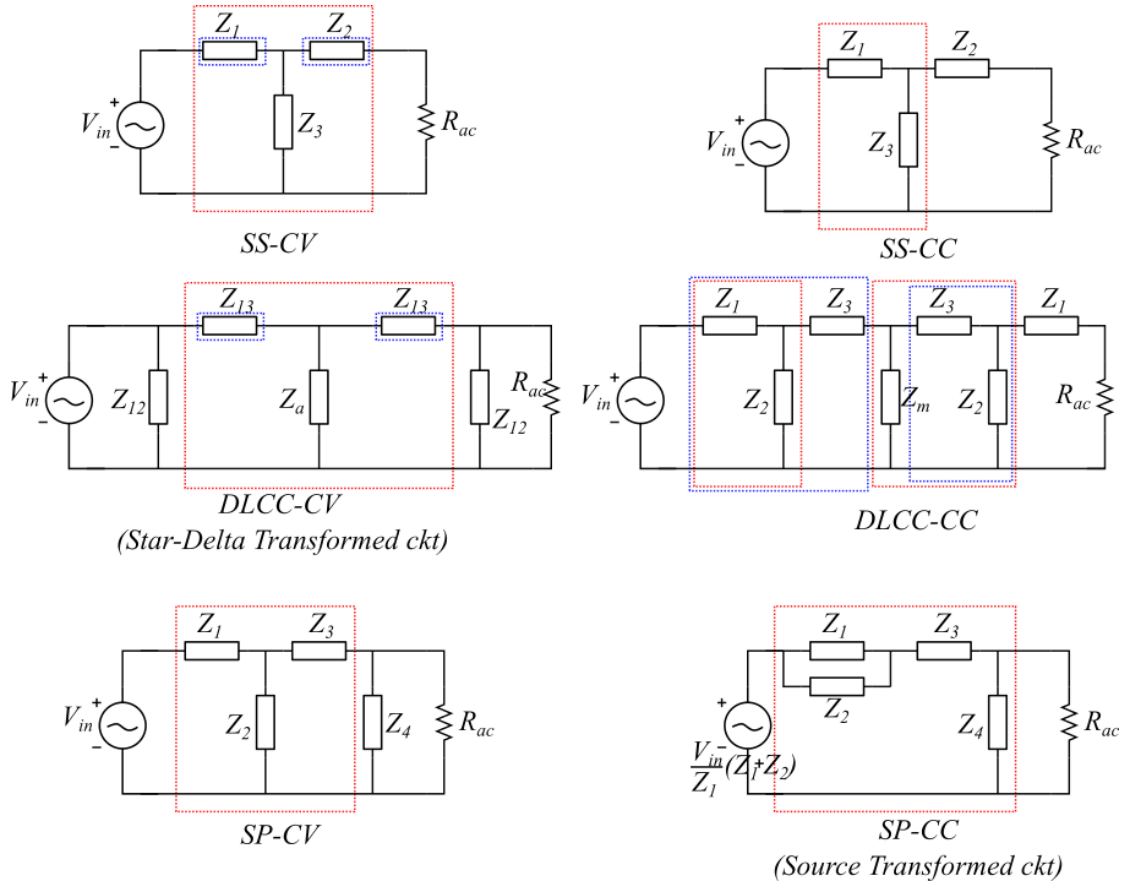


Figure 3.8: Representing different topologies using resonant tanks

The smallest possible network (with 3-components) for making V-V conversion (converting input voltage source to load independent voltage output) is a T-network which satisfies  $\frac{1}{Z_1} + \frac{1}{Z_2} + \frac{1}{Z_3} = 0$  (i.e  $Y_1 + Y_2 + Y_3 = 0$ ) where  $Z_i$  and  $Y_i$  represent component impedances and admittances respectively. Similarly, the smallest possible networks for V-C, C-V, and C-C conversions are reversed-

L, normal-L, and pi networks respectively, satisfying corresponding conditions as shown in Figure 3.6. [28] lists out elaborately all the possible smallest resonant tanks as shown in figure 3.7.

Any compensation network can be seen as a cascade of one or more such resonant tanks as shown in figure 3.8. Hence it reduces to solving a set of resonance conditions instead of solving complicated polynomial equations.

More than one solution can be possible, but all solutions may not satisfy ZPA. For example, in Figure 3.8, for SS-CV none of the two solutions satisfy ZPA, for DLCC-CV and DLCC-CC only the red-coloured box solution satisfies ZPA while blue one does not.

Sometimes bigger resonant tank solutions might be there (more than 3 components involved in resonance), which will not be included in our 2/3-component resonant tank solution adopted in this approach. It might be required to do some transformation to get those solutions before using this method. For example, in figure 3.8 in DLCC-CV a star-delta transformation of certain impedances is done, and in SP-CC a source transformation is required to arrive at the resonance condition.

Thus this is a good model, but does not give bigger resonant tank solutions directly. These can be found out only after doing some transformations. As per my knowledge, a general algorithm to know what transformation to do is not yet present. Finding such an algorithm can make this method more effective and general.

### Controlled-Source Model

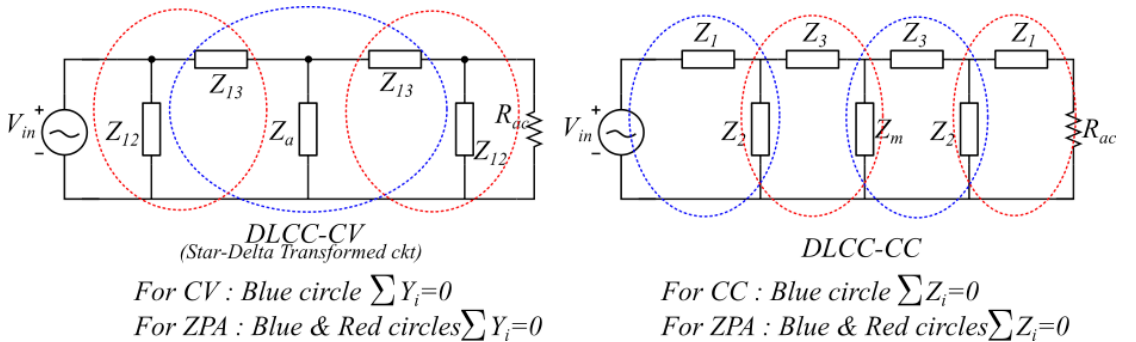


Figure 3.9: Visual representation of CC/CV and ZPA solutions with circles

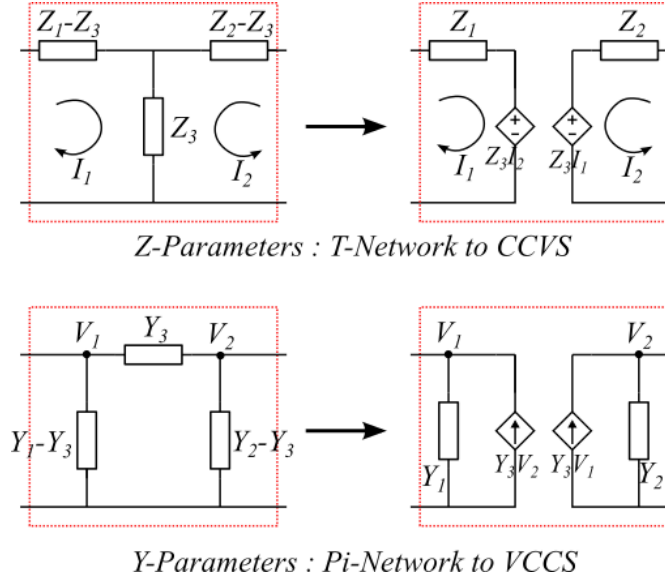


Figure 3.10: Modelling 2-port networks with impedance parameters as a Network or Controlled Source

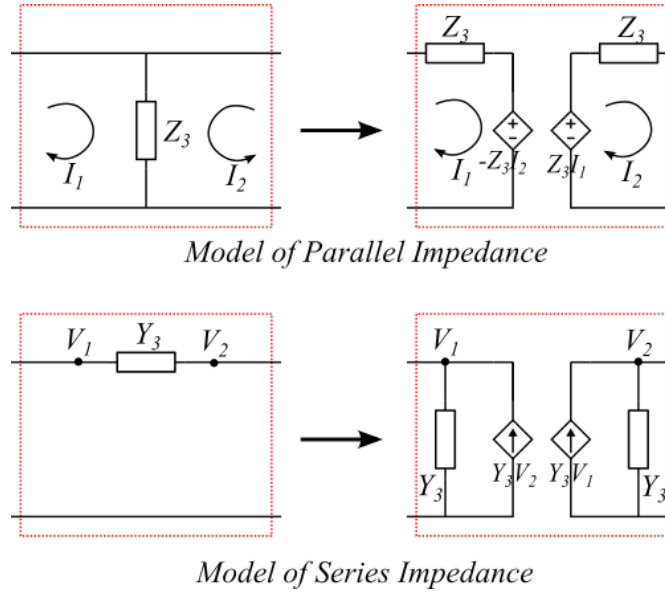


Figure 3.11: Representing different topologies using resonant tanks

Consider the DLCC topology. Conditions for CC with ZPA, and CV with ZPA are derived in [24] which can be simplified into resonant conditions and represented as shown in Fig.3.12 . The CC and CV conditions can be visually represented as the blue circles, and for ZPA both blue and red circles must be satisfied.

Trying to understand and explain this pattern is the motivation to develop the Controlled-Source Model (CSM). Though a rough idea of this model is present implicitly in transformer M-model and T-model, this model has not been directly used. For example, the work [24] uses this in some sense for arriving at CC mode resonant condition. But in some sense it gets equivalent to the gyrator model[21].

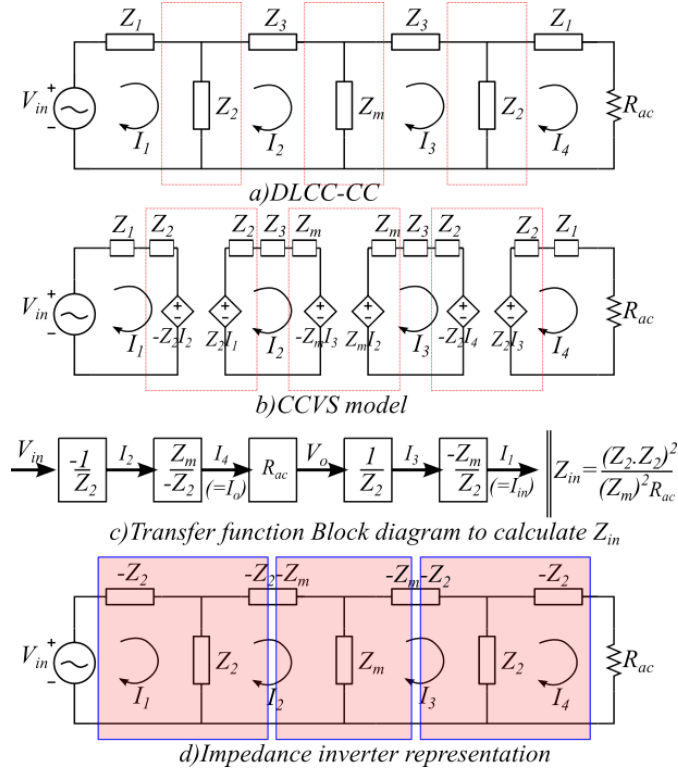


Figure 3.12: Modelling and Analysis of DLCC topology - CC mode

This model also helps in visualizing what happens to different current/voltage components in KVL/KCL equations, thus visually describes the equation.

To understand this model, first a recap 2-port parameters will be done.

A 2-port network can be modelled using impedance( $Z$ ) (or admittance( $Y$ )) parameters in 2 ways: a) T-network (or pi-network) b) CCVS (or VCCS) as shown in Figure 3.10 Using this we can model a T-network as a CCVS (and pi-network as a VCCS).

Simplifying this further by setting  $Z_1 = Z_2 = 0$  and  $Z_3 = Z$ , we can model a parallel-impedance as a CCVS (and a series-impedance as a VCCS) as shown in Figure 3.11.

This method of splitting down an impedance into CCVS/VCCS can help in understanding the reason behind the circle patterns: In DLCC-CC mode break the parallel-impedances  $Z_2$ ,  $Z_m$ ,  $Z_2$  into CCVS as in figure 3.12. By making  $Z_1 + Z_2 = 0$  and  $Z_m + Z_3 + Z_2 = 0$  (i.e first and third loops), the relations  $V_{in} = -I_2 Z_2$  and  $I_2 Z_m = -I_4 Z_2$  are obtained. This can be represented as a transfer function block diagram as shown in the same figure. Hence output current

$I_4 = \frac{Z_m}{Z_2^2} V_{in}$  is load-independent. Now, by making  $Z_2 + Z_3 + Z_m = 0$  and  $Z_2 + Z_1 = 0$  (i.e 2nd and 4th loops), one can obtain input current  $I_{in}$  as given by the transfer function block diagram. Thus  $Z_{in} = \frac{V_{in}}{I_{in}} = (\frac{Z_2 \cdot Z_2}{Z_m})^2 \cdot \frac{1}{R_{ac}} = -(\frac{X_2 \cdot X_2}{X_m})^2 \cdot \frac{1}{R_{ac}}$ , which is a real quantity, so ZPA is satisfied. A similar analysis can be done for DLCC-CV, SS and other topologies also.

Obtaining CC/CV condition is straight forward in this method. The ZPA condition holds here since we had cancelled all impedances and only CCVS remains, and if we transform the CCVS to T-network we get a impedance inverter which always satisfies ZPA which we will see in ZPA model. (It might be possible to understand ZPA using 2-port transfer-parameter-matrix(T) also like how they use in ZPA model ). This method essentially has broken a set of impedances and resonated a group of impedances. An algorithm has to be developed to know which components to break in-order to obtain our conditions. A deeper understanding and developing an algorithm(to avoid trial and error) can make this method more effective and general.

### Unified Model [13]

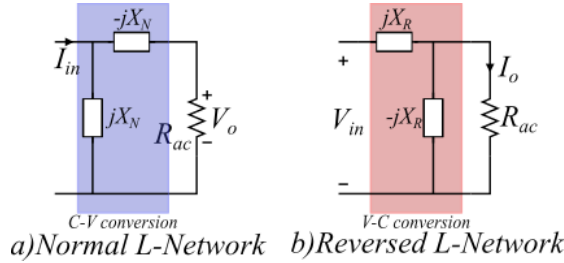


Figure 3.13: Normal and Reversed L-Networks

This is a refined version of the resonant-tank model, with C-V and V-C as the basic building blocks (Normal-L and Reversed-L networks), because even the V-V and C-C resonant-tanks can be seen as a cascade of V-C and C-V blocks.

The resonance condition for C-V and V-C is already known from resonant-tank model. Using this the simplified input impedance, and gains can be found out as given in table 3.1. Any compensation topology can be understood by splitting some of its impedances as a series/parallel combination of two impedances, and then grouping them into normal/reversed-L networks as shown in figure 3.14. At the resonant frequency  $\omega_{cc}$ , the impedances in normal-L (and reversed-

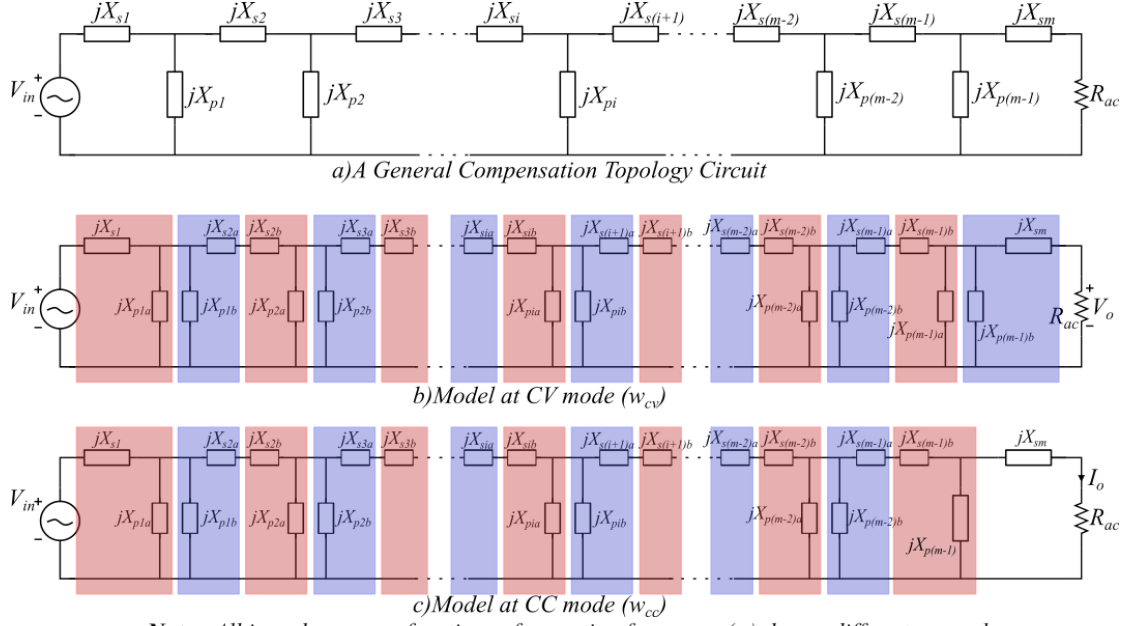


Figure 3.14: Modelling by breaking impedances and grouping into L-Networks to get CC and CV modes

	Normal L-Network	Reversed L-Network
Gain	$\frac{V_o}{I_{in}} = \frac{1}{jX_N}$	$\frac{I_o}{V_{in}} = \frac{1}{jX_R}$
$Z_{in}$	$\frac{jX_N \cdot (-jX_N + R_{ac})}{R_{ac}}$	$\frac{X_R^2}{R_{ac} - jX_R}$

Table 3.1: Simplified Gain and Input Impedance of L-Networks under resonance

L) network will be in resonance as given in table 3.2. Similar resonance condition can be obtained at  $w_{cv}$ . Note that  $X(w_{cc}) \neq X(w_{cv})$ , because last few resonance conditions are different for  $w_{cc}$  and  $w_{cv}$  in resonance condition. Thus CC and CV output is realized.

The gain at  $w_{cc}$  is simply the product of the gains of the cascaded resonant blocks as given in the table. Similarly in  $w_{cv}$  also.

By assuming resonant conditions are satisfied, the simplified input impedance can be found which can be derived by considering one T-block at a time and proceeding iteratively (Here T-block means a group of Normal and Reversed L networks as suggested by figure 3.15). ZPA condition is  $Im\{Z_{in}\} = 0$ , hence only real part will remain. The ZPA condition can be visualised as in figure 3.15.

The CC/CV resonance conditions and corresponding ZPA conditions can be converted in terms of actual impedances as shown for SS topology in figure 3.16.

The conditions given by this method are verified to be the same as the condi-



	CC mode equations(at $w = w_{cc}$ )	CV mode equations(at $w = w_{cv}$ )
Resonance Condition	$ \begin{aligned} X_{s1}(w_{cc}) &= -X_{p1a}(w_{cc}) = X_{R1C} \\ X_{p1b}(w_{cc}) &= -X_{s2a}(w_{cc}) = X_{N1C} \\ &\dots \\ X_{s(m-1)b}(w_{cc}) &= -X_{p(m-1)a}(w_{cc}) = X_{R(m-1)C} \\ -X_{p(m-1)b}(w_{cc}) &= X_{R(m-1)C} \end{aligned} $	$ \begin{aligned} X_{s1}(w_{cv}) &= -X_{p1a}(w_{cv}) = X_{R1V} \\ X_{p1b}(w_{cv}) &= -X_{s2a}(w_{cv}) = X_{N1V} \\ &\dots \\ X_{s(m-1)b}(w_{cv}) &= -X_{p(m-1)a}(w_{cv}) = X_{R(m-1)V} \\ X_{p(m-1)b}(w_{cv}) &= -X_{sm}(w_{cv}) = X_{N(m-1)V} \end{aligned} $
Gain (provided resonance conditions satisfied)	$G_{cc} = \frac{I_o}{V_{in}} = \frac{\prod_{i=1}^{m-2} X_{NiC}}{j \prod_{i=1}^{m-1} X_{RiC}}$	$G_{cv} = \frac{V_o}{I_{in}} = \frac{\prod_{i=1}^{m-1} X_{NiV}}{j \prod_{i=1}^{m-1} X_{RiV}}$
ZPA condition (provided resonance conditions satisfied)	$ \begin{aligned} &\sum_{i=1}^{m-2} \left( \prod_{x=1}^{i-1} -X_{Nx_C}^2 \right) (-X_{RiC} + X_{NiC}) \left( \prod_{x=i+1}^{m-1} -X_{Rx_C}^2 \right) \\ &(-X_{R(m-1)C} + X_{SmC}) \left( \prod_{i=1}^{m-2} -X_{NiC}^2 \right) = 0 \end{aligned} $	$ \begin{aligned} &\sum_{i=1}^{m-2} \left( \prod_{x=1}^{i-1} -X_{Nx_V}^2 \right) (-X_{RiV} + X_{NiV}) \left( \prod_{x=i+1}^{m-1} -X_{Rx_V}^2 \right) \\ &X_{NiV} \left( \prod_{x=i+1}^{m-1} -X_{Rx_V}^2 \right) = 0 \end{aligned} $
Input Impedance (provided resonance conditions satisfied)	$Z_{inCC} = \frac{1}{R_{ac} G_{cc} ^2}$	$Z_{inCV} = \frac{R_{ac}}{ G_{cv} ^2}$

Table 3.2: Equations in Unified Model

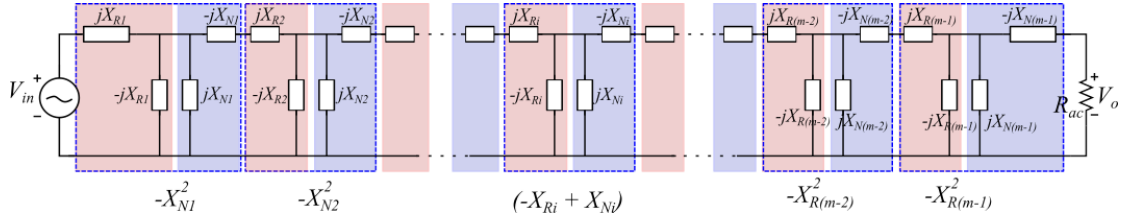


Figure 3.15: A visual representation of ZPA condition in CV mode (similar for CC mode also)

tions given by [28](SP topology) and [24] (DLCC topology) which are mentioned in figure 3.8.

Thus this method gives a unified approach with a proper algorithm for any compensation topology. Converting these equations in terms of actual impedances is sometimes tedious, but the design procedure suggested in [13] has no need for the converted equations, hence this is not a problem. This model gives a unified ZPA equation unlike the previous two models, but this equation is a bit lengthy

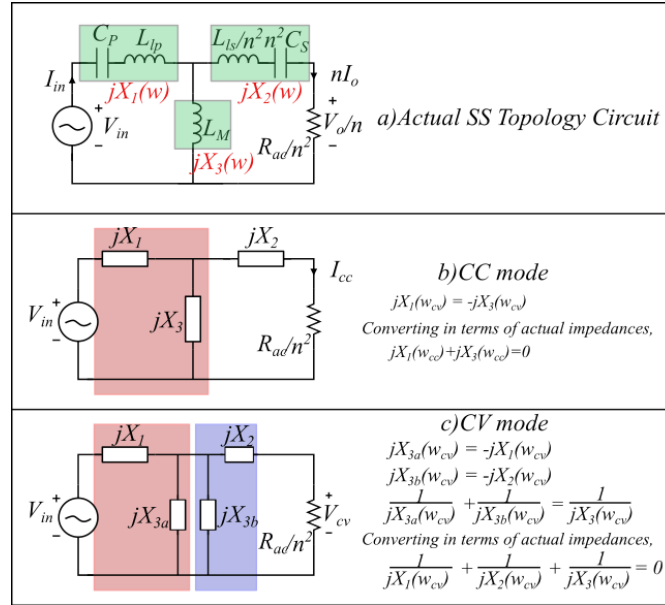


Figure 3.16: Using Unified Model in SS topology to get resonance conditions in terms of original impedances

to simplify and solve, which is one drawback still. A question exists if this method can give all possible solutions (CC,CV, with ZPA ) for any topology, though it does give all solutions for SS,SP, DLCC topologies.

### ZPA Model [16]

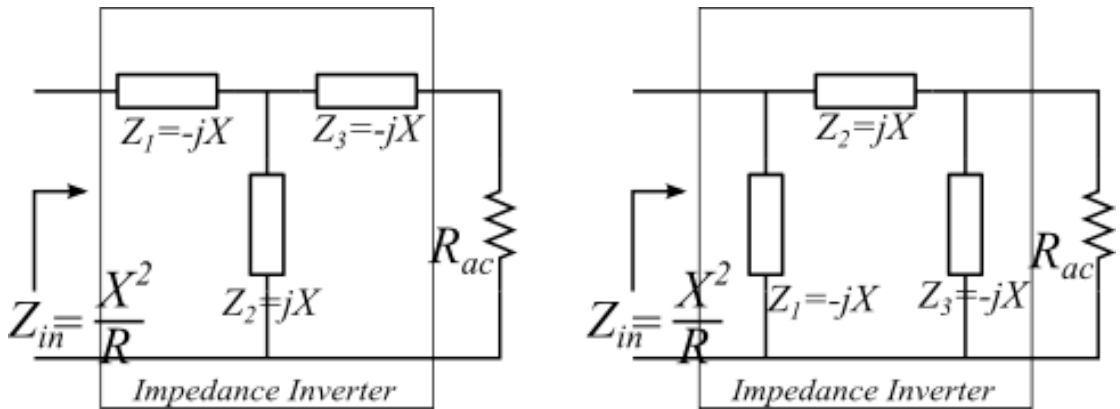


Figure 3.17: Impedance Inverter Circuits

This is a different kind of model, where components are grouped to ensure ZPA conditions. CC/CV conditions are obtained by some calculations.

Consider a T-network made of purely reactive impedances with a resistive load. If and only if  $Z_1 = -Z_2 = Z_3$  (figure 3.17) it will have a purely resistive input impedance  $Z_{in}$  which can be mathematically proved.  $Z_{in} = -\frac{Z_2^2}{R_{ac}} = \frac{X_2^2}{R_{ac}}$  (where

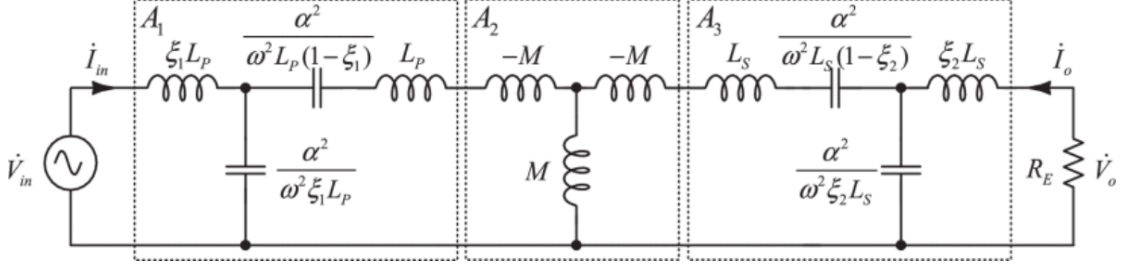


Figure 3.18: ZPA block modelling of DLCC topology [16]

$Z_2 = jX_2$ ), so it is called an impedance inverter since  $R_{ac}$  appears inverted in  $Z_{in}$  [8]. We can see that in SS topology this condition holds in CC mode and not in CV mode, hence only CC mode has ZPA.

Bigger topologies can be modelled as a cascade of such T-networks. Ensuring  $Z_1 = -Z_2 = Z_3$  for each network will ensure ZPA. CC and CV conditions have to be obtained using previous three models or calculate mathematically. Qu *et al.*[16] got the CC mode condition for DLCC topology with Resonant-Tank model. Then he expresses all components in terms of just 2 parameters (by eliminating other variables using ZPA and CC equations) and mathematically calculates CV condition (using 2-port transfer function parameter matrix)

### Summary of the models

Four models have been discussed. It would be good to develop an intuitive model combining ZPA and CC/CV models to get a deeper understanding of its working and to simplify calculations. The following table summarizes the models discussed.

### 3.3.2 Zero Phase Angle (ZPA)

It means making the input phase angle  $\theta_{in}$  zero (angle between input voltage and current), i.e making input impedance  $Z_{in}$  purely real by cancelling out the reactive portion by resonance. Mathematically  $Im\{Z_{in}\} = 0$ . This might occur in more than one frequency (i.e many solutions might be possible). This leads to the bifurcation phenomenon which will be explained later.

Mathematically, Active power provided by the source every cycle is  $P_{in} =$

Model	Description
General Condition	Express as thevenin or norton equivalent and $Z_{eq}$ is made 0 or $\infty$ for CV/CC. For ZPA solve $Im\{Z_{in}\} = 0$
Resonant-Tank Model	Bigger circuits are modelled as cascade of small resonant tanks for CV/CC. ZPA has to be mathematically calculated
Controlled-Source Model	Certain impedances are modelled as controlled sources and a group of impedances are nullified(resonated) for CV/CC. If all impedances are nullified ZPA surely occurs(by ZPA model), else need to calculate mathematically
Unified Model	Big compensation topologies are modelled as cascade of L-networks by splitting certain impedances to satisfy CV/CC. A general mathematical equation is derived for ZPA
ZPA model	Here CV/CC condition has to be mathematically calculated or by previous models. ZPA is ensured by modelling the topology as a cascade of impedance inverters

Table 3.3: Summary of Compensation Topology Models

$V_{in} \cdot I_{in} \cdot \cos(\theta_{in})$ ;  $V_{in}$ ,  $I_{in}$  are rms values,  $P_{in}$  is maximum when  $\theta_{in} = 0$ . By ensuring ZPA, we can use a lower supply rating to give the required active power to load. In other words, input provides maximum active power when operated at ZPA.

Conceptually, a part of input power is utilized in increasing the potential energy of reactive elements(say for establishing magnetic field of inductor). This energy returns back to source. Thus the source needs to pump in more than the required active power required by the load. By ensuring ZPA, the resonance takes care of it, i.e this to and fro motion of power happens within the reactive components, such that their potential energy is constant, so source and load are not affected at steady state as shown in the figure.

### 3.3.3 Zero Voltage Switching (ZVS)

Making input impedance( $Z_{in}$ ) slightly inductive can result in ZVS of the switching device during TURN ON, thus reducing switching losses[4]. Once we complete our design for ZPA in CC and CV modes, ZVS can be achieved through a small change through a) Parameter tuning [16] where we change a component value slightly, b)Frequency tuning[24] where we operate at a slightly higher or lower frequency

than the ZPA frequency ( $f_{cc}$  or  $f_{cv}$ ). A sensitivity analysis has to be done to see how the introduction of this small change impacts the gain, etc. for different loads in both CC and CV modes[16].

### 3.3.4 Bifurcation

We saw that ZPA condition is  $Im\{Z_{in}\} = 0$ . We'll get a polynomial in  $\omega$ , which may have many solutions. [25,26] give some mathematical tools and conditions for analysing bifurcation in basic compensation topologies. If we plan to use a simple control system and somehow if our system goes to another ZPA operating point it might be problematic. So we can a)Design to have only one ZPA (or) b)Ensure that undesirable instabilities don't occur. In our design we will need ZPA at two frequencies(at  $f_{cc}$  and  $f_{cv}$ ) for the CC and CV modes, hence we need to ensure large-signal instabilities don't occur

### 3.3.5 Frequency-splitting

[19] explains that there will be two peaks in the power curve above a certain coupling( $k$ ) using an analogy of two pendulums connected with a spring. [12] says that if our control system is not proper these peaks can cause a damage due to high power transfer.

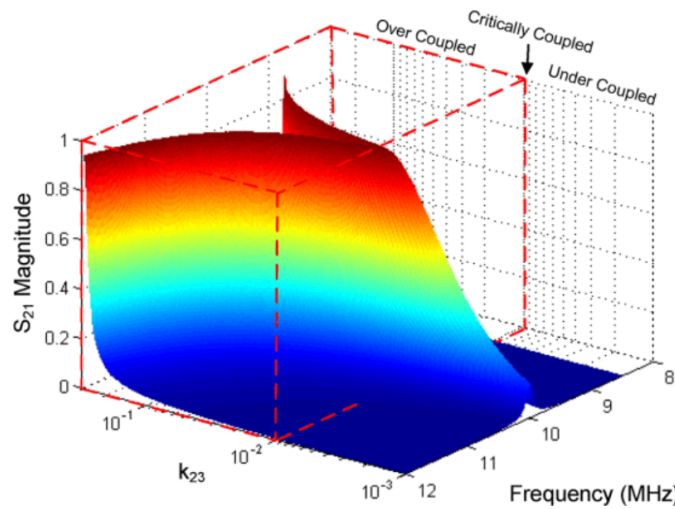


Figure 3.19: Plot by [19] depicting frequency splitting with coupling coefficient( $k$ )

### 3.3.6 Filtering action

Usually the filtering takes place implicitly and First Harmonic Approximation[FHA] is valid, which we had assumed while modelling the input and output ports of compensation topology.

A proper mathematical way of analysing harmonics' attenuation would be to find input impedance( $Z_{in}(\omega)$ ) and output impedance( $Z_{out}(\omega)$ , which is same as thevenin impedance) as suggested in [4]. From their bode plots we'll notice a high-Q peak at the resonance point. But finding  $Z_{in}(\omega)$  and plotting by hand will be difficult for higher order topologies. Some have done deeper analysis , for example [11] considers effect of harmonics on ZVS switching.

### 3.3.7 High circulating currents/voltage stresses

In some topologies, high circulating currents or high voltages are observed across passive elements and switches. For example [18] reports high voltage stress in primary side coil and capacitor of SS topology, and higher circulating current in primary side of PS topology (figure 3.20 ). This impacts in the following ways:

- (a) **Device Stress:** Device stress will be more, so higher rated devices have to be used
- (b) **Size:** If our topology has an inductor, core size will increase for carrying higher currents, hence it will become bulky.
- (c) **Efficiency:** Due to higher rated switches, their on-state resistance will be more and hence higher conduction losses. Due to high currents, the  $I^2R$  conduction losses of inductors and coil will be high. Thus high circulating currents is probably the major cause of efficiency degradation by conduction loss

**Zero coupling allowance:** This is a special case where coupling coefficient  $k=0$  (i.e no EV is there to receive power). For example, in SS topology,  $k=0$  causes a short circuit of the input source causing huge primary circulating currents(because  $k = 0 \Rightarrow L_M = 0$ , and  $L_{lp}$  and  $C_p$  impedances are nullified at resonance). Hence control-system has to keep track if receiver(vehicle) is present or not, and open circuit the inverter switches if there is no receiver.

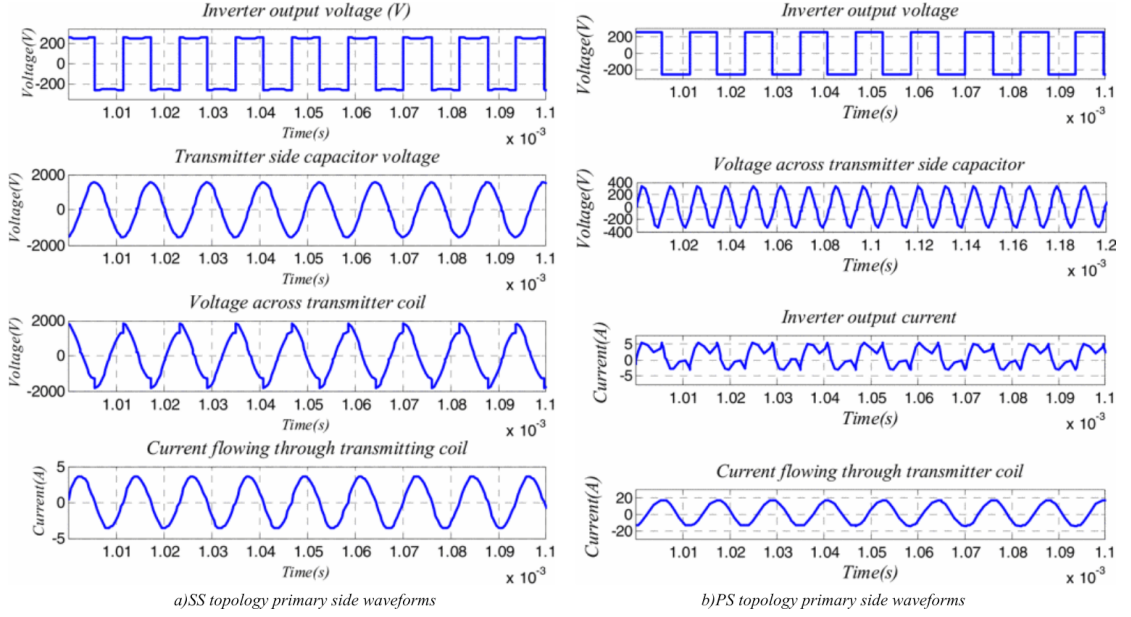


Figure 3.20: Stress on Primary side components of SS and PS topologies in design by [18]

Erickson and Maksimovic[4] discuss a method to understand this for resonant DC-DC converters. For Zero/light load and no load conditions (i.e  $R_{bat} = 0$  and  $R_{bat} = \infty$ ), plot bode plots of input impedance  $Z_{in}$  and observe at our operating frequency. Using mathematical theorems he stated that the curve for any  $R_{ac} = (0, \infty)$  will lie between above two curves, thus we can get an idea of upper and lower limit of the circulating currents by plotting for just  $R_{ac} = 0$  and  $R_{ac} = \infty$ . This method of drawing hand-bode plots may not be that simple in bigger topologies.

### 3.3.8 Efficiency

We're talking about efficiency of compensation network, hence only conduction losses are here. The losses of a compensation topology arise due to ESR of inductors and coil. High circulating currents is a factor as we saw already. There may be other factors which I haven't come across. Zhang *et al.*[29] try a mathematical approach to choose components to achieve maximum efficiency for basic topologies(SS,SP,PS,PP) and proves that only secondary side affects efficiency in these basic topologies, and only by optimizing the secondary capacitance the conduction losses can be minimized.

### 3.3.9 Parameter Variation(PV) and misalignment tolerance

The coupling constant( $k$ ) is variable, and hence Mutual and leakage inductances ( $M, L_{lp}, L_{ls}$ ) are also variable. This is especially true in Dynamic WPT (DWPT) applications. Sensitivity analysis must be done to understand its impact on gain,  $z_{in}$ , efficiency, etc. For example, in SS topology CV mode,  $w_{cv} = \frac{1}{\sqrt{L_{lp} \cdot C_p}}$ , hence if coupling varies then our output voltage won't be load-independent. But SS topology CC mode doesn't get affected since  $w_{cc} = \frac{1}{\sqrt{L_p \cdot C_p}}$ . For SP topology, ZPA condition depends on coupling( $k$ ), and in PS & PP topologies, ZPA condition depends on both coupling( $k$ ) and load( $R_{bat}$ ) (This is because in basic topologies  $C_p$  is usually set in-order to satisfy ZPA, and  $C_p$  is a function of  $k$  in SP, function on  $k$  &  $R_{load}$  in PS and PP)[20].

### 3.3.10 Maximum Power Transfer(MPT)

This is a separate application in itself and different works have been done by researchers. Sample *et al.*[19] has worked on maximizing and delivering a constant power to secondary, inspite of misalignments and large distances. This will be useful in Dynamic WPT applications, wireless laptop charging, etc. For analysis purposes, the scattering matrix parameter  $S_{21}$  is used, which is a measure of power transferred from the source(in primary side) to the load(in secondary side) through the coupling coil.  $S_{21}$  can be related with the voltage gain of the 2-port. Experimentally,  $S_{21}$  can be found using a Vector Network Analyzer (VNA). They show that above a certain coupling( $k$ ) it is possible to provide a maximum and constant coupling-independent power by frequency tuning control.

Koh *et al.*[8] presents a work on impedance matching for maximum power transfer and a strategy to distribute source power to several receivers in required ratio. This is useful in multi-receiver applications where a single charger(primary side) charges more than one EV.

In our application we need CC-CV and ZPA which is done by fixing the frequency at  $f_{cc}$  and  $f_{cv}$ , hence above approaches can't be used directly. But it might be possible to integrate these understandings into our system in some other



manner, which will require a deeper understanding.

### 3.3.11 Others: Size, Bidirectional power flow

To overcome shortcomings of the basic topologies (SS,SP,PS,PP), larger topologies are used as described in next section. But using more components will increase the size of the system (especially topologies consisting many inductors) which is not beneficial for EVs. There are other features of interest like bidirectional power-flow/V2G (Vehicle-to-Grid), etc.

## 3.4 Summary of basic topologies

Our design procedure equations will be mainly based on CC/CV, ZPA and ZVS. The basic topologies(SS,SP,PS,PP) cannot satisfy CC & CV along with ZPA in both modes (CC and CV) simultaneously as shown in figure 3.21. Hence we have to go for bigger topologies. S-SP topology is the smallest one which can satisfy all these requirements, hence we will try implementing this, closely following [14].

Topology	Possible mode charge to implement	ZPA	Angular Resonant Frequency
SS	CC	Yes	$\omega = \frac{1}{\sqrt{L_1 C_p}} = \frac{1}{\sqrt{L_2 C_s}}$
	CV	No	$\omega = \frac{1}{\sqrt{L_p C_p}} = \frac{1}{\sqrt{L_s C_s}}$
SP	CC	No	$\omega = \frac{1}{\sqrt{L_p C_p}} = \frac{1}{\sqrt{L_s C_s}}$
	CV	Yes	$\omega = \frac{1}{\sqrt{1-k^2} \sqrt{L_p C_p}} = \frac{1}{\sqrt{L_2 C_s}}$
PS	CV	Yes	$\omega = \frac{1}{\sqrt{L_1 C_p}} = \frac{1}{\sqrt{L_2 C_s}}$ and $L_x = L_1$
PP	CC	Yes	$\omega = \frac{1}{\sqrt{1-k^2} \sqrt{L_1 C_p}} = \frac{1}{\sqrt{L_2 C_s}}$ and $L_x = (1-k^2)L_1$

Figure 3.21: Comparison of basic topologies in terms of CC/CV and ZPA by [24]

## CHAPTER 4

### STEADY STATE ANALYSIS AND DESIGN OF S-SP TOPOLOGY

We have already discussed steady state modelling techniques in **chapter 3** (Input and output port model and Compensation topology models). This chapter will explain the Steady state analysis and design of S-SP topology and output filter.

#### 4.1 Choosing the topology

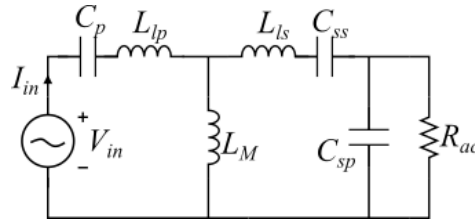


Figure 4.1: S-SP Topology

- The basic topologies cannot satisfy all the four conditions (CC,CV,ZPA at CC, ZPA at CV). So we need to have some extra degree of freedom to achieve all four conditions. This is done by adding extra components.

- The smallest topology which can satisfy all the four conditions is S-SP topology[14]. Hence we are choosing this. A S-SP topology consists of a series capacitance in primary side, and a series and a parallel capacitance in the secondary side as shown in the figure.

- So the secondary parallel capacitor( $C_{sp}$ ) will be connected to rectifier. Hence an LC filter must be used[15] , because using a C-filter will cause high currents in  $C_{sp}$  capacitor.

## 4.2 Steady State Requirements (design objective)

The following are our requirements:

Battery:  $V_{bat,cv} = 270V$ ;  $I_{bat,cc} = 12.22A$ ; ( $P = 3.3kW$ )

Frequency:  $f_{cc}, f_{cv}$  must be in  $81.38kHz - 90kHz$  range (SAE J2954 Standard)

Input DC-Bus: Let  $V_{dc}$  be around  $250V$

From this the compensation topology requirements can be decided. After deciding the topology the filter specifications also can be decided.

### Compensation Topology Requirements

1. Gain requirement

$$CC : \frac{I_{bat}}{V_{dc}} = \frac{2\sqrt{2}}{\pi} \cdot G_{cc} \cdot \frac{\pi}{2\sqrt{2}} \implies \frac{12.22}{250} = G_{cc} \implies G_{cc} = 0.0488$$

$$CV : \frac{V_{bat}}{V_{dc}} = \frac{2\sqrt{2}}{\pi} \cdot G_{cv} \cdot \frac{2\sqrt{2}}{\pi} \implies \frac{270}{250} = \frac{8}{\pi^2} G_{cv} \implies G_{cv} = 1.3324$$

2. CC and CV modes : Will be handled in next section

3. ZPA condition : Will be handled in next section

### Filter Requirements

1. Choice of filter:

- It has to be an LC filter.
- This is because if we use a C-filter, the voltage at rectifier output will be almost a DC(ripples will be too small). So the waveform at rectifier input( $V_o$ ) will be a square wave which is also the voltage across capacitor  $C_{sp}$ . So  $V_o$  being a square wave has high frequency harmonic content(3rd,5th,etc.).  $C_{sp}$  impedance is low for high frequencies, so these harmonic voltages will cause high frequency currents through  $C_{cp}$  which will cause high losses due to ESR of capacitor. Instead if we use LC filter, only the current  $I_o$  will be a square wave which is not a problem(it will be a problem in topologies like SS,PS because they end with an inductor).

2. Cut-off frequency of filter:

- The compensation topology output waveform lies in  $81.38kHz - 90kHz$

- So we should choose the cut-off as  $\frac{1}{\sqrt{L_f C_f}} < 80kHz$  or  $502.65krad/sec$  to block the AC components and only pass the DC.
- So we can take  $L_f = 250\mu H$ ;  $C_f = 400nF$  which is around  $1/25^{th}$  of cut-off frequency

### 4.3 Steady State Model equations of S-SP topology

The S-SP topology is modelled using unified model[13] mentioned in Chapter 3 .The model for CC and CV modes is shown in 4.2.

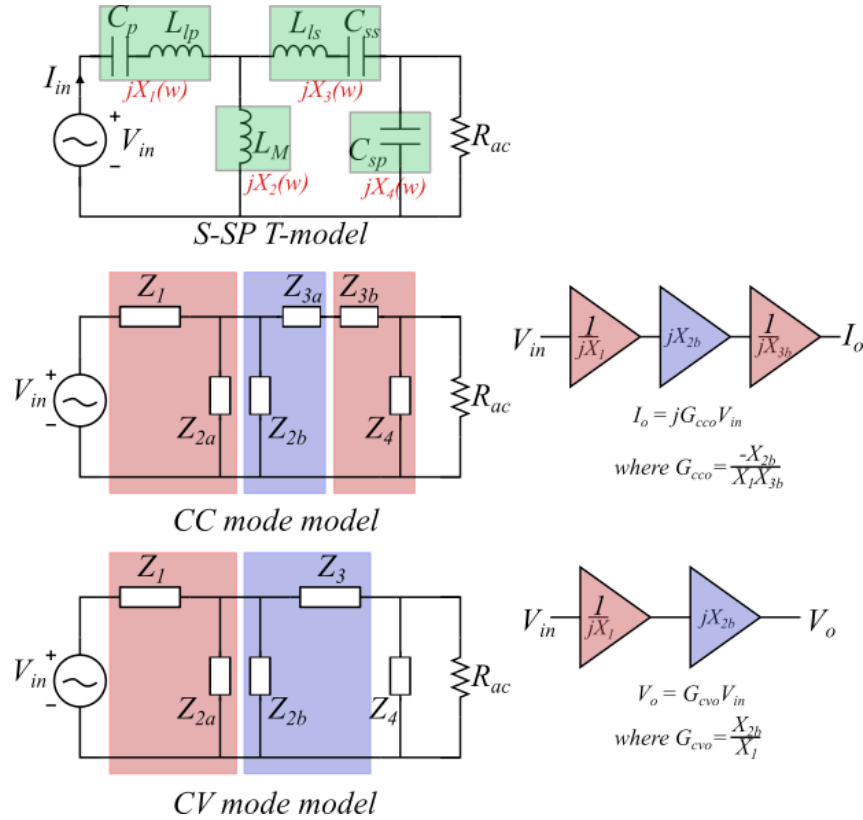


Figure 4.2: S-SP topology Unified Model

The table below lists down all steady-state equations of S-SP topology. The meaning of these equations is described shortly below:

1. First, the components are represented as  $Z_1, Z_2, Z_3, Z_4$  for simplicity in notation. This i'm calling as Basic equations.
2. Second, the actual impedances are transformed(broken down) to get the unified model.

3. Third, the resonant conditions required to achieve CC/CV (load-independent output) is mentioned
4. Fourth, the gains in CC/CV modes are given which are valid when CC/CV resonance is present.
5. Fifth, the ZPA conditions for CC/CV modes are given which are valid when CC/CV resonance is present.

CC mode	CV mode
1) Basic Equations	
$Z_1(w_{cc}) = jX_1 = j \left( w_{cc}L_{lp} - \frac{1}{w_{cc}C_p} \right)$ $Z_2(w_{cc}) = jX_2 = j(w_{cc}M)$ $Z_3(w_{cc}) = jX_3 = j \left( w_{cc}L_{ls} - \frac{1}{w_{cc}C_{ss}} \right)$ $Z_4(w_{cc}) = jX_4 = j \left( -\frac{1}{w_{cc}C_{sp}} \right)$	$Z_1(w_{cv}) = jX'_1 = j \left( w_{cv}L_{lp} - \frac{1}{w_{cv}C_p} \right)$ $Z_2(w_{cv}) = jX'_2 = j(w_{cv}M)$ $Z_3(w_{cv}) = jX'_3 = j \left( w_{cv}L_{ls} - \frac{1}{w_{cv}C_{ss}} \right)$ $Z_4(w_{cv}) = jX'_4 = j \left( -\frac{1}{w_{cv}C_{sp}} \right)$
2) Transform Equations (to transform to unified model)	
$\frac{X_{2a}X_{2b}}{X_{2a} + X_{2b}} = X_2; X_2 \rightarrow X_{2a}, X_{2b}$ $X_{3a} + X_{3b} = X_3; X_3 \rightarrow X_{3a}, X_{3b}$	$\frac{X'_{2a}X'_{2b}}{X'_{2a} + X'_{2b}} = X'_2; X'_2 \rightarrow X'_{2a}, X'_{2b}$
3) CC/CV Resonant equations	
$X_1 = -X_{2a}$ $X_{2b} = -X_{3a}$ $X_{3b} = -X_4$	$X'_1 = -X'_{2a}$ $X'_{2b} = -X'_3$
4) Gain equation	
$G_{cc} = \frac{-X_{2b}}{X_1X_{3b}}$	$G_{cv} = \frac{X'_{2b}}{X'_1}$
5) ZPA equation	
$X_{2b}X_{3a} + (X_{2a} + X_{2b})X_{3b} = 0$	$X'_{2b}X'_3 + (X'_{2a} + X'_{2b})X'_4 = 0$

Table 4.1: Unified model Steady-State Equations of S-SP topology

They above equations be also expressed in terms of actual impedances  $Z_1$  to  $Z_4$  as shown in table below. This is explained in detail in Appendix-I.

$CC : \frac{1}{X_1} + \frac{1}{X_2} + \frac{1}{X_3 + X_4} = 0$	$CV : \frac{1}{X'_1} + \frac{1}{X'_2} + \frac{1}{X'_3} = 0$
$ZPA_{CC} : X_2 + X_3 = 0$	$ZPA_{CV} : X'_2 + X'_3 + X'_4 = 0$

Table 4.2: Steady-State actual Steady-State Equations of S-SP Topology

## 4.4 Simplified Equations:

The equations above can be simplified further. In the design procedure, first we're fixing  $C_{sp}$  and  $f_{cv}$  as will be explained in next section. So we know  $X'_4$ .

### 4.4.1 CV mode

In CV mode, using the CC/CV resonant equations, Gain eqn and ZPA eqn given in the table, it is possible to find the *ratio of the variables* as shown below since we have 5 variables and 4 equations. (for fast calculation, you can substitute  $X'_1 = 1$  and calculate other terms to get the ratio easily)

$$\begin{aligned} X'_1 : X'_{2a} : X'_{2b} : X'_3 : X'_4 &= 1 : -1 : G_{cv} : -G_{cv} : \frac{-G_{cv}^2}{1 - G_{cv}} \\ \Rightarrow X'_1 : X'_2 : X'_3 : X'_4 &= 1 : \frac{G_{cv}}{1 - G_{cv}} : -G_{cv} : \frac{-G_{cv}^2}{1 - G_{cv}} \\ \Rightarrow X'_1 : X'_2 : X'_3 : X'_4 &= \frac{1 - G_{cv}}{-G_{cv}^2} : \frac{1}{-G_{cv}} : \frac{1 - G_{cv}}{G_{cv}} : 1 \end{aligned}$$

So now, if we know  $X'_4$  we can find out all other impedances in CV mode using the above ratio. Now we know  $M$  and  $C_{sp}$  (Since we know  $X'_2, X'_4, f_{cv} \Rightarrow M = \frac{1}{G_{cv} w_{cv}^2 C_{sp}}$ ).

### 4.4.2 CC mode

We know  $M$  and  $C_{sp}$ . We need to find  $f_{cc}$  and other component values.

- First,  $X_2 = w_{cc}M$ ;  $X_4 = -1/w_{cc}C_{sp}$  (still we dont know  $w_{cc}$  though)
- Find other impedances in terms of  $X_2, X_4$  using all CC mode equations.  
We'll get  $X_1 = \frac{(X_2 - X_4)}{(G_{cc} * X_4)}$ ;  $X_3 = -X_2$ ;
- We'll also get  $G_{cc} = 1/X_2 = 1/w_{cc}M$ . In CV mode we had found  $M$  in terms of  $C_{sp}$ , so we can rewrite as:  $w_{cc} = \frac{G_{cv} w_{cv}^2 C_{sp}}{G_{cc}}$ .
- Note that  $w_{cc} \propto C_{sp}$  so by incrementing  $C_{sp}$  we can increment  $f_{cc}$  to fix at some value above  $81.38kHz$

### 4.4.3 Components Calculation:

We know  $f_{cc}, f_{cv}, C_{sp}, M$ . We also need to find out  $L_p, L_s, C_p, C_{ss}$  using  $X_1, X_2, X_3, X_4, X'_1, X'_2, X'_3, X'_4$ .

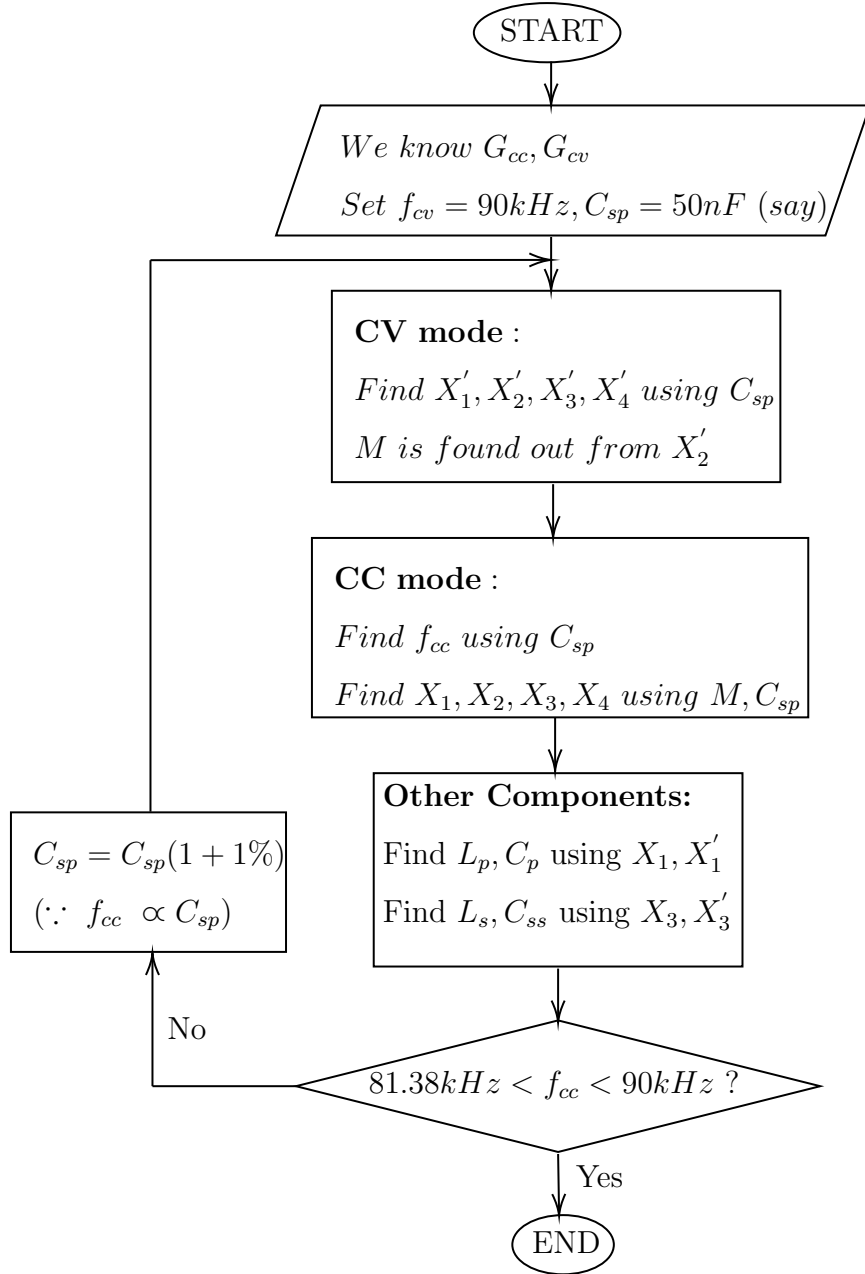
We'll get linear equations basic equations mentioned in table, which can be solved to get  $L_p, L_s, C_p, C_{ss}$

$$\begin{aligned}
\bullet \quad X_1 &= \left( w_{cc} L_{lp} - \frac{1}{w_{cc} C_p} \right); X'_1 = \left( w_{cv} L_{lp} - \frac{1}{w_{cv} C_p} \right) \\
&\implies L_p = M + \frac{w_{cv} X'_1 - w_{cc} X_1}{w_{cv}^2 - w_{cc}^2}; C_p = \frac{w_{cv}^2 - w_{cc}^2}{(w_{cc} X'_1 - w_{cv} X_1) w_{cv} w_{cc}} \\
\bullet \quad X_3 &= \left( w_{cc} L_{ls} - \frac{1}{w_{cc} C_{ss}} \right); X'_3 = \left( w_{cv} L_{ls} - \frac{1}{w_{cv} C_{ss}} \right) \\
&\implies L_s = M + \frac{w_{cv} X'_3 - w_{cc} X_3}{w_{cv}^2 - w_{cc}^2}; C_{ss} = \frac{w_{cv}^2 - w_{cc}^2}{(w_{cc} X'_3 - w_{cv} X_3) w_{cv} w_{cc}}
\end{aligned}$$

## 4.5 Design Procedure of Compensation Topology

The below design procedure as suggested by [14] can be used to set the component values of S-SP topology. The equations discussed in previous section are directly used here.

We are setting some values for  $f_{cv}$  and  $C_{sp}$  initially and finding out if  $f_{cc}$  is in the required range for satisfying the SAE standards. If not, we're incrementing  $C_{sp}$  and iterating the procedure. Finally we should also check if the component values are reasonable.



This will achieve CC/CV and ZPA .This is confirmed by  $Z_{th}$  and  $\theta_{in}$  plots in 4.3. Note that there are other solutions for CC and CV conditions, but they don't satisfy ZPA condition.

For ZVS we can increment  $f_{cc}$  and decrement  $f_{cv}$  by say 1-2% to make  $Z_{in}$  slightly inductive as indicated by 4.3. So we have set  $f_{cc} = 83kHz, f_{cv} = 88kHz$ . Now it wont satisfy CC/CV properly and the gains will change slightly, but the control system will take care of that small change.



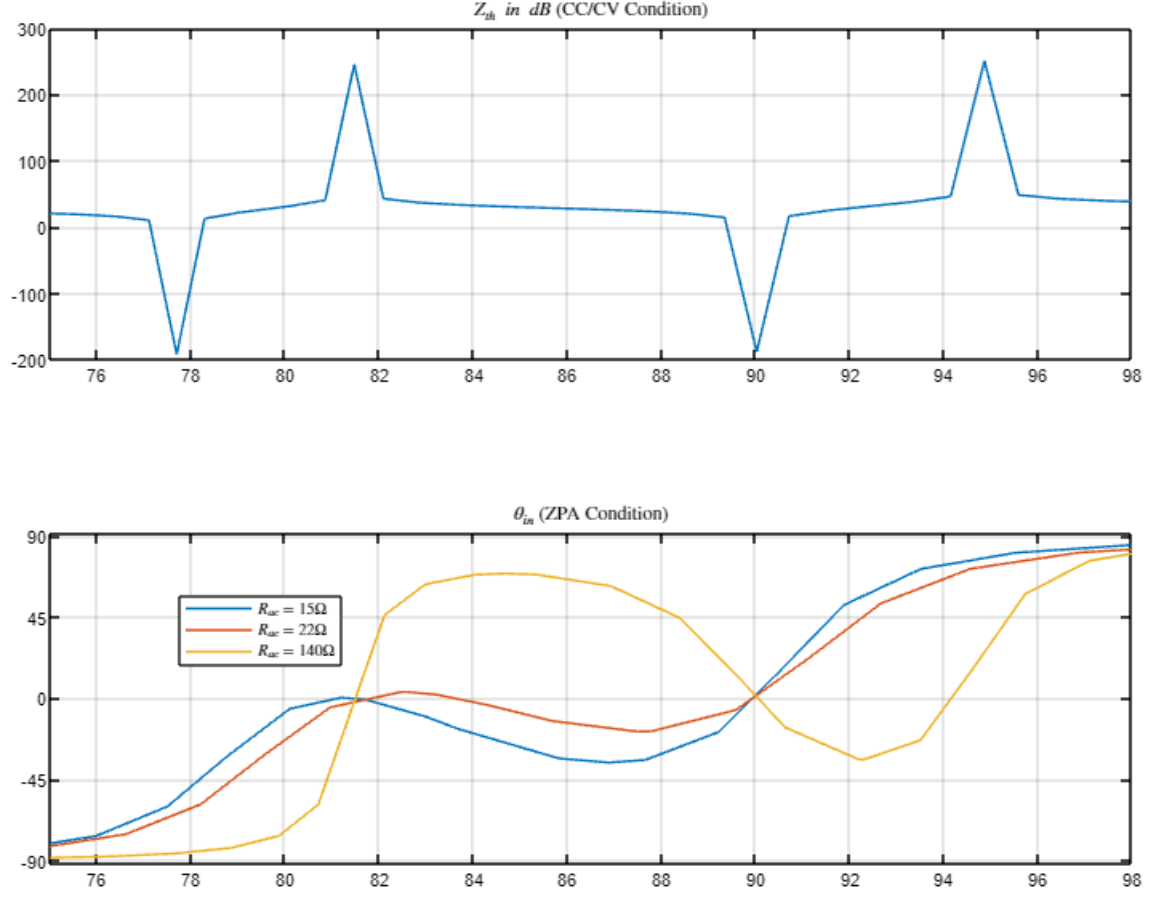


Figure 4.3: Plot of Thevenin impedance  $Z_{th}$  and Input phase angle  $\theta_{in}$  over 75-98 kHz input frequency

## 4.6 Final Results

The final results are tabulated in the table below:

	Values	Comments
Battery	$V_{bat,cv} = 270V$ ; $I_{bat,cc} = 12.22A$ ; ( $P = 3.3kW$ )	
Frequencies	$f_{cc} = 81.5kHz$ ; $f_{cv} = 90kHz$	SAE J2954 Standard
Compensation Topology	$L_p = 288\mu H$ ; $L_s = 288\mu H$ ; $k = 0.14$ $C_p = 12.17nF$ ; $C_{ss} = 13.25nF$ ; $C_{sp} = 60nF$	Satisfies required Gain, CC/CV, ZPA
Filter	$L_f = 250\mu H$ ; $C_f = 400nF$	Satisfies cutoff frequency

Table 4.3: WPT system Steady-State Design

## 4.7 Conclusion

In this chapter we did Steady-State analysis of S-SP topology using Unified model and designed it using an iterative procedure. The filter was also chosen based on topology and frequency requirements. CC/CV, ZPA, ZVS for S-SP topology were achieved.

# CHAPTER 5

## DYNAMIC MODELLING OF S-SP TOPOLOGY AND WPT SYSTEM

The aim of this chapter is to model the dynamics of the WPT system. A WPT system has both DC and AC currents and voltages, similar to resonant DC-DC converters. So proper states must be chosen, which is our first task.

The second task is modelling. First it i model the compensation topology(purely AC) before modelling the entire WPT system(AC+DC). A compensation topology is a higher order system as we'll see(order=10). So the third task is to use suitable approximations to reduce the order to 4.

There are several mathematical models and mathematical order-reduction techniques. What is used here is a combination of some of these models and techniques which are intuitive rather than just mathematical. Here intuitive means the model circuit is obtained by certain simple transformations on the original circuit.

Finally we'll include the DC side(LC-filter and rectifier) also into this model thus modelling the entire WPT system. Over the entire course we'll be applying these modelling techniques to a S-SP topology side-by-side.

### 5.1 Choice of States

The first question is "How should we choose the state variables?". In case of a DC-DC buck converter, the average inductor current and average capacitor voltage can be taken as states as mentioned in table 5.1. This works because the DC-component dominates and the harmonic component ripples are negligible compared to the DC component. Hence we were only interested in DC component, because considering ripples in the model will make computations difficult and modelling these minute details of ripple waveform is unnecessary.

Component	States
Capacitor	Average voltage $\langle v(t) \rangle_{T_s}$ (considered over one switching cycle)
Inductor	Average current $\langle i(t) \rangle_{T_s}$ (considered over one switching cycle)

Table 5.1: States in DC-DC converter

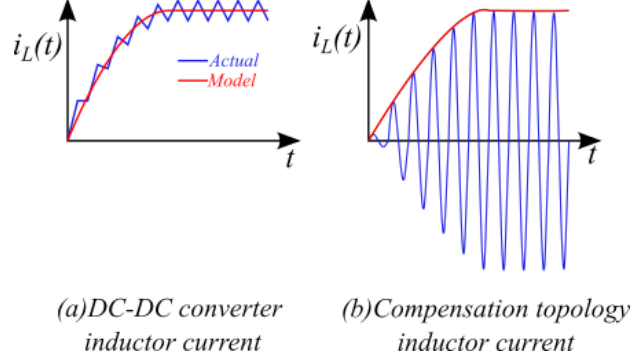


Figure 5.1: Illustration of Actual Vs Modelled quantities waveforms

In case of a WPT system, due to high quality factor of compensation topology the fundamental component is dominant and the DC and harmonic components are negligible (like ripples riding on the fundamental waveform). The fundamental waveform is oscillating very fast wrt time and so is not a good choice for state variable. Instead, since the fundamental waveform can be described by its amplitude and phase, these can be chosen as states and these states are varying slowly with time.

So two states amplitude and phase ( $A, \phi$ ) are needed to describe a single circuit element (inductor/capacitor) whose time domain representation is  $a(t) = A \cos(\omega t - \phi)$ . Alternatively the sinusoidal fourier coefficients ( $a_n, b_n$ ) can be taken as states (which is equivalent to taking dq components, because  $d = a_n, q = -b_n$ ). Alternatively a single complex variable (phasor) can be taken as state which will reduce the order of matrix while solving. This technique of expressing inductor current in different ways to get different states is shown in table 5.2 which is similar for capacitor voltage also

You can compare this with motor control analogy. AC machine currents are sinusoidal. So we do a dq transform to get d and q components which are DC, and the AC waveform can be fully reconstructed from d,q components. So now we can easily design a PI controller as if designing for a DC system.

So how should we choose our states?

	$i_L(t)$	States
Amplitude and Phase	$I_L \cos(\omega t - \phi)$	$(I_L, \phi)$
Complex Phasor	$\text{Re}\{\mathbf{I}_L e^{j\omega t}\}$	$\mathbf{I}_L$ where $\mathbf{I}_L = I_L e^{-j\phi}$
DQ component/ Fourier Series	$I_{Ld} \cos(\omega t) - I_{Lq} \sin(\omega t)$	$(I_{Ld}, I_{Lq})$ or $(a_n, -b_n)$ where $I_{Ld} = \text{Re}\{\mathbf{I}_L\} = I_L \cos(\phi)$ $I_{Lq} = \text{Im}\{\mathbf{I}_L\} = -I_L \sin(\phi)$ and $(a_n, b_n)$ are the sinusoidal fourier components

Table 5.2: States in Compensation Topology for inductor current

- Usually using  $(A, \phi)$  only small signal models[3] can be realized because there will be many non-linearities. Also it will be mathematical, and may not be possible to directly get the circuit model from time-domain circuit.
- Sinusoidal fourier series  $(a_n, b_n)$  or exponential fourier series is used in GSSA modelling[6]. It will make it mathematical instead of getting a circuit model directly, though the final result might be similar.
- So we are using d and q component as our states to get a dq phasor model which is a large signal circuit model directly by doing a transformation on the time-domain circuit which is intuitive and straight-forward.[10,9].
- There are other terminologies like EDF, etc[27]. which might be helpful while modelling.

Note that you can use peak-peak quantities or RMS quantities, the model of compensation topology won't change. But using RMS quantities is helpful while combining with the DC side (for complete WPT model). Hence We will Use RMS quantities.

## 5.2 Modelling of Compensation Topology

Now we will try to derive the model from the time domain circuit. This procedure is same as deriving steady state phasor circuit, only difference is amplitude and phase are varying with time.

### 5.2.1 Time domain to Phasor domain

This subsection explains how a time domain circuit can be transformed into the phasor domain[9]. The next subsection will explain how a Phasor domain-circuit

can be converted to dq-domain[10].

- **Resistor:** Consider a current  $i(t) = \mathbf{I}e^{j\omega t}$  passing through a resistor. This will cause a voltage  $v(t) = \mathbf{V}e^{j\omega t}$  across the resistor. How are the phasors  $\mathbf{V}$  and  $\mathbf{I}$  related? We know that  $v(t) = Ri(t) \implies \mathbf{V}e^{j\omega t} = \mathbf{I}Re^{j\omega t} \implies \mathbf{V} = \mathbf{I}R$  relates the phasor current and voltage. Note:  $\mathbf{I} = Ie^{j\phi}$  where  $I$  is amplitude and  $\phi$  is phase of  $i(t)$ .

- **Inductor:** Consider a current  $i(t) = \mathbf{I}e^{j\omega t}$  passing through an inductor. Let the voltage it be  $v(t) = \mathbf{V}e^{j\omega t}$ . We know  $v(t) = L\frac{di(t)}{dt} \implies \mathbf{V}e^{j\omega t} = j\omega L\mathbf{I}e^{j\omega t} + L\frac{d\mathbf{I}}{dt}e^{j\omega t} \implies \mathbf{V}e^{j\omega t} = (j\omega L\mathbf{I} + L\frac{d\mathbf{I}}{dt})e^{j\omega t}$ ; Thus in the phasor domain a current phasor  $\mathbf{I}$  causes a voltage phasor  $\mathbf{V} = (j\omega L\mathbf{I} + L\frac{d\mathbf{I}}{dt})$  which is an impedance and an inductor. At steady state  $d\mathbf{I}/dt = 0$ , so  $\mathbf{V} = j\omega L\mathbf{I}$  (an impedance, which is what we are using in steady state sinusoidal analysis). Thus an inductor in time domain is modelled as an inductance in series with an impedance in the phasor domain as shown in the figure.

- **Capacitor:** Consider a voltage  $v(t) = \mathbf{V}e^{j\omega t}$  applied across a capacitor. It will cause a current  $i(t) = \mathbf{I}e^{j\omega t}$  across the capacitor. How are the phasors  $\mathbf{V}$  and  $\mathbf{I}$  related? The time domain relation is  $i(t) = C\frac{dv(t)}{dt} \implies \mathbf{I}e^{j\omega t} = (j\omega C\mathbf{V} + C\frac{d\mathbf{V}}{dt})e^{j\omega t} \implies \mathbf{I} = j\omega C\mathbf{V} + C\frac{d\mathbf{V}}{dt}$ ; So if we have a capacitor in time domain, if we do phasor transformation we will have a capacitor and an admittance in phasor domain as shown in the figure. We can do a quick cross-check. In steady state the capacitor appears like an open circuit, so  $\mathbf{I} = j\omega C\mathbf{V}$  which is what we'll expect in steady-state sinusoidal model also.

- **Mutual inductance:**  $i_1(t) = L\frac{di_1(t)}{dt} + M\frac{di_2(t)}{dt}$ ;  $i_2(t) = L\frac{di_2(t)}{dt} + M\frac{di_1(t)}{dt}$ ; Now we can do a phasor transformation and we'll get a mutual inductance, and a mutual coupled impedance as shown in the figure 5.2.

To simplify this process, we can define our transform operator like this (just like fourier transform shortcuts):

- $\frac{d}{dt}(x(t)) \rightarrow (j\omega + \frac{d}{dt})(\bar{X})$
- $k(x(t)) \rightarrow k(\bar{X})$

Now we'll see how this can be applied to our S-SP topology. The time domain circuit can be transformed into phasor domain circuit as shown in the figure.

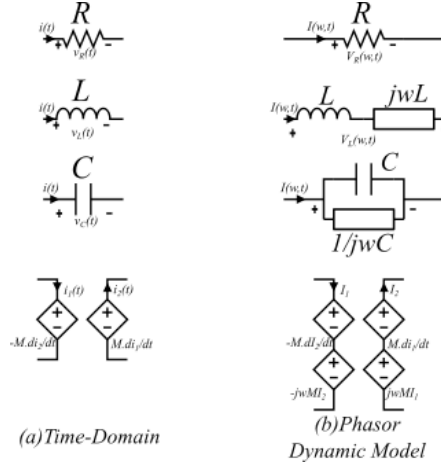


Figure 5.2: Phasor transforms of circuit elements

The time domain circuit is an AC circuit (all currents and voltages are oscillating sinusoids). The phasor domain circuit is a complex DC circuit (The currents and voltages are complex numbers with a real and imaginary part, and they are not sinusoids). Hence transient analysis is easier in our dynamic phasor circuit. We can use laplace transform on this also and solve it easily as shown in figure 5.3.

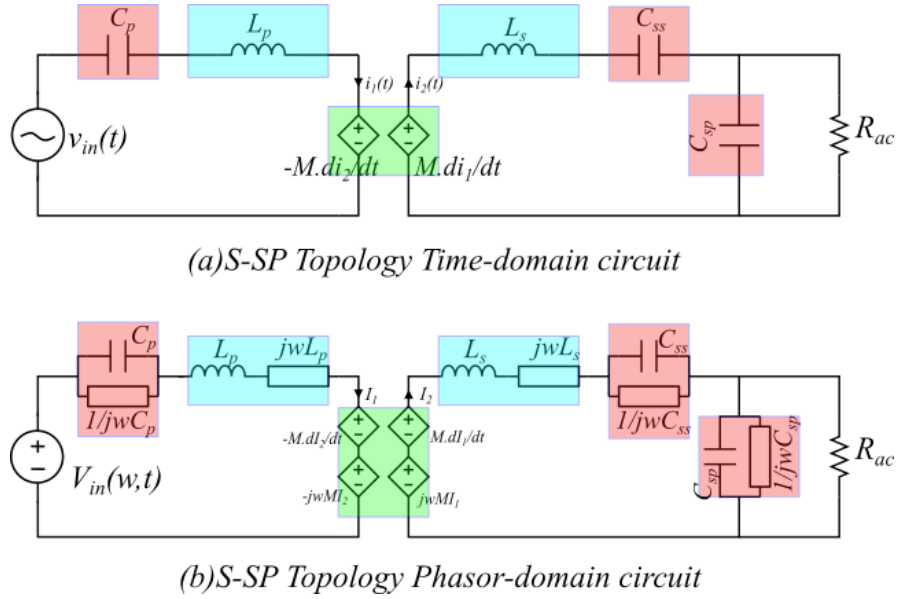


Figure 5.3: S-SP topology Time-Phasor domain transformation

## 5.2.2 Phasor domain to DQ domain

If we wish to handle with real quantities instead of complex quantities, we can separate the real and imaginary parts and write corresponding equations to get a dq transformed circuit[10]. For example the phasor  $\mathbf{V}$  can be written as  $\mathbf{V} =$

$V_d + jV_q$  , similarly for other currents and voltages and substitute them in the phasor equations. This procedure is illustrated for a capacitor as shown:

#### Phasor Transform of Capacitor

$$i(t) = \bar{I}e^{j\omega t} ; v(t) = \bar{V}e^{j\omega t}$$

$$i(t) = C \frac{dv(t)}{dt}$$

$$\Rightarrow \bar{I}e^{j\omega t} = C \frac{d}{dt} \{ \bar{V}e^{j\omega t} \}$$

$$= C \frac{d\bar{V}}{dt} e^{j\omega t} + j\omega C \bar{V} e^{j\omega t}$$

$$\Rightarrow \bar{I} = C \frac{d\bar{V}}{dt} + j\omega C \bar{V}$$

#### DQ Transform of Capacitor

$$\bar{I} = I_d + jI_q ; \bar{V} = V_d + jV_q$$

$$\bar{I} = C \frac{d\bar{V}}{dt} + j\omega C \bar{V}$$

$$\Rightarrow (I_d + jI_q) = C \left( \frac{dV_d}{dt} + j \frac{dV_q}{dt} \right) + j\omega C (V_d + jV_q)$$

$$\Rightarrow I_d = C \frac{dV_d}{dt} - \omega C V_q$$

$$\text{and } I_q = C \frac{dV_q}{dt} + \omega C V_d$$

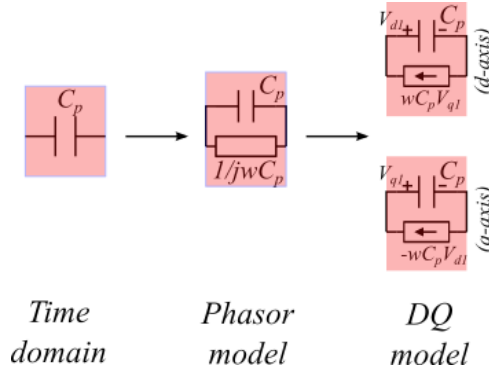


Figure 5.4: Transforming a capacitor

In the dq model ' $j\omega$ ' terms in phasor model will create a cross-coupling between d and q components (because  $j\omega$  (or simply  $j$ ) adds 90 degrees, so if we have  $\mathbf{V} = j\omega L \mathbf{I}$ , the q-component of current  $\mathbf{I}$  will affect the d component voltage .  $V_d + jV_q = j\omega L(I_d + jI_q) \Rightarrow V_d + jV_q = -j\omega L I_q + j\omega L I_d$ .

The dq model of S-SP topology is shown in the figure

For transient analysis of DC circuits we use Laplace transformed circuits. We can do the same for the phasor circuit and DQ circuits as these are DC excited circuits[9]. This is shown in the figure.



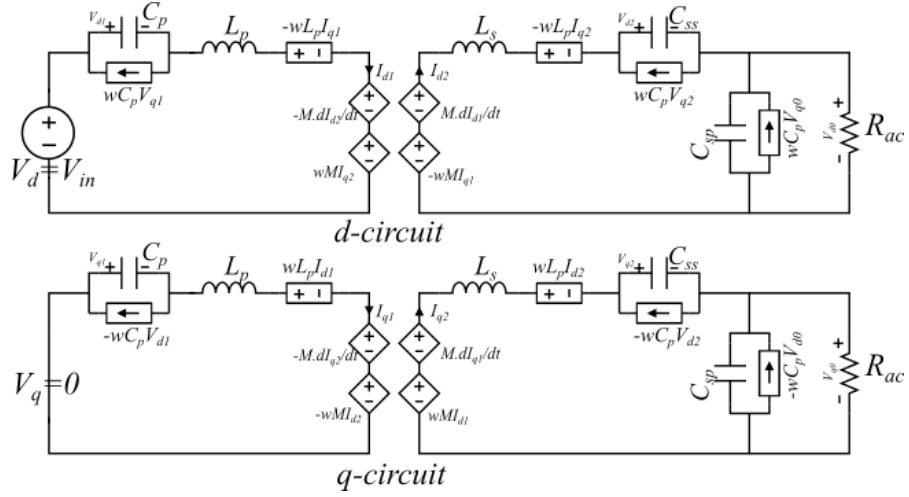


Figure 5.5: S-SP topology DQ model

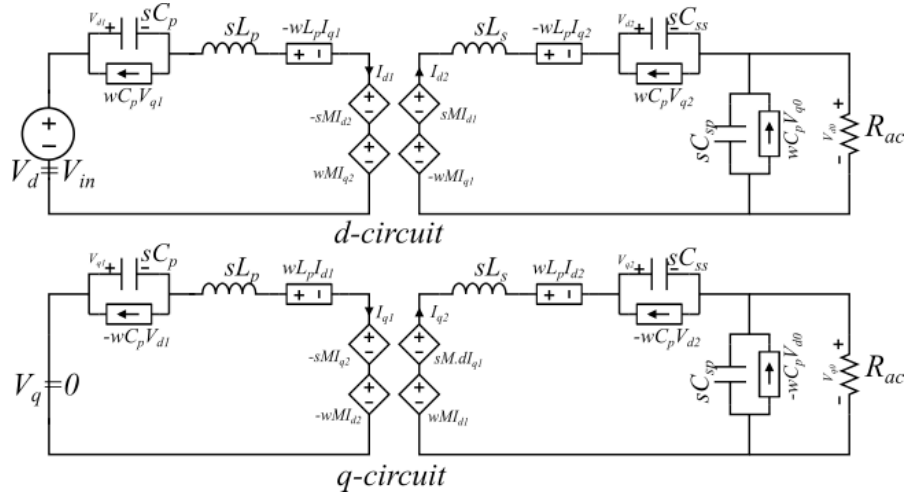


Figure 5.6: S-SP topology DQ model (laplace transformed)

### 5.3 State Equations of S-SP topology

The order of this topology is expected to be 10(two inductor currents and 3 capacitor voltages; and each quantity has 2 components real(d) and imaginary(q). Hence  $(2 + 3) \times 2 = 10$  states). The equations of S-SP topology can be written using the DQ-domain laplace transformed circuit as shown below:

$$\begin{aligned}
V_{in} &= sL_p I_{d1} - wL_p I_{q1} - sM I_{d2} + wM I_{q2} + V_{d1} \\
0 &= sL_p I_{q1} + wL_p I_{d1} - sM I_{q2} - wM I_{d2} + V_{q1} \\
0 &= -sM I_{d1} + wM I_{q1} + sL_s I_{d2} - wL_s I_{q2} + V_{d2} + V_{do} \\
0 &= -sM I_{q1} - wM I_{d1} + sL_s I_{q2} + wL_s I_{d2} + V_{q2} + V_{qo} \\
0 &= -I_{d1} + sC_p V_{d1} - wC_p V_{q1} \\
0 &= -I_{q1} + sC_p V_{q1} + wC_p V_{d1} \\
0 &= -I_{d2} + sC_{ss} V_{d2} - wC_{ss} V_{q2} \\
0 &= -I_{q2} + sC_{ss} V_{q2} + wC_{ss} V_{d2} \\
0 &= -I_{d2} + \left(sC_{sp} + \frac{1}{R_{ac}}\right) V_{do} - wC_{sp} V_{qo} \\
0 &= -I_{q2} + \left(sC_{sp} + \frac{1}{R_{ac}}\right) V_{qo} + wC_{sp} V_{do}
\end{aligned}$$

Output equation

$$\begin{aligned}
V_{bat} &= \frac{2}{\pi} \sqrt{V_{do}^2 + V_{qo}^2}; I_{bat} = \frac{\pi}{4} \sqrt{I_{do}^2 + I_{qo}^2} \\
(or) V_{bat} &= \frac{2}{\pi} |V_o|; I_{bat} = \frac{\pi}{4} |I_o|
\end{aligned}$$

The same can be represented in matrix format also as shown below:

$U = AX \implies X = A^{-1}U$  gives required transfer functions

$$\begin{bmatrix} V_{in} \\ 0 \\ 0 \\ 0 \\ 0 \\ 0 \\ 0 \\ 0 \\ 0 \\ 0 \end{bmatrix} = \begin{bmatrix} sL_p & -wL_p & -sM & wM & 1 & 0 & 0 & 0 & 0 & 0 \\ wL_p & sL_p & -wM & -sM & 0 & 1 & 0 & 0 & 0 & 0 \\ -sM & wM & sL_s & -wL_s & 0 & 0 & 1 & 0 & 1 & 0 \\ -wM & -sM & wL_s & sL_s & 0 & 0 & 0 & 1 & 0 & 1 \\ -1 & 0 & 0 & 0 & sC_p & -wC_p & 0 & 0 & 0 & 0 \\ 0 & -1 & 0 & 0 & wC_p & sC_p & 0 & 0 & 0 & 0 \\ 0 & 0 & -1 & 0 & 0 & 0 & sC_{ss} & -wC_{ss} & 0 & 0 \\ 0 & 0 & 0 & -1 & 0 & 0 & wC_{ss} & sC_{ss} & 0 & 0 \\ 0 & 0 & -1 & 0 & 0 & 0 & 0 & 0 & sC_{sp} & -wC_{sp} \\ 0 & 0 & 0 & -1 & 0 & 0 & 0 & 0 & wC_{sp} & sC_{sp} \end{bmatrix} \begin{bmatrix} I_{d1} \\ I_{q1} \\ I_{d2} \\ I_{q2} \\ V_{d1} \\ V_{q1} \\ V_{d2} \\ V_{q2} \\ V_{do} \\ V_{qo} \end{bmatrix}$$

$$H_{cc}(s) \approx \frac{V_{qo}}{V_{in}}; H_{cv}(s) \approx \frac{V_{do}}{V_{in}}; (\text{TF is after an approximation explained in next section})$$

We'll get  $U = AX$ ; where  $U$  represents the source which excites the system,  $A$  is the nodal matrix(MNA matrix) which consists of impedance terms like  $sL$ , etc. (and also  $jwL$ , etc.).  $X$  is the state matrix. So  $X = A^{-1}U$  is the solution which contains transfer functions of all state-variables. Notice that there is a non-linearity in getting the output( $I_{bat}$ ) and also it is of order 10. With this we can get the transfer function and bode plots using matlab easily, and using this bode plot a controller can be designed.

## 5.4 Order-reduction techniques and approximations

The order of this topology is 10 as we saw (two inductor currents and 3 capacitor voltages; and each quantity has 2 components real(d) and imaginary(q). Hence  $(2 + 3) \times 2 = 10$  states). There is also a non-linearity in getting the output( $I_{bat}$ ).

Sometimes we might get more insight if we reduce it to lower orders which we can probably hand-calculate. This is possible by making some approximations which lead to simplification. We will see some of those approximations now.

### 5.4.1 C-L or SVADP approximation

A capacitor can be approximated to an inductance at low frequencies as shown in the figure. [3] derives it mathematically and calls it SVADP approximation. [10] derives it in time domain. [9] derives it in laplace domain, which I'll describe here. The capacitor in time domain becomes a parallel combination of capacitance and impedance in phasor domain. We can take laplace transform of this phasor circuit for simpler calculations. Its impedance will be  $Z = 1/(sC + jwC)$ . We can do some mathematical simplifications like multiplying conjugate, rearranging, etc. and finally express in terms of a frequency dependent capacitor  $C(s) = C(1 + s^2/w^2)$  as shown below.

$$\begin{aligned}
 \bar{I} &= C \frac{d\bar{V}}{dt} + jwC\bar{V} \\
 \implies \bar{I} &= sC\bar{V} + jwC\bar{V} [\text{laplace transform}] \\
 \implies \bar{V} &= \frac{1}{sC + jwC} \bar{I} [\text{rearrange}] \\
 \implies \bar{V} &= \frac{s - jw}{(s^2 + w^2)C} \bar{I} [\text{multiply conjugate}] \\
 \implies \bar{V} &= \frac{s - jw}{w^2C \left(1 + \frac{s^2}{w^2}\right)} \bar{I} [\text{take } w^2 \text{ common}] \\
 \implies \bar{V} &= \frac{s - jw}{w^2C(s)} \bar{I} \left[ \text{where } C(s) = C \left(1 + \frac{s^2}{w^2}\right) \right] \\
 \implies \bar{V} &= \left( \frac{s}{w^2C(s)} + \frac{1}{jwC(s)} \right) \bar{I} [\text{split numerator}] \\
 \text{For } s \ll w, C(s) &\approx C, \text{ so} \\
 \bar{V} &= \left( \frac{s}{w^2C} + \frac{1}{jwC} \right) \bar{I}
 \end{aligned}$$

If d and q components (or the amplitude) change very slowly compared to the oscillating frequency of sinusoid,  $s \ll w$ . So  $C(s) \approx C$ . So  $Z = 1/jwC + s/w^2C$ .

This looks like an impedance  $1/j\omega C$  and an inductance  $1/\omega^2 C$  in series as shown in the figure. Thus a phasor capacitor approximately behaves like an inductance for slowly varying amplitude as shown in figure 5.7. Similarly a phasor inductance can also be approximated to a capacitance for slowly varying amplitude.

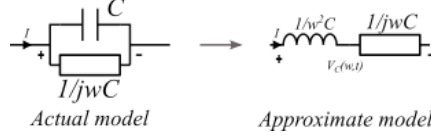


Figure 5.7: SVADP approximation

We can apply this approximation to all capacitors in the S-SP topology to get a reduced order model of order 6 (3 inductor currents, each current has d and q components, so  $3 \times 2 = 6$ ). Instead we can actually keep the last capacitor( $C_{sp}$ ) unchanged for more accuracy and still we'll get order 6 as shown in the figure 5.8(2 inductor currents, 1 capacitor voltage; d & q components for each quantity)

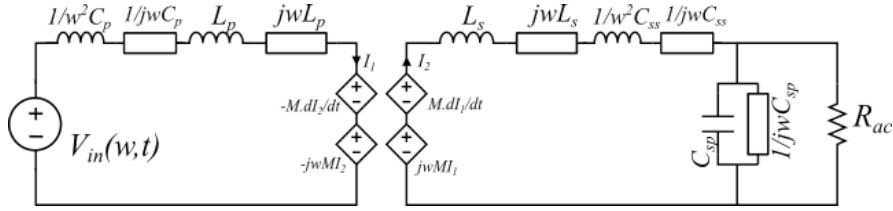


Figure 5.8: S-SP topology SVADP approximation

#### 5.4.2 Neglecting Mutual-Inductance dynamics partly

The dynamic part of mutual inductance can be partially neglected as shown in the figure. Partially means only the CCVS dynamic part is neglected (but mutual inductance is included in self inductance also right,  $L_p = L_{lp} + L_m$ ). This is used in [10]. The reason is not clear for me. It might have come due to a calculation mistake, but somehow it doesn't affect the model much. So this is probably a good approximation. Some questions yet to be answered are 1. Why this approximation should work?, 2. Under what cases will this approximation be invalid?. We can simplify the S-SP topology with this approximation as shown in figure 5.9.

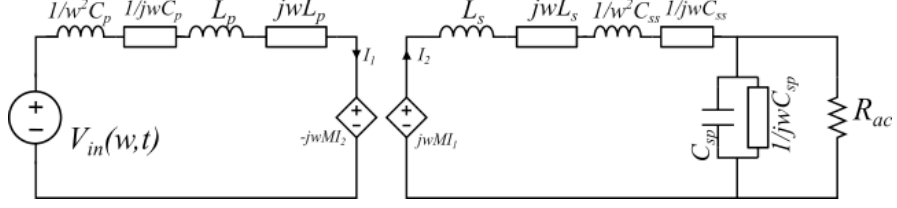


Figure 5.9: S-SP topology Mutual Inductance approximation

### 5.4.3 Static element approximation

Some elements can be approximated as static elements (just keeping the steady state impedances and leaving out the dynamic part). This seems to be used in [1] and [23]. The reason probably is that some components don't affect the dynamics much. In the case of S-SP topology, I'm using this approximation to neglect the dynamics part of  $C_{sp}$  capacitance (Maybe  $C_{sp}$  doesn't affect dynamics much because it is a large capacitance). So it appears as a static impedance only as shown in figure 5.10. So the model is further reduced from order 6 to order 4, the states being  $I_{d1}, I_{q1}, I_{d2}, I_{q2}$ . An observation is that this approximation does not work properly when applied to other capacitors like  $C_p, C_{ss}$ , or inductors  $L_p, L_s$ .

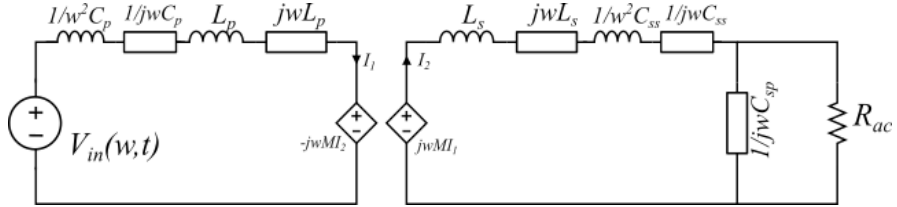


Figure 5.10: S-SP topology Static  $C_{sp}$  approximation

### 5.4.4 Constant phase approximation

This approximation is used in [6]. From the steady state unified model, the output current (or voltage) is at a constant phase with  $V_{in}$  as shown in figure 5.11. For example in CC mode,  $I_o/V_{in} = jk$  at steady state where  $k$  is the gain. Also  $V_o = I_o R_{ac}$ . Hence  $I_o, V_o$  are  $90^\circ$  phase shifted wrt  $V_{in}$ .  $V_{in}$  has only d-component, and q-component is zero since we are taking  $V_{in}$  as reference. Hence  $I_o, V_o$  have only q-component since they are  $90^\circ$  shifted from  $V_{in}$ . Hence q-component is zero for  $I_o, V_o$  at CC mode-steady state. (Similarly d-component of  $I_o, V_o$  is zero in CV mode-steady state).

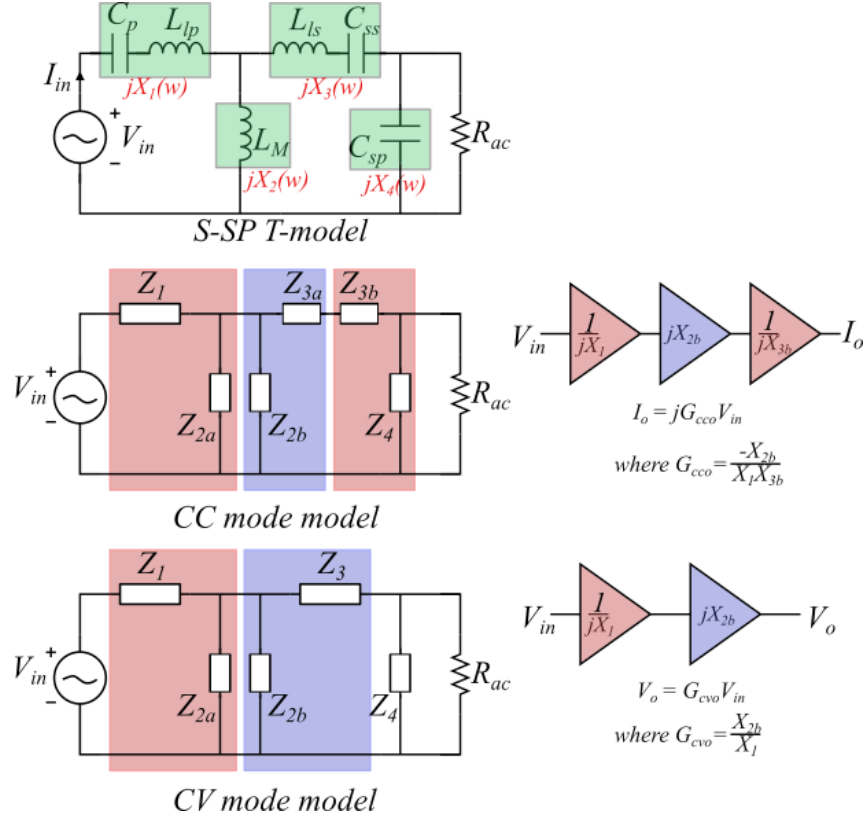


Figure 5.11: Steady-State Unified Model of S-SP topology

Now we are going to extend this steady state relation to transient also for CC mode case(similar analysis can be done for CV mode also). Assume q-components of  $I_o, V_o$  are negligible compared to d-components in transient also  $I_{oq}(t) \ll I_{od}(t)$ ,  $V_{oq}(t) \ll V_{od}(t)$ . Hence  $I_{bat} = \frac{2}{\pi} \sqrt{I_{od}^2 + I_{oq}^2} \approx \frac{2}{\pi} I_{oq}$ . Still it is of order 4, but the non-linearity in  $I_{bat}$  is removed. So we can get a large signal transfer function  $I_{bat}/V_{in}$ . (If we don't apply this approximation we'll have to linearize it to get the transfer function  $I_{bat}/V_{in}$  and it would be a small signal model)

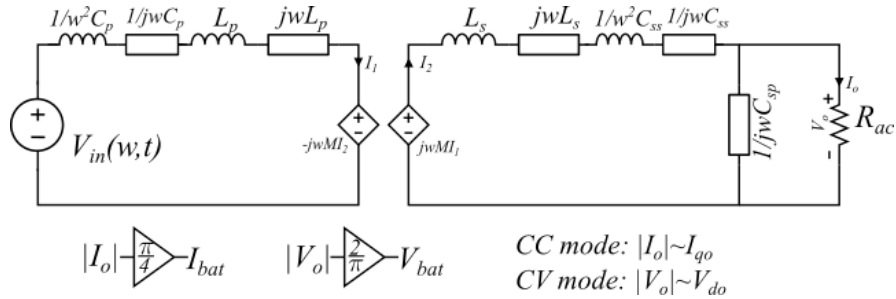


Figure 5.12: S-SP topology Constant Phase approximation

### 5.4.5 Other mathematical approximations

There are other possible approximations. They seem to be mathematical, and we might have to work to see if they can be explained intuitively in terms of the circuit. Some of them are listed here:

**1.Approximation by [3]:** In steady state we can express one state  $X_1$  in terms of another state  $X_2$  ( $X_1 = kX_2$ ). Now we can assume this relation holds true to a first order during transient also (i.e  $dx_1/dt = k \cdot dx_2/dt$ ). By substituting this in the original state equations we can reduce the order.

**2.Approximation by [23]:** It starts with an approximation that amplitude and phase are almost constant. Using this a simple model is derived. Then this approximate model is substituted in the actual equations to get a more accurate model. This can be done again and again iteratively to get more accurate but complicated models.

### 5.4.6 Comparison of Approximations

The following bode plot and step response shows how each of these approximations mimic the actual response to some extent.

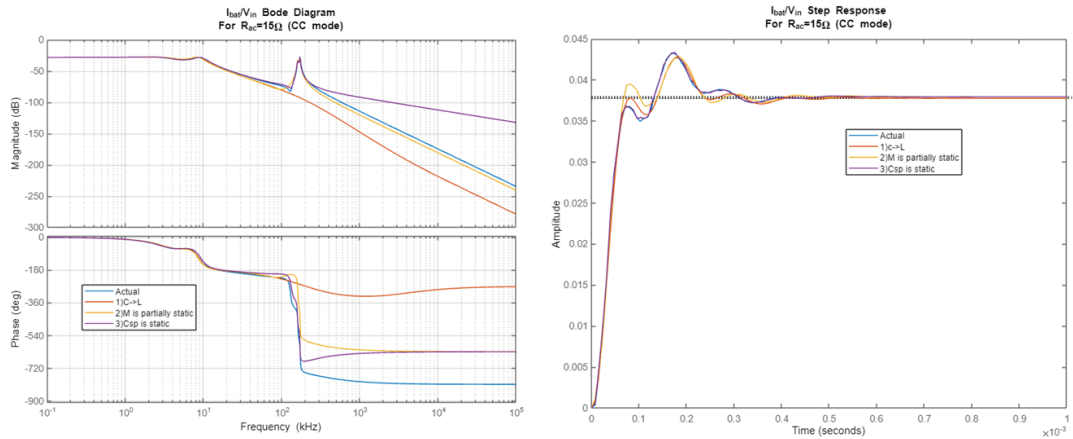


Figure 5.13: Comparison of Approximations Plots

## 5.5 The Final reduced-order model of S-SP topology

By using all the approximations we get the reduced order model as shown in figure 5.14. Bode and Step plots comparing the 4th order model with the actual 10th order model for a particular load is shown in figure 5.15

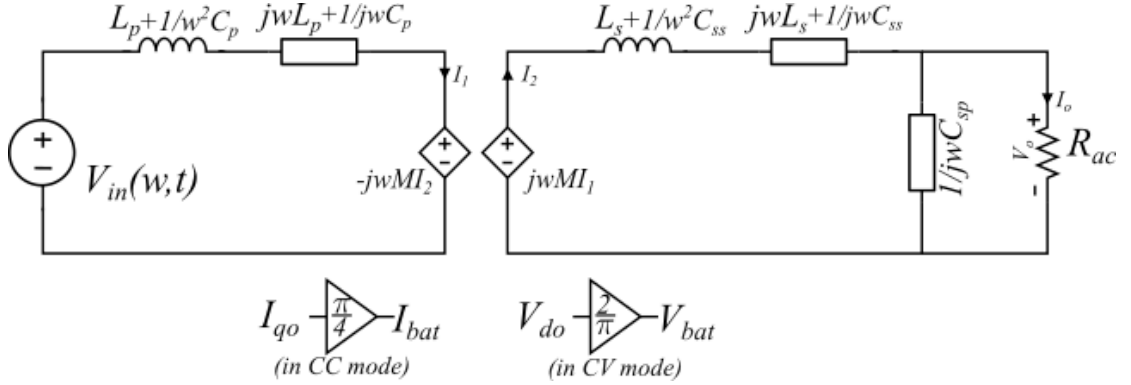


Figure 5.14: The Reduced-Order Model of S-SP Topology

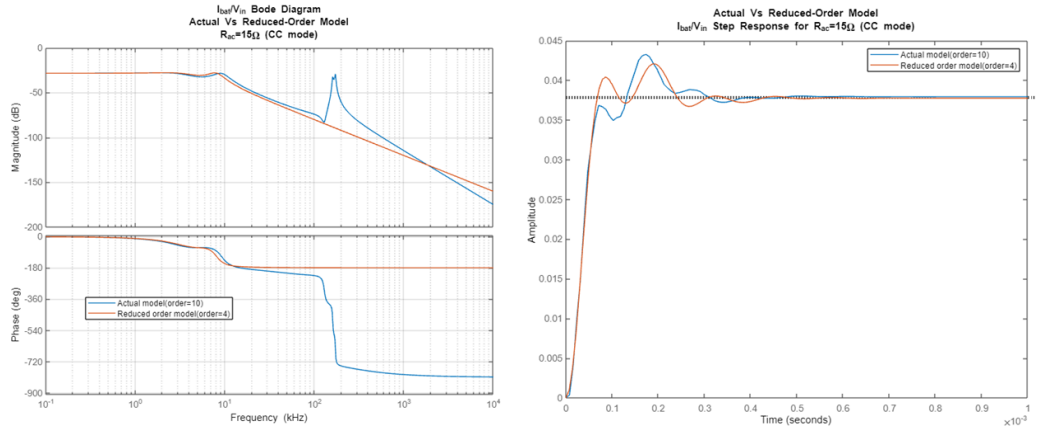


Figure 5.15: Comparison of Actual and Reduced-Order Model

The model seems to hold good enough upto 1/10th of the resonance frequency (1/10th of 81.5kHz). Similar observation can be done for other loads and in CV mode also.

## 5.6 Combined WPT model

Till now only the compensation-topology has been modelled. For a detailed modelling we may have to consider the DC side components like rectifier, filter at output



and DC-bus voltage, inverter at input. This section explains that procedure.

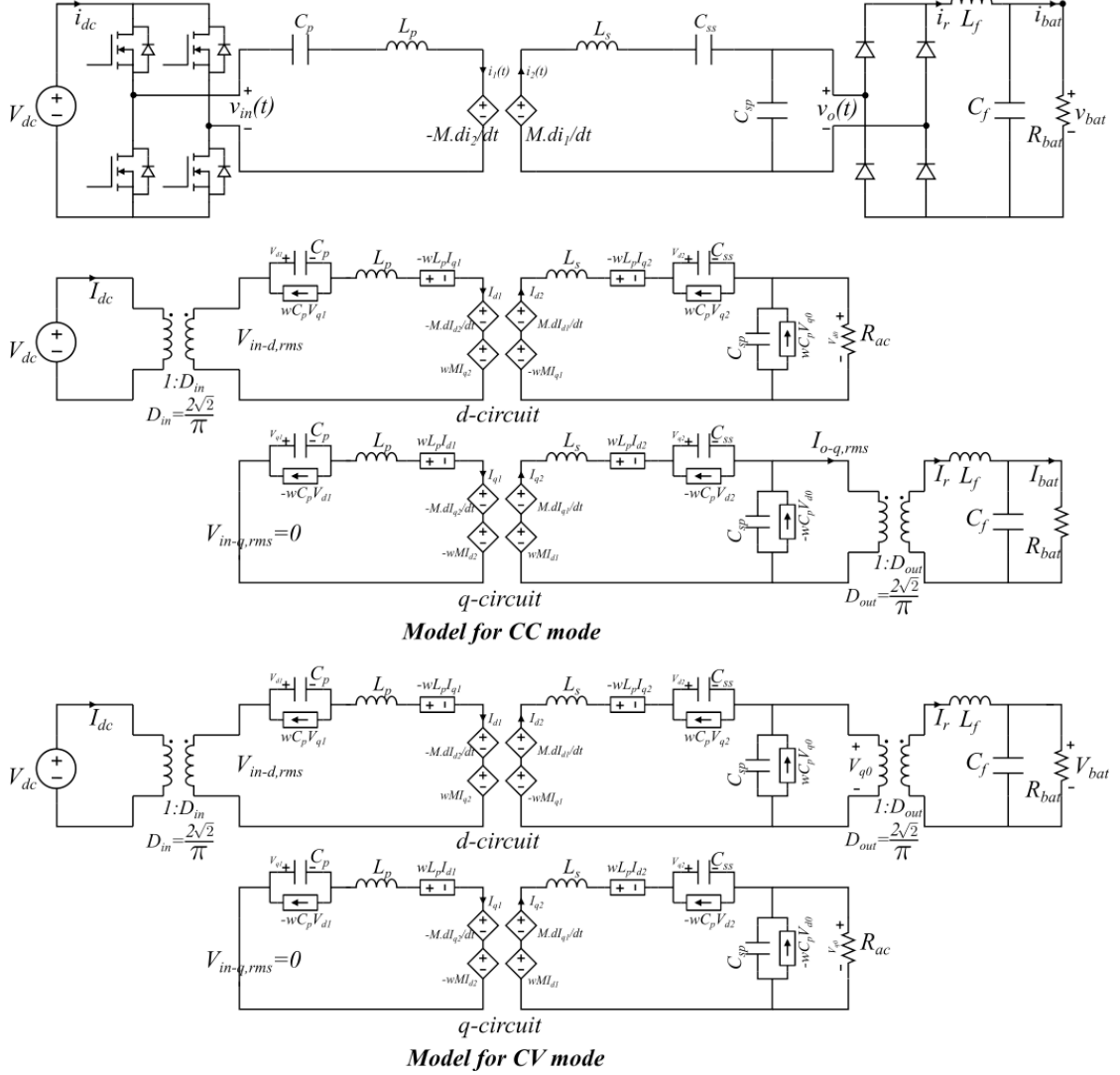


Figure 5.16: Dynamic Model of the entire WPT System

In the input side, the d side voltage  $V_d = V_{in}$  is only affected by the inverter, because we are taking  $V_{in}$  along d-axis as our reference. By drawing the waveform of current  $i_{dc}$  we would notice that only the d-component of  $I_{in}$  (input current of compensation topology) will affect  $i_{dc}$ . The q-component won't have any impact on  $i_{dc}$  even if ZPA was not present. Hence the inverter is modelled as a transformer

In the output side, using approximation-4 (phase of output current is  $\pm 90^\circ$  in CC mode and phase of output voltage is  $0/180^\circ$  in CV mode) either d or q-component will be present dominantly so the rectifier can be modelled as a transformer and connected along that axis only (d or q).

Note that rms amplitudes are used as states so that this kind of transformer representation is possible. If we use peak amplitudes as states then this represen-

tation would not be possible.

## 5.7 The Monotonicity theorem

The battery resistance varies in this manner: CC mode:  $15\Omega < R_{ac} < 22\Omega$  CV mode:  $22\Omega < R_{ac} < 140\Omega$  So  $R_{ac}$  can take a range of values. So what  $R_{ac}$  should we consider for designing a controller? [4] says that the bode plot responses will be monotonic with load resistance for resonant converters by using a mathematical theorem. This works for resonant converters also.

- **CC mode:** Transfer function  $I_{bat}/V_{in}$  is plotted for  $R_{ac} = 15, 18, 22$ . We see that  $R_{ac} = 18\Omega$  plot comes between  $R_{ac} = 15\Omega$  and  $R_{ac} = 22\Omega$ . Plot for any other  $R_{ac}$  in this range will also be sandwiched between the plots corresponding to 15 and 22  $\Omega$ . Hence it is enough to consider these limiting plots and design a controller for these, and this controller will automatically work well for other plots also. Also In time domain the settling time and maximum overshoot of intermediate loads are sandwiched between  $R_{ac} = 15$  and  $22\Omega$ .

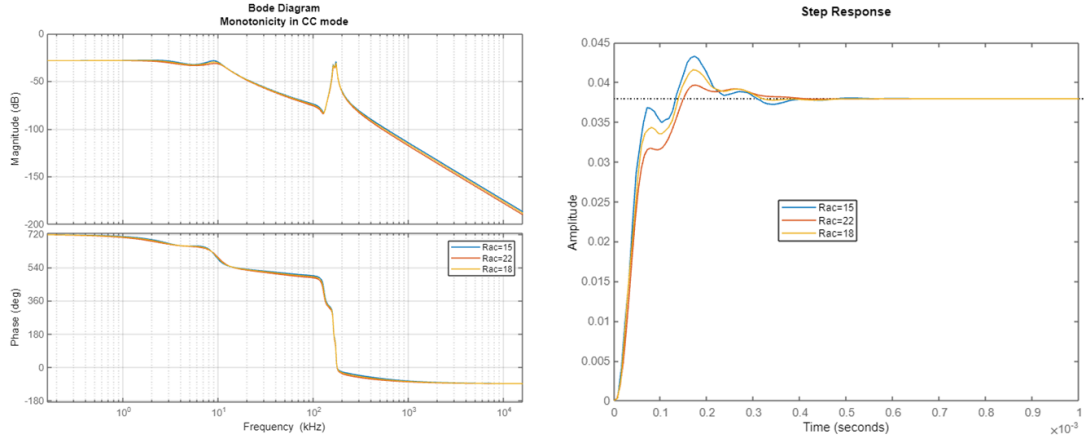


Figure 5.17: Illustration of Monotonicity Theorem (CC mode)

- **CV mode:** Bode plot for the transfer function  $V_{bat}/V_{in}$  is plotted for  $R_{ac} = 22, 140\Omega$  and in-between values. Here again you can see that plots of intermediate values of  $R_{ac}$  are sandwiched between  $R_{ac} = 22, 140\Omega$  plots. In time domain the settling time and maximum overshoot of intermediate loads are sandwiched between  $R_{ac} = 22$  and  $140\Omega$ . Hence it is enough to analyse for the extreme cases  $R_{ac}=22, 140\Omega$ .

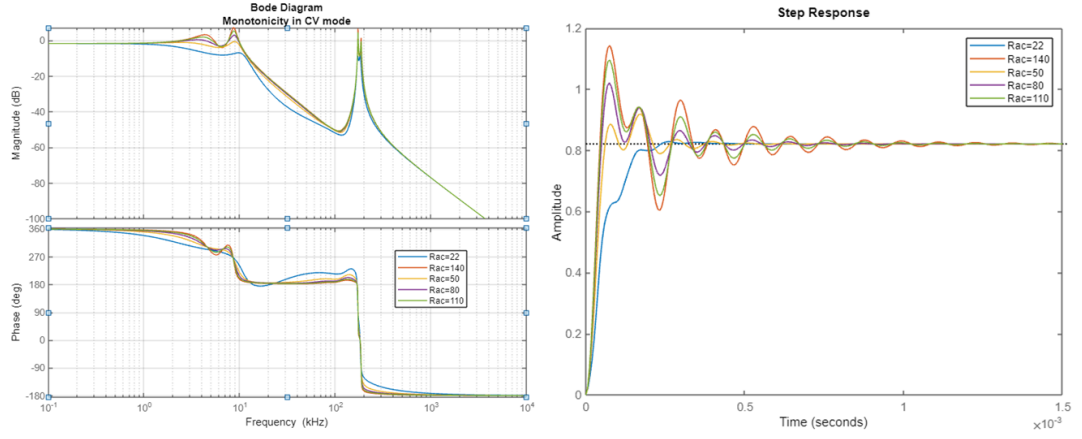


Figure 5.18: Illustration of Monotonicity Theorem (CV mode)

The response is constant for frequencies  $f \leq 1kHz$ . So if we want to design a PI controller to get 1kHz bandwidth closed-loop system, we can simply take the plant as a gain block in both CC and CV modes. Then we can test how it would work for exact system using the exact phasor model matrix equations in matlab which is easy to do.

## 5.8 Conclusion

We saw phasor dq modelling of the compensation topology and approximations to reduce the order and remove the non-linearity. We combined the DC side also into the model getting a linear large-signal dynamic model of the WPT system. The monotonicity theorem is explained which is useful for controller design.

# CHAPTER 6

## CONTROL SYSTEM

This chapter explains how a control system can be designed for controlling our WPT system in CC/CV modes for charging the battery.

### 6.1 Choosing a control strategy

Some of the commonly used control techniques are described below:

1. **Frequency control:** Here the switching frequency( $f_{sw}$ ) is the control variable. Changing the impedance changes the thevenin impedance of the compensation topology, hence the transfer function from input to output will change. This is the principle behind this technique. But here we are trying to implement ZPA/ZVS, so we have to fix our frequency at  $f_{cv}$  or  $f_{cc}$ . Hence this strategy is not suitable here.
2. **Phase shift control:** Here the gating signals to the switches are given as phase shifted square waves, which effectively forms a quasi square wave of duty cycle  $d$  at the input of compensation topology. By changing the phase shift value the duty  $d$  can be controlled. By changing the duty the fundamental component of quasi-square wave can be controlled  $V_{in} = \frac{4V_{dc}}{\pi} \sin(\frac{\pi d}{2})$ , hence the output voltage can be controlled. This is the principle behind this technique. This technique can achieve CC and ZPA, and sometimes ZVS also. But achieving ZVS might not be simple. This is because for a square waveform( $d \approx 1$ ) a small input phase angle is enough. But for a quasi-square waveform a larger input phase angle is required so that diode conducts when the switch is turned on, which is not possible when  $d$  is lesser(say 0.5) because CC/CV operation needs almost zero phase angle(ZPA)[14] otherwise output will not be load-dependent.
3. **Voltage regulation control:** Here the DC-bus voltage( $V_{dc}$ ) is controlled to control the output voltage/current. This method can accomplish both CC/CV and ZPA/ZVS for a wide load range.

In this work phase-shift control and voltage regulation control were tried and verified to give same output. The same controller was used in both cases with minor modifications.

## 6.2 Controller Block Diagram

Separate PI controllers will be designed for CC and CV modes. The battery voltage and current ( $v_{bat}, i_{bat}$ ) are taken as feedback for PI controllers.  $v_{bat}$  is used to switch between CC and CV modes when it reaches 270V. It will work in CC mode when  $V_{bat} < 270V$  and in CV mode when  $V_{bat} > 270V$ . The gating signals will be quasi-square waves in phase-shift control with switching frequencies as  $f_{cc}, f_{cv}$ . Thus the control requirements can be accomplished. The block diagram is shown in figure 6.1.

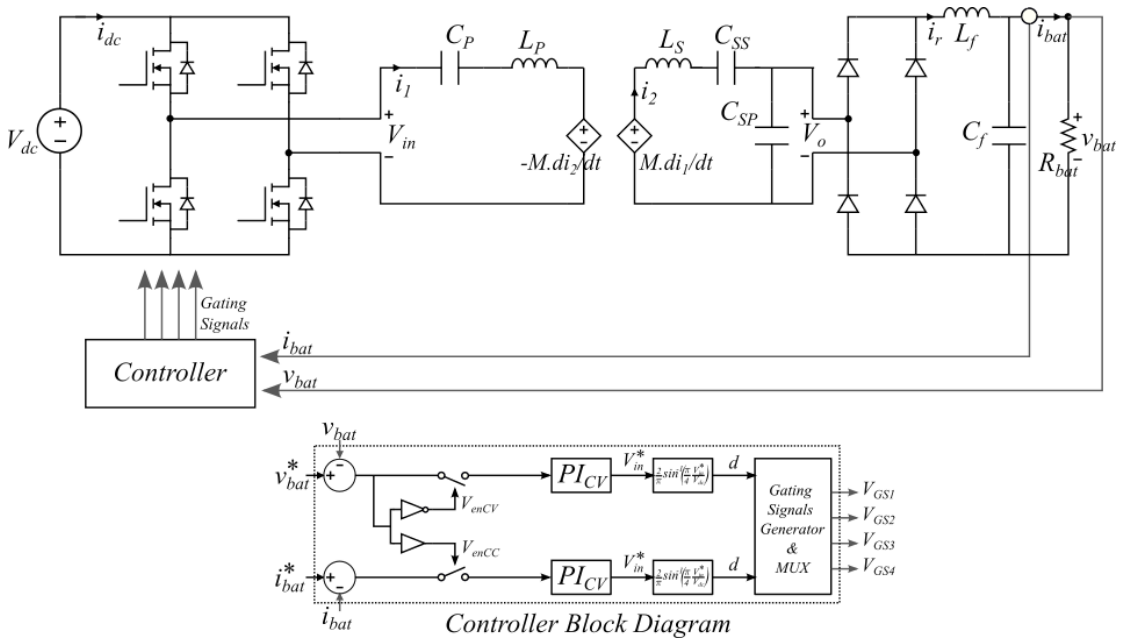


Figure 6.1: Control block diagram of the WPT system

### 6.3 Controller Design

This section explains how the PI controller parameters  $K_p, K_i$  are set. The exact 10th order model for S-SP topology is used for plant transfer function  $G_{plant}(s)$  with the help of matlab for taking matrix inversion.

### 6.3.1 CC mode Controller Design

The requirements in CC mode are given first, using which an appropriate controller can be calculated. The final design results are given at the end. The controller is

designed for  $R_{ac} = 15\Omega$  because it has more overshoot, and so it'll likely work for  $R_{ac} = 22\Omega$  also.

#### Requirements

$$G_c(s) = \frac{K}{s} \left(1 + \frac{s}{w_c}\right)$$

$$G_{plant}(s) = \frac{I_{bat}}{V_{in}}$$

$$\text{Required } w_{BW} = 1kHz$$

*Phase margin already good*

#### Calculations

$$G_{cc0} = G_{plant}(j.w_{BW}) = 0.0387$$

$$\text{Choose } w_c = 10 \times w_{BW}$$

$$G_{plant}(j.w_{BW}).G_c(j.w_{BW}) = 1$$

$$\implies K = \frac{w_{BW}}{G_{cc0}}$$

$$K_p = \frac{K}{w_c}; K_i = K$$

#### Design for CC mode (using $R_{ac} = 15\Omega$ )

$$G_c(s) = K_p + \frac{K_i}{s}$$

$$K_p = 2.5850$$

$$K_i = 162.42 \times 10^3$$

$$PM = 83.4^\circ \text{ at } BW = 1kHz$$

### 6.3.2 CV mode Controller Design

The requirements in CC mode are given first, using which an appropriate controller can be calculated. The final design results are given at the end. The controller is designed for  $R_{ac} = 140\Omega$  because it has more oscillations, and so it'll likely work for  $R_{ac} = 22\Omega$  also.

#### Requirements

$$G_c(s) = \frac{K}{s} \left(1 + \frac{s}{w_c}\right)$$

$$G_{plant}(s) = \frac{V_{bat}}{V_{in}}$$

$$\text{Required } w_{BW} = 1kHz$$

*Phase margin already good*

### Calculations

$$G_{cv0} = G_{plant}(j.w_{BW}) = 0.8548$$

$$\text{Choose } w_c = 10 \times w_{BW}$$

$$G_{plant}(j.w_{BW}).G_c(j.w_{BW}) = 1$$

$$\Rightarrow K = \frac{w_{BW}}{G_{cv0}}$$

$$K_p = \frac{K}{w_c}; K_i = K$$

### Design for CV mode (using $R_{ac} = 140\Omega$ )

$$G_c(s) = K_p + \frac{K_i}{s}$$

$$K_p = 0.1182$$

$$K_i = 7.4286 \times 10^3$$

$$PM = 92^\circ \text{ at } BW = 1kHz$$

## 6.4 Bode Plots of Controller and Closed-loop response

The theoretical bode-plots and step-response obtained in CC and CV modes for the extreme load conditions are shown in this section. These plots confirm that the controller works properly.

### 6.4.1 CC mode

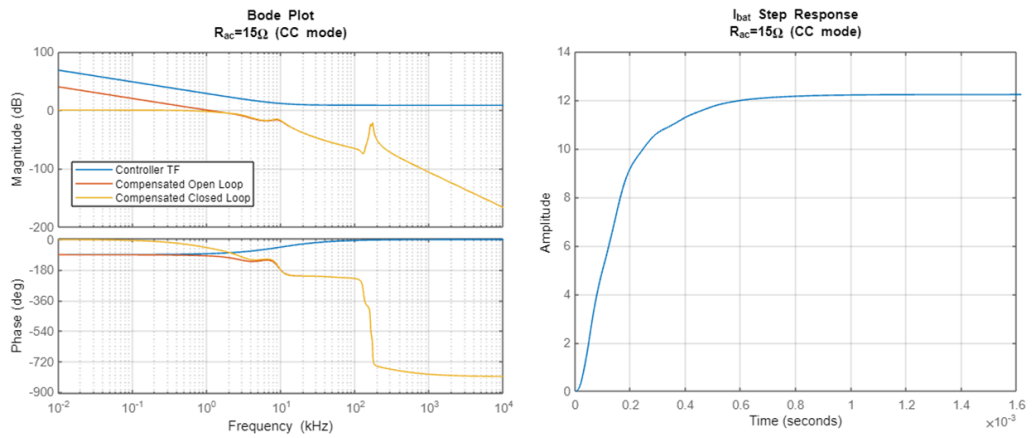


Figure 6.2: Closed Loop Response(15Ω - CC mode)

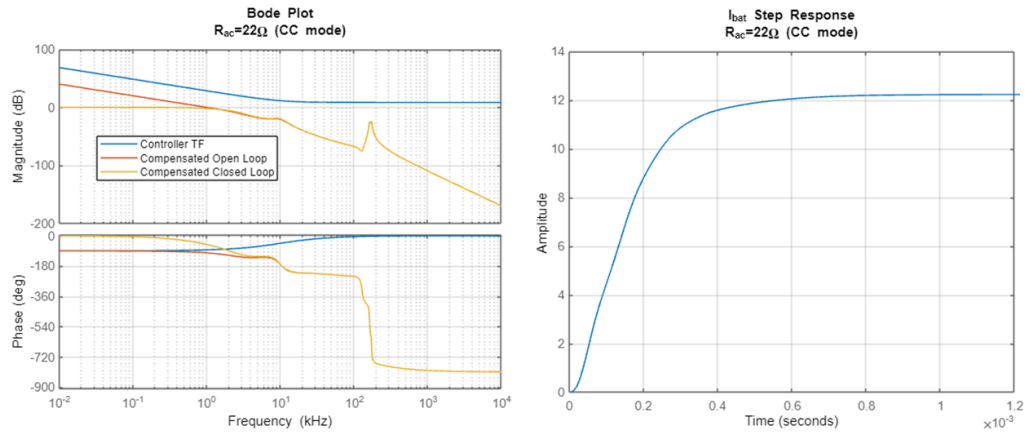


Figure 6.3: Closed Loop Response( $22\Omega$  - CC mode)

## 6.4.2 CV mode

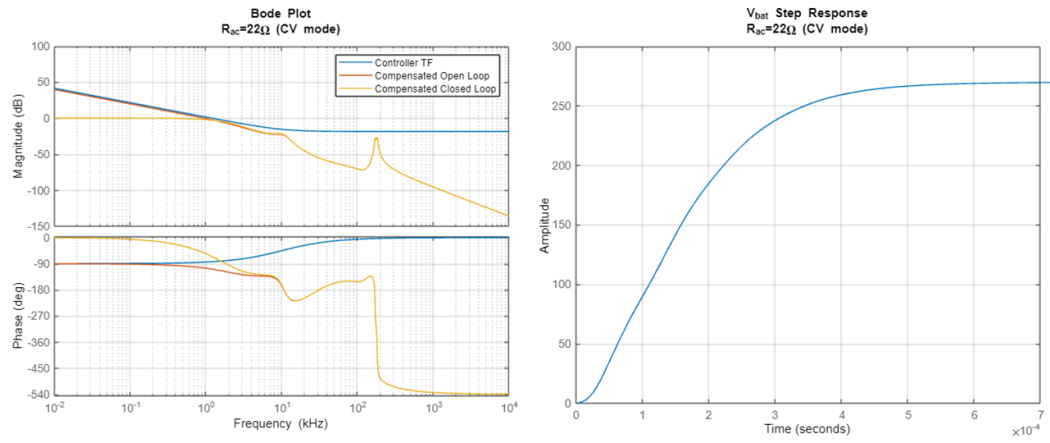


Figure 6.4: Closed Loop Response( $22\Omega$  - CV mode)



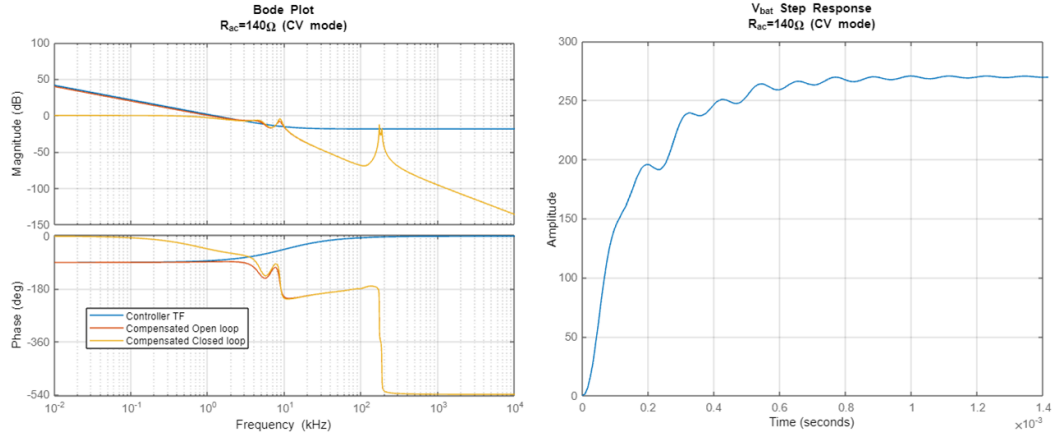


Figure 6.5: Closed Loop Response( $140\Omega$  - CV mode)

## 6.5 Conclusion

Thus a controller is designed for the WPT system which includes separate PI controllers for each mode and a switching logic to switch between two modes. The controller is designed based on DC-bus voltage regulation strategy which is the most suitable one for our application.

# CHAPTER 7

## SIMULATION RESULTS

The simulations done to verify steady state analysis, dq model and transient analysis will be presented in this chapter.

### 7.1 Steady State Simulations

The simulations for steady state analysis done using LTspice will be presented in this section. Fig. 7.1 indicates load independent CV mode frequencies at 78kHz and 90kHz, and load independent CC mode frequencies at 81.5kHz and 90kHz. However, only 81.5kHz and 90kHz frequencies satisfy ZPA condition and comply with the SAE J2954 standard, hence only these two frequencies will be used.

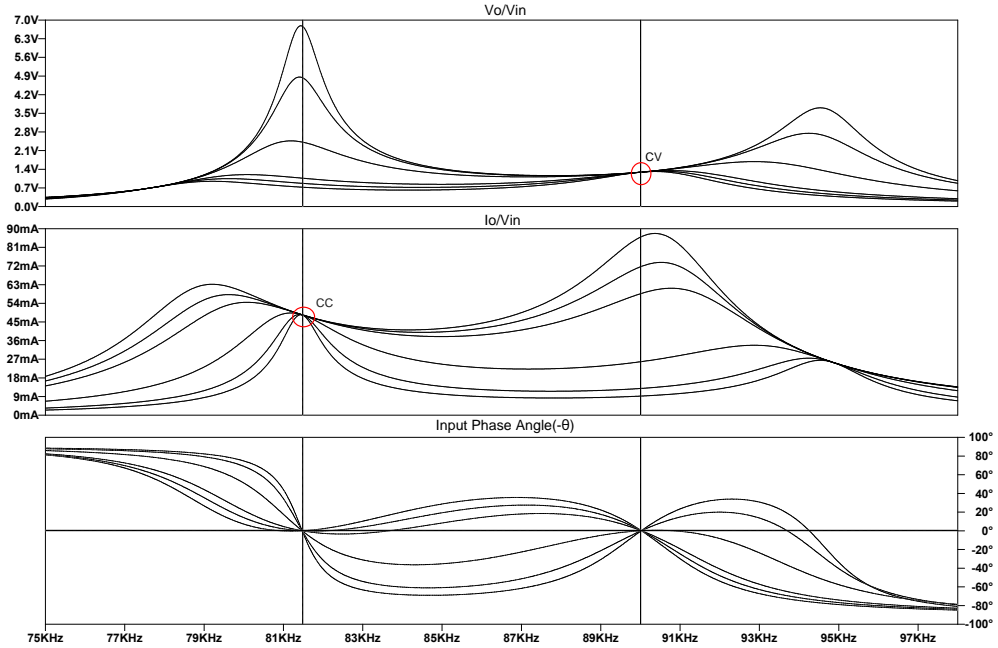


Figure 7.1: Output voltage and current gains and input phase angle for different loads

The plots of voltage ( $V_{in}$ ) and current ( $I_{in}$ ) at compensation topology input confirm ZPA as indicated by Fig. 7.2(a) and Fig. 7.3(a), which are obtained by modelling output port as an ac resistance ( $R_{ac}$ ). However, the input phase angle

slightly deviates from zero when rectifier with LC filter is connected at output. The deviation is more for small  $R_{ac}$  as in Fig. 7.2(b), and is negligible for very large  $R_{ac}$  as in Fig. 7.3(b).

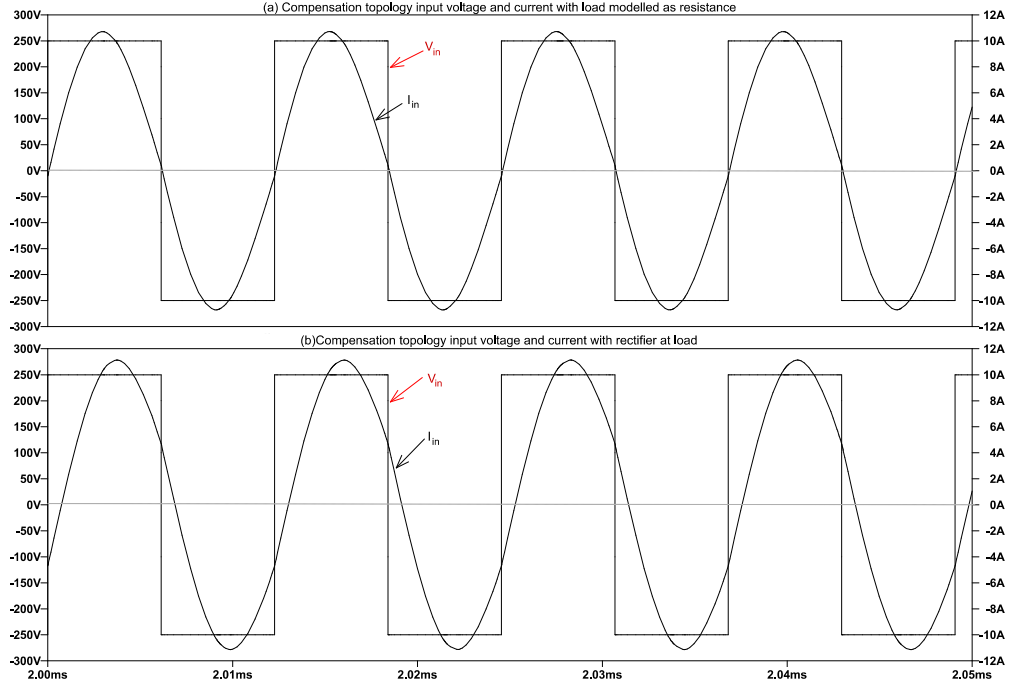


Figure 7.2: Compensation topology input waveforms with  $R_{ac} = 15\Omega$  for (a)load modelled as pure resistance (b) load is rectifier

The reason is as follows. The input phase angle ( $\theta_{in}$ ) will be equal to output phase angle ( $-\theta_{in}$ ) in CV mode and negative of output phase angle ( $-\theta_{in}$ ) in CC mode, with respect to fundamental components. This is a property of the compensation topology and is proved in Appendix-I. This is illustrated in Fig. 7.4 and in Fig. 7.5. In Fig. 7.4,  $V_{in}$  to  $I_o$  phase is  $90^\circ$  and  $I_{in}$  to  $V_o$  phase is also  $90^\circ$ . Hence output phase angle directly affects input phase angle in cc mode. Similarly in Fig. 7.5,  $V_{in}$  to  $V_o$  phase is expected to be  $0^\circ$  (some slight deviation is here though) and  $I_{in}$  to  $I_o$  phase is  $0^\circ$ . Hence output phase angle must equal input phase angle in cv mode also.

The phase at output would be zero if load was a resistance. But the load is an inverter, and the output current ( $I_o$ ) will be a square waveform. So the output voltage will have harmonic distortion, especially in DCM mode where  $V_o$  becomes zero for sometime as shown in Fig. 7.6. So the zero crossing of fundamental component ( $V_{o,1}$ ) and actual ( $V_o$ ) are displaced, which is approximately the output

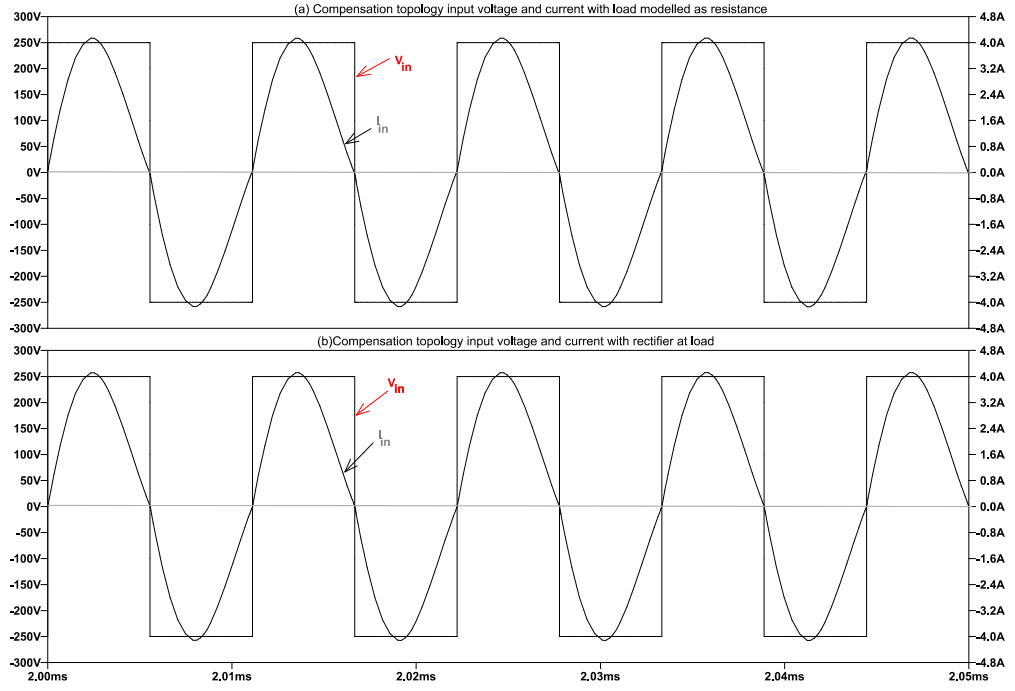


Figure 7.3: Compensation topology input waveforms with  $R_{ac} = 140\Omega$  for (a) load modelled as pure resistance (b) load is rectifier

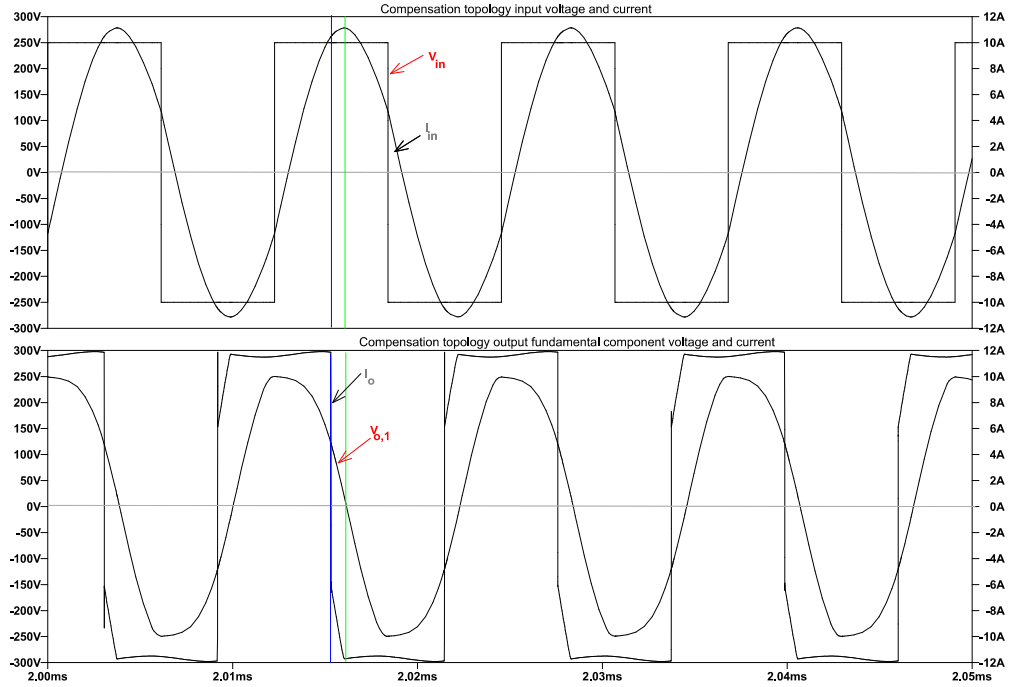


Figure 7.4: Compensation topology input and output waveforms with  $R_{ac} = 15\Omega$  depicting input-output phase relation in cc mode

phase angle (assuming output current is approximately still a square wave and its fundamental component is not phase shifted). For higher  $R_{ac}$  the output current is

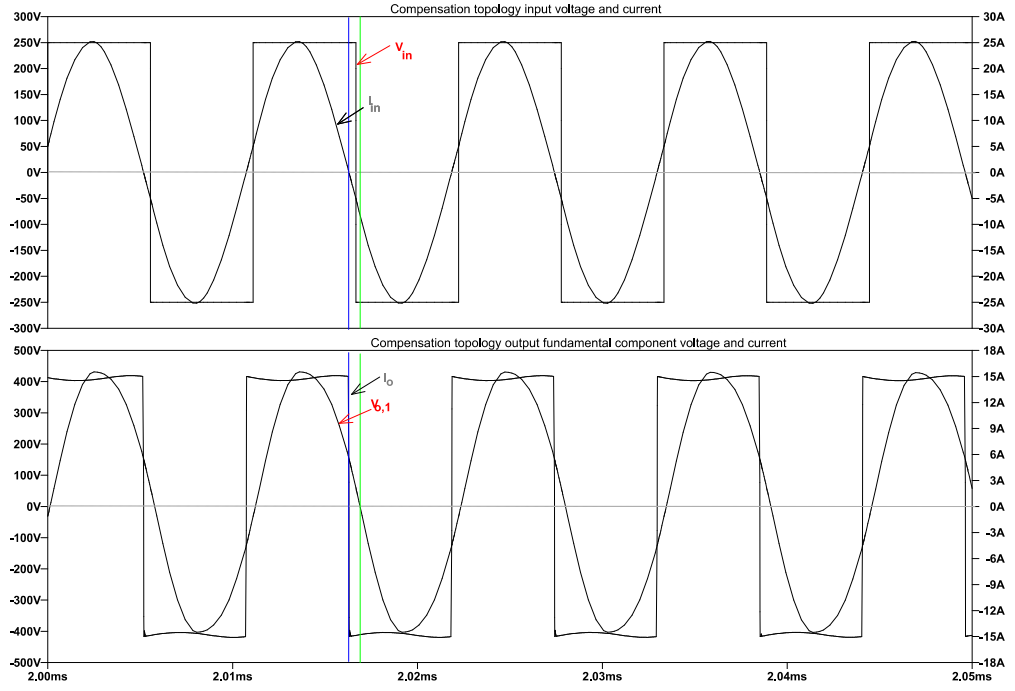


Figure 7.5: Compensation topology input and output waveforms with  $R_{ac} = 22\Omega$  depicting input-output phase relation in cv mode

low , so the capacitor current and voltages are not distorted much, hence resembles ideal scenario.

## 7.2 DQ Model Verification

The dq model of S-SP topology is implemented in matlab simulink whose circuit diagram is shown in Fig. 7.7. The actual sinusoidal waveform ( $V_o(t)$ ) and waveform obtained using dq transformed circuit ( $V_{do}$ ) is shown in Fig. 7.8. The q-component ( $V_{qo}$ ) can be neglected in comparison with d-component ( $V_{do}$ ) in cv mode as seen from the plot. Similarly in cc mode the q-component of current will only be considered.

## 7.3 Transient Waveform Simulations

The battery transient current waveforms (CC mode) are shown for  $R_{ac} = 15\Omega, 22\Omega$  are shown in Figures 7.10 and 7.10. The current  $I_{bat}$  settles at 271V at steady

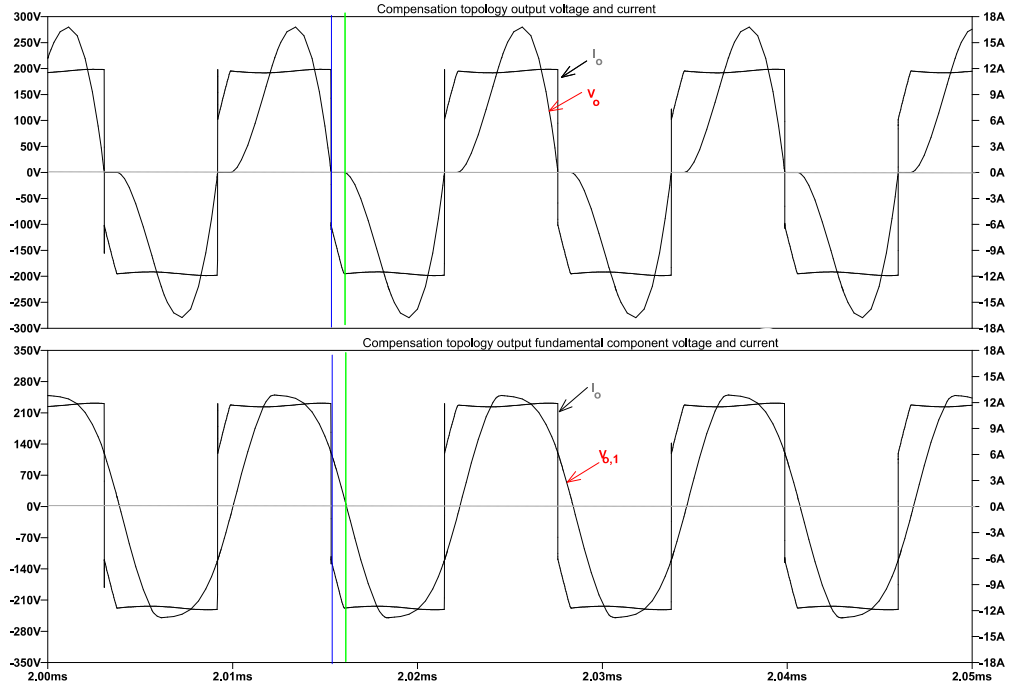


Figure 7.6: Compensation topology output waveforms with  $R_{ac} = 15\Omega$  depicting phase deviation at output

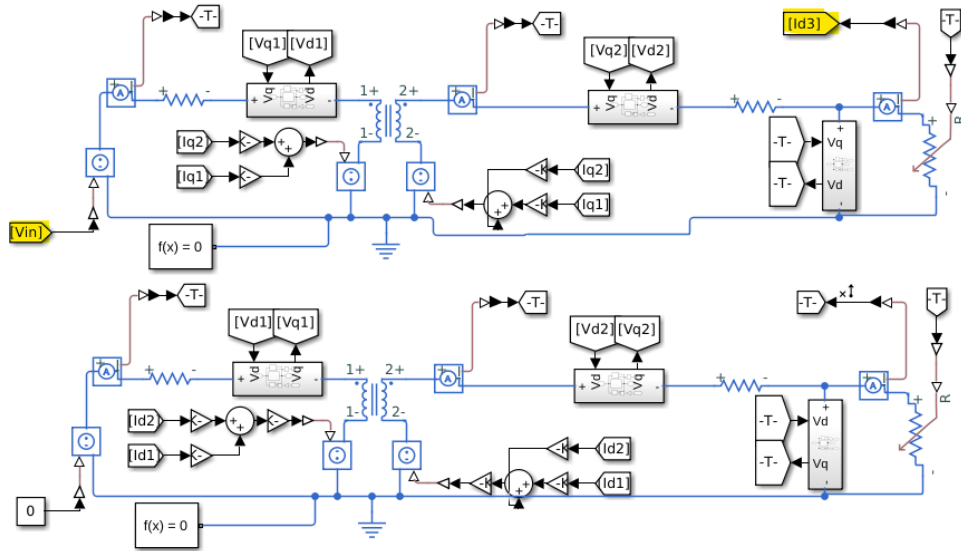


Figure 7.7: Circuit diagram of dq model (10th order)

state as expected

The battery transient voltage waveforms (CV mode) are shown for  $R_{ac} = 22\Omega, 140\Omega$  are shown in Figures 7.11 and 7.12. The voltage  $V_{bat}$  settles at 271V at steady state as expected. Without the controller there was a big overshoot in  $R_{ac} = 140\Omega$  case which is solved now.

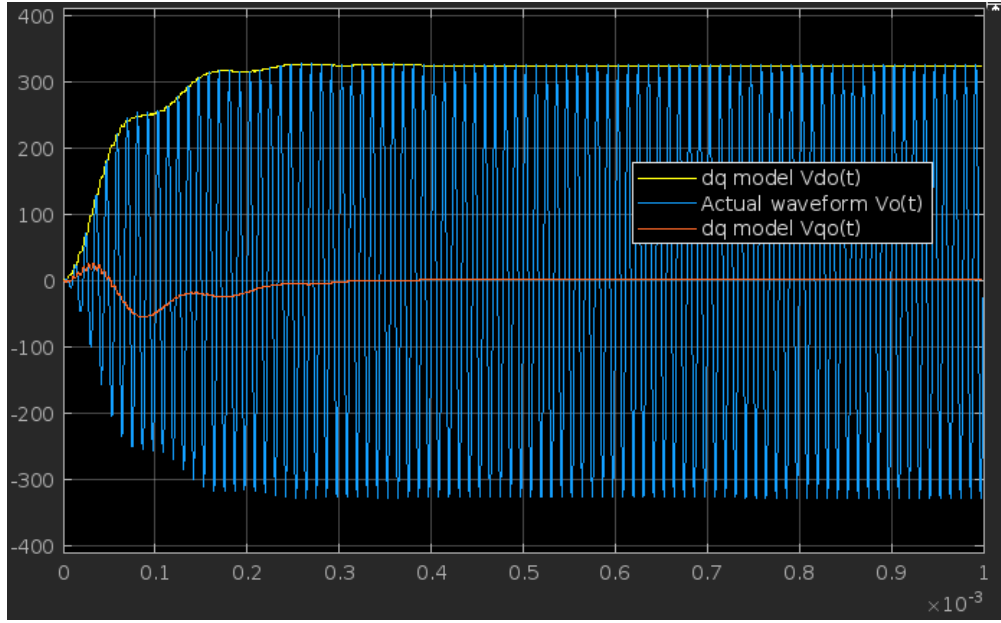


Figure 7.8: Simulation of dq model (10th order) and actual waveform

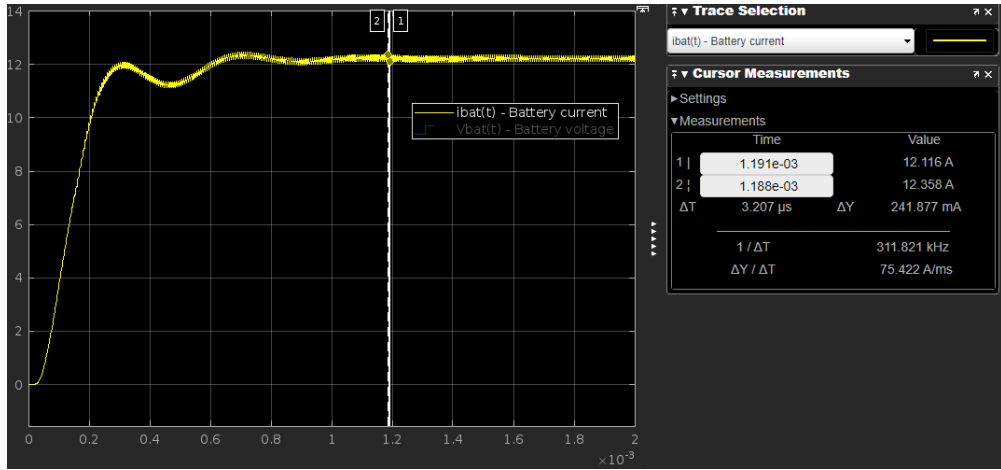


Figure 7.9:  $I_{bat}$  closed-loop waveform in cc mode for  $R_{ac} = 15\Omega$

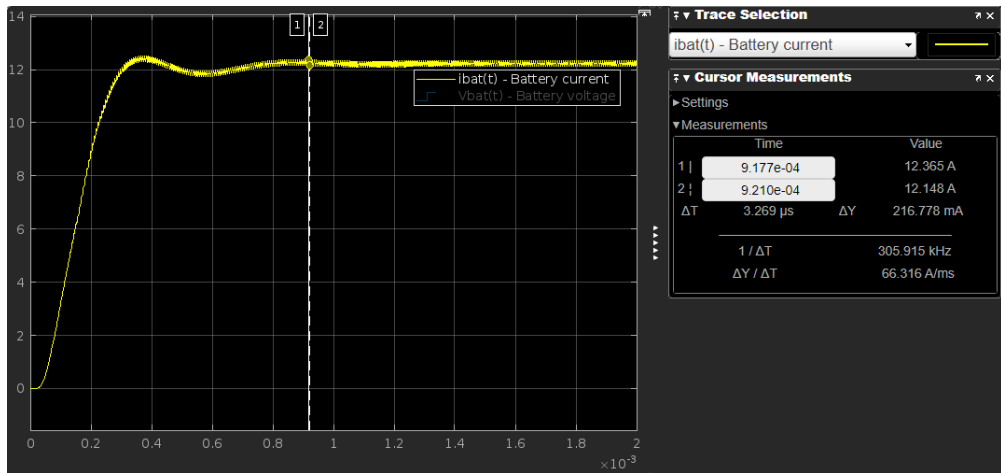


Figure 7.10:  $I_{bat}$  closed-loop waveform in cc mode for  $R_{ac} = 22\Omega$

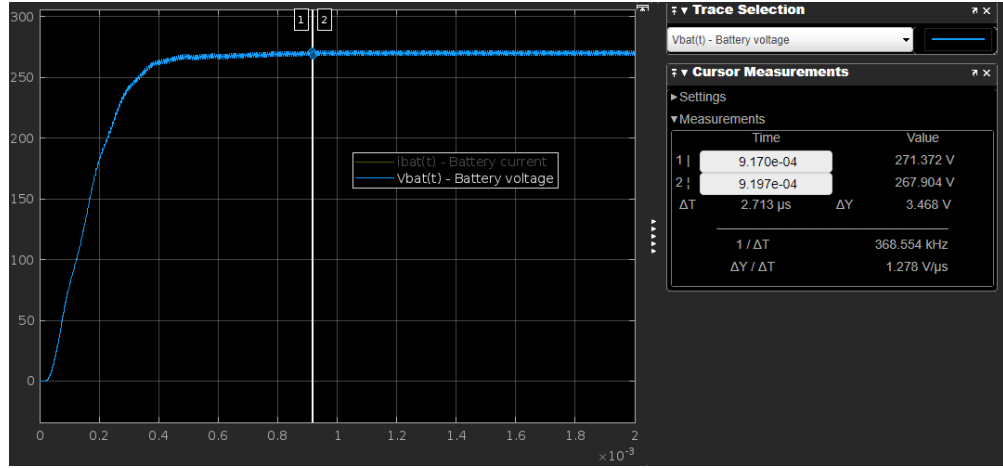


Figure 7.11:  $V_{bat}$  closed-loop waveform in cv mode for  $R_{ac} = 22\Omega$

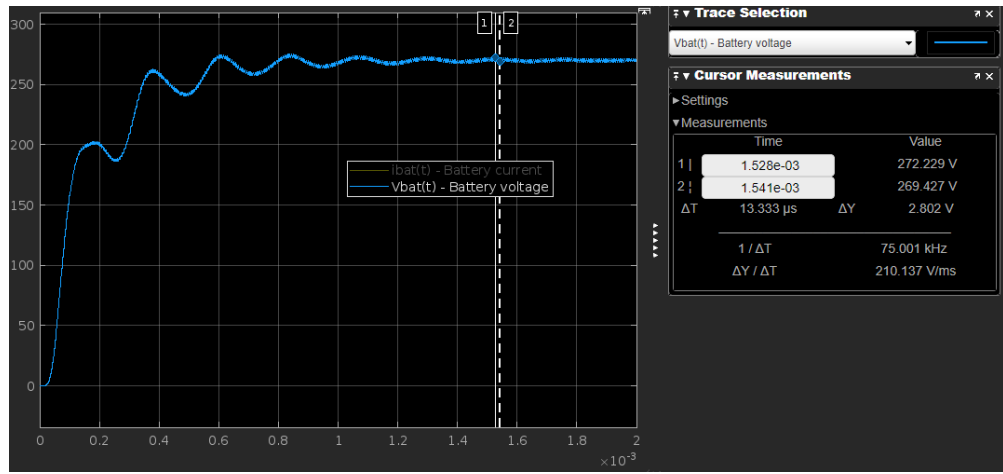


Figure 7.12:  $V_{bat}$  closed-loop waveform in cv mode for  $R_{ac} = 140\Omega$

## 7.4 Conclusion

This chapter has thus presented simulations required to verify the theoretical analysis.



# CHAPTER 8

## CONCLUSION AND FUTURE SCOPE

### 8.1 Conclusion

This thesis has designed a S-SP topology based WPT system along with a control system by a proper understanding of steady-state and dynamic models. The proposed system has tried to minimize the number of components, by choosing the smallest possible topology and also eliminating the need of additional components like switches and secondary DC-DC converter.

### 8.2 Future Scope

1. **Overcoming disadvantages in S-SP topology:** The S-SP topology is the smallest possible topology, but it has some disadvantages, such as high sensitivity to mutual inductance( $M$ ). This is because the CC/CV and ZPA equations somewhere have  $M$  separatively. Currently changing the topology(say to LCC), which changes the equations such that  $M$  doesn't have individual effect but only  $L_{lp} + M$  has effect on the equations, so that change in  $M$  doesn't affect the circuit in a common way. It can be explored if something easier can be done.

2. **Developing an intuitive synthesized model:** Currently the models try to visualize a big resonant network as a cascaded network of small resonant tanks. Many a times the equations derived from the models might be complex, but the simplified form of equations seems to be stunningly simple, for example DLCC topology equations. This thesis has done some attempt to explain the equations using controlled-source model in chapter 3, but still it looks complicated. If it is possible to understand how the resonant elements interact as a whole then the design procedure can probably become simplified.

## CHAPTER 9

### APPENDIX I - Actual equations and integrated ZPA model

The actual equations in terms of actual impedances  $X_1, X_2, X_3, X_4$  (without transformation into unified model) are derived here and summarized towards the end. The resonant tank approach[28] is used for CC/CV LIO(Load-Independent Output) condition. The ZPA is also derived using same strategy. (Note that it is always possible to mathematically simplify the unified model equations, or the equations obtained by other models and arrive at these equations)

#### 9.1 CC/CV LIO Analysis of S-SP topology using Resonant Tank Model

##### 9.1.1 CV mode LIO analysis

A resonant T-circuit (satisfying  $\frac{1}{X'_1} + \frac{1}{X'_2} + \frac{1}{X'_3} = 0$ ) does voltage-voltage (V-V) conversion as explained by the resonant tank model. This gives a load-independent output voltage  $V_o$  with gain  $G_{cv} = \frac{-X'_3}{X'_1}$

##### 9.1.2 CC mode LIO analysis

Consider the circuit in figure 9.1 (a). If we ensure  $\frac{1}{X_1} + \frac{1}{X_2} + \frac{1}{X_3+X_4} = 0$ , this circuit will give a load independent voltage  $V_o = -\frac{X_3+X_4}{X_1} \cdot V_{in}$  at the output.

Now, if we connect a dummy voltage source equal to  $V_o$  to the output terminal it won't affect the circuit's node voltages and branch currents in any way. So we can rewrite the circuit as figure 9.1(b) using substitution theorem.

Now we can do a source transformation by converting the dummy voltage source to dummy current source as in figure 9.1 (c). It is just a dummy current

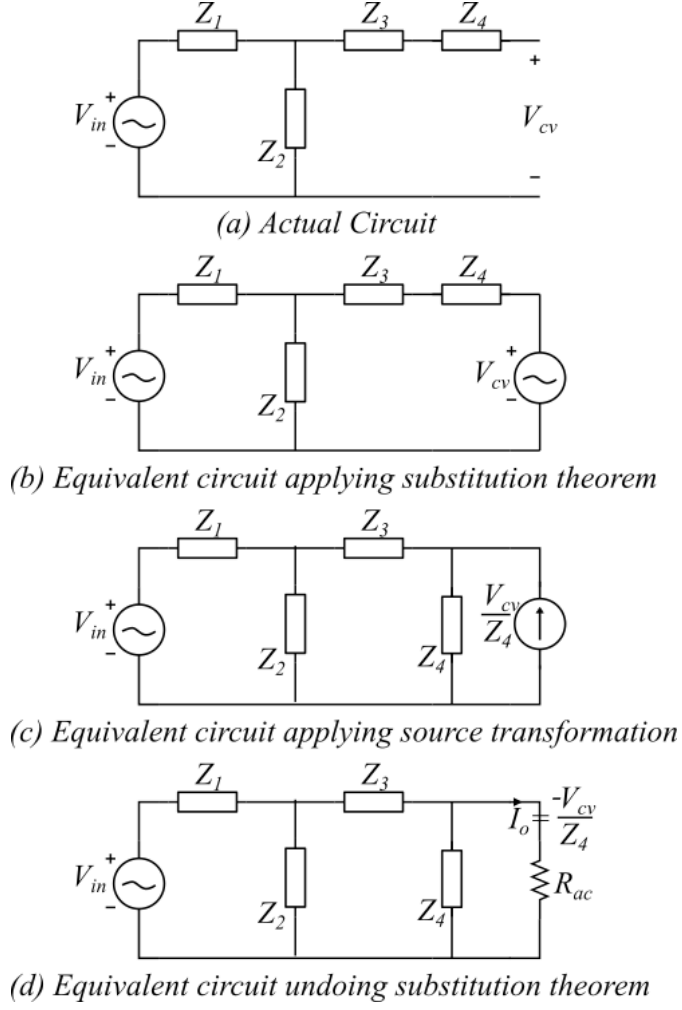


Figure 9.1: CC mode LIO condition derivation

source, so even if we remove it and add a load or short circuit it, the current will be same and independent of load as shown in figure 9.1 (d).

Thus the resonant condition  $\frac{1}{X_1} + \frac{1}{X_2} + \frac{1}{X_3+X_4} = 0$  gives a load-independent current output  $I_o$  with gain  $G_{cc} = -j \cdot \frac{X_3+X_4}{X_1X_4}$ .

## 9.2 Integrated ZPA analysis using resonant tank approach

### Introduction:

A couple of strategies have been proposed to determine ZPA condition.

- Lu *et al.*[13] has proposed a unified mathematical ZPA equation for a slightly transformed circuit which is valid for all topologies. However, the mathemat-

ical equation can be bit complicated especially for higher order topologies. (Unified Model)

- Qu *et al.*[16] has proposed a resonant tank based approach to achieve ZPA. This method can be used to obtain the load-independent output condition and ZPA condition in one mode, CC or CV. However, the conditions for the other mode have to be mathematically derived.
- Sohn *et al.*[21] has proposed a gyrator based model. This model explains well the input and output phase relation. Though this work does not try for ZPA, it qualitatively explains how ZVS can be achieved, but the input phase angle can be too large also.
- Other works like [28,24] have derived the ZPA condition mathematically.

In all of the above works, CC/CV and ZPA conditions are treated differently and obtained using separate strategies. This work explains how the resonant tank techniques used to achieve CC/CV can be directly applied to achieve ZPA also. Thus CC/CV and ZPA conditions can be achieved with the same technique, instead of using a separate method for ZPA. The analysis is found to give the same results for SS,SP,S-SP[14,28],DLCC[24] topologies and can be used for any other topology.

### 9.2.1 CV mode ZPA analysis:

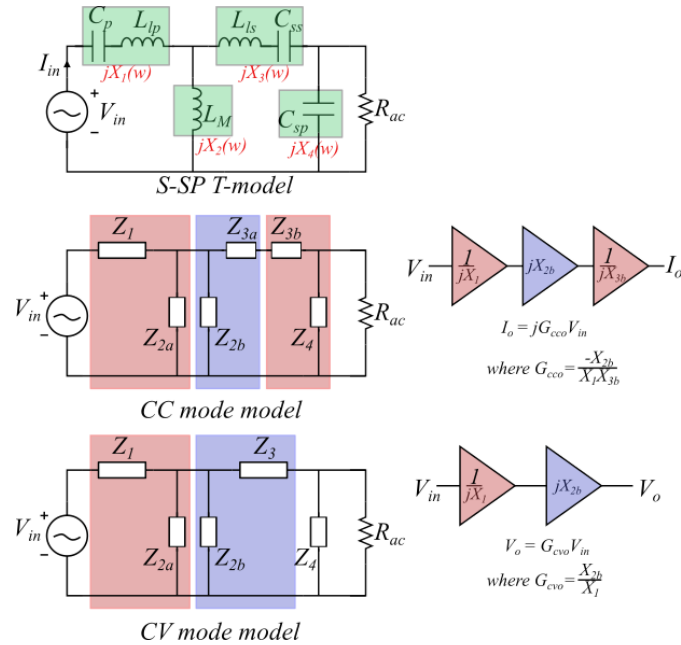


Figure 9.2: Unified Model of S-SP topology

The ZPA analysis procedure will be explained now for CV mode.

$V_{in}$  to  $V_o$  conversion is achieved by the T-resonant tank  $\left(\frac{1}{X'_1} + \frac{1}{X'_2} + \frac{1}{X'_3} = 0\right)$ .  $V_o$  will be at a phase of  $0^\circ/180^\circ$  wrt  $V_{in}$ . This can be clearly seen by applying the unified model. This is because each L-network will contribute a phase of  $\pm 90^\circ$ , and V-V conversion will require an even number of blocks, hence  $0^\circ/180^\circ$ . This result has been pointed out in [6]

$I_o = V_o/R_{ac}$  is the current required by the load for this value of  $V_o$ .  $I_o$  will be in phase with  $V_o$  because it is a resistive load. The input current  $I_{in}$  will be determined based on the topology and load current requirement  $I_o$ .

If we ensure the resonant condition  $X'_2 + X'_3 + X'_4 = 0$ , which corresponds to a  $\pi$ -network which does C-C transformation,  $I_{in}$  will be at a phase of  $0^\circ/180^\circ$  with  $I_o$ . This is because C-C transformation requires an even number of L-shaped resonant tanks of the unified model and each L-circuit contributes a phase of  $\pm 90^\circ$ .

Thus by ensuring C-C resonant condition along with V-V resonant condition, input ZPA is achieved along with CV LIO.

The mathematical explanation is given below

$$\begin{aligned}
\angle V_o - \angle V_{in} &= 0^\circ/180^\circ \\
\angle I_o - \angle V_o &= \theta_{out} = 0^\circ \\
\angle I_{in} - \angle I_o &= 0^\circ/180^\circ \\
\text{From above equations,} \\
\angle I_{in} - \angle V_{in} &= \angle I_o - \angle V_o \\
\text{(or) } \theta_{in} &= \theta_{out} \\
\implies \theta_{in} &= 0^\circ \text{ (ZPA)}
\end{aligned}$$

The above condition  $\theta_{in} = \theta_{out}$  has been proved using the gyrator model in [21]. The input phase angle will be same as the output phase angle provided the V-V and C-C resonant conditions are satisfied. This is a property of the resonant topology and will be true (wrt fundamental components) irrespective of the output. The output angle is approximately zero as it can be modelled like an AC resistance  $R_{ac}$ , but if there is some output phase angle the same angle will be present in the input side.

## CV mode Input Impedance

The value of input impedance  $Z_{in}$  can be calculated by equating input and output power. The apparent complex power supplied by the source is  $S = V_{in}I_{in}^*$ . During the initial transients,  $S$  has both active and passive components. The active power goes to the load resistance and the reactive power is drawn by the resonant tanks to charge up their potential energy. At steady state the resonant tanks are sufficiently charged up and will draw no more power from the source because of the sustainable nature of resonant tanks. So the input apparent power is purely active power and this goes completely to the load  $R_{ac}$ .

$$\begin{aligned}
V_{in}I_{in}^* &= V_oI_o^* \\
\Rightarrow V_{in} \left( \frac{V_{in}^*}{Z_{in}^*} \right) &= V_o \left( \frac{V_o^*}{R_{ac}} \right) \\
\Rightarrow \frac{|V_{in}|^2}{Z_{in}} &= \frac{|V_o|^2}{R_{ac}} \quad (\because Z_{in}^* = Z_{in}, \text{ as } Z_{in} \text{ is purely real due to ZPA}) \\
\Rightarrow Z_{in} &= \frac{R_{ac}}{|V_o/V_{in}|^2} \\
\Rightarrow Z_{in} &= \frac{R_{ac}}{|G_{cv}|^2}
\end{aligned}$$

[13] derives the above expression using the ZPA mathematical equation and CV resonant conditions. Here it is derived more directly by equating the power.

## CV mode Reverse Gain:

The reverse current gain  $I_{in}/I_o$  can now be found out as follows:

$$\begin{aligned}
Z_{in} &= \frac{R_{ac}}{|G_{cv}|^2} \\
\Rightarrow \frac{V_{in}}{I_{in}} &= \frac{V_o}{I_o} \frac{1}{|G_{cv}|^2} \\
\Rightarrow \frac{V_{in}}{I_{in}} &= \frac{V_o/G_{cv}}{I_o \cdot G_{cv}^*} \\
\Rightarrow I_{in} &= I_o \cdot G_{cv}^* \quad (\because V_o = V_{in} \cdot G_{cv})
\end{aligned}$$

The reverse current gain  $I_{in}/I_o$  is conjugate of the forward voltage gain  $V_o/V_{in}$ , provided the V-V and C-C resonant conditions are satisfied. This kind of pattern is

noticeable in CC mode also as derived in the next section. This is like a transformer or gyrator as explained in the gyrator model. But one can try to dig deeper and understand why this happens in terms of the circuit, i.e what is the relation between the seemingly independent V-V resonant T-circuit and C-C resonant  $\pi$ -circuit which causes their gains to behave like this.

### 9.2.2 CC mode ZPA analysis:

$V_{in}$  to  $I_o$  conversion is achieved by the resonance condition  $\frac{1}{X_1} + \frac{1}{X_2} + \frac{1}{X_3 + X_4} = 0$ . In the unified model, V-C conversion will require odd number of L-circuits, hence  $I_o$  will be at a phase of  $\pm 90^\circ$  with  $V_{in}$ . This will cause a voltage  $V_o = I_o R_{ac}$  across the load. If we resonate  $X_2$  and  $X_3$  (a L-circuit) as  $X_2 + X_3 = 0$ , V-C conversion takes place. So  $I_{in}$  will be purely dependent on  $V_o$  and will be at a phase of  $\mp 90^\circ$  with  $V_o$ . It is  $\mp 90^\circ$  (not  $\pm 90^\circ$ ) because reverse gain ( $G_{cc}^*$ ) will be conjugate of forward gain ( $G_{cc}$ ) which will be described towards the end of this section.

$$\angle I_o - \angle V_{in} = \pm 90^\circ$$

$$\angle V_o - \angle I_o = -\theta_{out} = 0^\circ$$

$$\angle I_{in} - \angle V_o = \mp 90^\circ \quad (\because I_{in}/V_o = G_{cc}^*)$$

*From above equations,*

$$\angle I_{in} - \angle V_{in} = -(\angle I_o - \angle V_o)$$

$$(or) \quad \theta_{in} = -\theta_{out}$$

$$\implies \theta_{in} = 0^\circ \text{ (ZPA)}$$

Hence ZPA is achieved.

## CC mode Input Impedance

The input impedance can be calculated just like in CV mode.

$$\begin{aligned}
V_{in}I_{in}^* &= V_oI_o^* \\
\Rightarrow V_{in} \left( \frac{V_{in}^*}{Z_{in}^*} \right) &= (I_oR_{ac})I_o^* \\
\Rightarrow \frac{|V_{in}|^2}{Z_{in}} &= |I_o|^2 R_{ac} \quad (\because Z_{in}^* = Z_{in}, \text{ as } Z_{in} \text{ is purely real due to ZPA}) \\
\Rightarrow Z_{in} &= \frac{1}{R_{ac} \cdot |I_o/V_{in}|^2} \\
\Rightarrow Z_{in} &= \frac{1}{R_{ac} \cdot |G_{cc}|^2}
\end{aligned}$$

## CC mode Reverse Gain:

The reverse gain  $I_{in}/V_o$  is calculated here.

$$\begin{aligned}
Z_{in} &= \frac{1}{R_{ac} \cdot |G_{cc}|^2} \\
\Rightarrow \frac{V_{in}}{I_{in}} &= \frac{I_o}{V_o} \frac{1}{|G_{cc}|^2} \\
\Rightarrow \frac{V_{in}}{I_{in}} &= \frac{I_o/G_{cc}}{V_o \cdot G_{cc}^*} \\
\Rightarrow I_{in} &= V_o \cdot G_{cc}^* \quad (\because I_o = V_{in} \cdot G_{cc})
\end{aligned}$$

## 9.2.3 Comments

The input impedance  $Z_{in}$  and reverse gains  $(G_{cc}^*, G_{cv}^*)$  are calculated directly from power equations which is a surface level approach. [21] has tried a circuit level approach by explaining using gyrators. [14] has done a mathematical work. It will be good to try to understand at a deeper level, using the resonant circuits to explain this phenomenon. By doing this one might understand how changing each individual component affects the gain and input phase angle, which might help one to overcome phase issues at output, or to get ZVS at input.



### 9.3 Summary of equations

The above equations can be summarized as follows:

CC mode	CV mode
$CC : \frac{1}{X_1} + \frac{1}{X_2} + \frac{1}{X_3 + X_4} = 0$	$CV : \frac{1}{X'_1} + \frac{1}{X'_2} + \frac{1}{X'_3} = 0$
$ZPA_{CC} : X_2 + X_3 = 0$	$ZPA_{CV} : X'_2 + X'_3 + X'_4 = 0$
$G_{cc} = -j \cdot \frac{X_3 + X_4}{X_1 X_4}$	$G_{cv} = \frac{-X'_3}{X'_1}$
$Z_{in} = \frac{1}{ G_{cc} ^2 R_{ac}}$ $\theta_{in} = -\theta_{out} = 0^\circ$ $I_o = G_{cc} V_{in} ; I_{in} = G_{cc}^* V_o$	$Z_{in} = \frac{R_{ac}}{ G_{cv} ^2}$ $\theta_{in} = \theta_{out} = 0^\circ$ $V_o = G_{cc} V_{in} ; I_{in} = G_{cc}^* I_o$

## REFERENCES

1. **Aditya, W. S., K.** (2016). Linearization and control of series-series compensated inductive power transfer system based on extended describing function concept.
2. **Biswas, S., L. Huang, V. Vaidya, K. Ravichandran, N. Mohan, and S. V. Dhople** (2016). Universal current-mode control schemes to charge li-ion batteries under dc/pv source. *IEEE Transactions on Circuits and Systems I: Regular Papers*, **63**(9), 1531–1542.
3. **Dominguez, A., L. A. Barragan, J. I. Artigas, A. Otin, I. Urriza, and D. Navarro** (2017). Reduced-order models of series resonant inverters in induction heating applications. *IEEE Transactions on Power Electronics*, **32**(3), 2300–2311.
4. **Erickson, R. W. and D. Maksimovic**, *Fundamentals of Power Electronics*. Springer, 2001, 2ed edition.
5. **Grepow** (2019). What are the 3 stages of lithium battery charging? URL <https://www.grepow.com/blog/what-are-the-3-stages-of-lithium-battery-charging/>.
6. **Hu., A. P.** (2001). Selected resonant converters for ipt power supplies. *Ph.D thesis, Electrical and Electronic Engineering, The University of Auckland*.
7. **JhunJhunwala, A.** (2020). Nptel lecture : Fundamentals of electric vehicles, lecture-31, charging batteries. URL <https://www.youtube.com/watch?v=tyeSahlzt3Y>.
8. **Koh, K. E., T. C. Beh, T. Imura, and Y. Hori** (2014). Impedance matching and power division using impedance inverter for wireless power transfer via magnetic resonant coupling. *IEEE Transactions on Industry Applications*, **50**(3), 2061–2070.
9. **Lee, S., B. Choi, and C. T. Rim** (2013). Dynamics characterization of the inductive power transfer system for online electric vehicles by laplace phasor transform. *IEEE Transactions on Power Electronics*, **28**(12), 5902–5909.
10. **Lee, S. and S.-H. Lee** (2020). dq synchronous reference frame model of a series-series tuned inductive power transfer system. *IEEE Transactions on Industrial Electronics*, **67**(12), 10325–10334.
11. **Li, S., W. Li, J. Deng, T. D. Nguyen, and C. C. Mi** (2015). A double-sided lcc compensation network and its tuning method for wireless power transfer. *IEEE Transactions on Vehicular Technology*, **64**(6), 2261–2273.
12. **Liu, X., X. Yuan, C. Xia, and X. Wu** (2021). Analysis and utilization of the frequency splitting phenomenon in wireless power transfer systems. *IEEE Transactions on Power Electronics*, **36**(4), 3840–3851.

13. **Lu, J., G. Zhu, D. Lin, Y. Zhang, J. Jiang, and C. C. Mi** (2019). Unified load-independent zpa analysis and design in cc and cv modes of higher order resonant circuits for wpt systems. *IEEE Transactions on Transportation Electrification*, **5**(4), 977–987.
14. **Lu, J., G. Zhu, D. Lin, Y. Zhang, H. Wang, and C. C. Mi** (2021). Realizing constant current and constant voltage outputs and input zero phase angle of wireless power transfer systems with minimum component counts. *IEEE Transactions on Intelligent Transportation Systems*, **22**(1), 600–610.
15. **Qu, J. Y. L. J. W. S.-C., X. and C. Tse** (2019). Design for continuous-current-mode operation of inductive-power-transfer converters with load-independent output. *IET Power Electronics*, **12**(10), 2458–2465.
16. **Qu, X., H. Chu, S.-C. Wong, and C. K. Tse** (2019). An ipt battery charger with near unity power factor and load-independent constant output combating design constraints of input voltage and transformer parameters. *IEEE Transactions on Power Electronics*, **34**(8), 7719–7727.
17. **Qu, X., H. Han, S.-C. Wong, C. K. Tse, and W. Chen** (2015). Hybrid ipt topologies with constant current or constant voltage output for battery charging applications. *IEEE Transactions on Power Electronics*, **30**(11), 6329–6337.
18. **Ravikiran, V. and R. K. Keshri**, Comparative evaluation of s-s and p-s topologies for wireless charging of electrical vehicles. In *IECON 2017 - 43rd Annual Conference of the IEEE Industrial Electronics Society*. 2017.
19. **Sample, A. P., D. T. Meyer, and J. R. Smith** (2011). Analysis, experimental results, and range adaptation of magnetically coupled resonators for wireless power transfer. *IEEE Transactions on Industrial Electronics*, **58**(2), 544–554.
20. **Shevchenko, V., O. Husev, R. STRZELECKI, B. Pakhaliuk, N. Poliakov, and S. Natalia** (2019). Compensation topologies in ipt systems: Standards, requirements, classification, analysis, comparison and application. *IEEE Access*, **PP**, 1–1.
21. **Sohn, Y. H., B. H. Choi, G.-H. Cho, and C. T. Rim** (2016). Gyrator-based analysis of resonant circuits in inductive power transfer systems. *IEEE Transactions on Power Electronics*, **31**(10), 6824–6843.
22. **Sohn, Y. H., B. H. Choi, E. S. Lee, G. C. Lim, G.-H. Cho, and C. T. Rim** (2015). General unified analyses of two-capacitor inductive power transfer systems: Equivalence of current-source ss and sp compensations. *IEEE Transactions on Power Electronics*, **30**(11), 6030–6045.
23. **Sun, J. and H. Grotstollen**, Averaged modeling and analysis of resonant converters. In *Proceedings of IEEE Power Electronics Specialist Conference - PESC '93*. 1993.
24. **Vu, V.-B., D.-H. Tran, and W. Choi** (2018). Implementation of the constant current and constant voltage charge of inductive power transfer systems with the double-sided lcc compensation topology for electric vehicle battery charge applications. *IEEE Transactions on Power Electronics*, **33**(9), 7398–7410.

25. **Wang, C.-S., G. Covic, and O. Stielau**, General stability criterions for zero phase angle controlled loosely coupled inductive power transfer systems. *In IECON'01. 27th Annual Conference of the IEEE Industrial Electronics Society (Cat. No.37243)*, volume 2. 2001.
26. **Wang, C.-S., G. Covic, and O. Stielau** (2004). Power transfer capability and bifurcation phenomena of loosely coupled inductive power transfer systems. *IEEE Transactions on Industrial Electronics*, **51**(1), 148–157.
27. **Zahid, Z. U., Z. M. Dalala, C. Zheng, R. Chen, W. E. Faraci, J.-S. J. Lai, G. Lisi, and D. Anderson** (2015). Modeling and control of series-series compensated inductive power transfer system. *IEEE Journal of Emerging and Selected Topics in Power Electronics*, **3**(1), 111–123.
28. **Zhang, W. and C. C. Mi** (2016). Compensation topologies of high-power wireless power transfer systems. *IEEE Transactions on Vehicular Technology*, **65**(6), 4768–4778.
29. **Zhang, W., S.-C. Wong, C. K. Tse, and Q. Chen** (2014). Analysis and comparison of secondary series- and parallel-compensated inductive power transfer systems operating for optimal efficiency and load-independent voltage-transfer ratio. *IEEE Transactions on Power Electronics*, **29**(6), 2979–2990.